NATURAL RESOURCES

GEOLOGIC MAP OF THE SHELTON VALLEY 7.5-MINUTE QUADRANGLE, MASON COUNTY, WASHINGTON

by Michael Polenz, Mitchell D. Allen, Gabriel Legorreta Paulín, Daniel W. Eungard, Recep Cakir, Spenser P. Scott, and Shannon A. Mahan

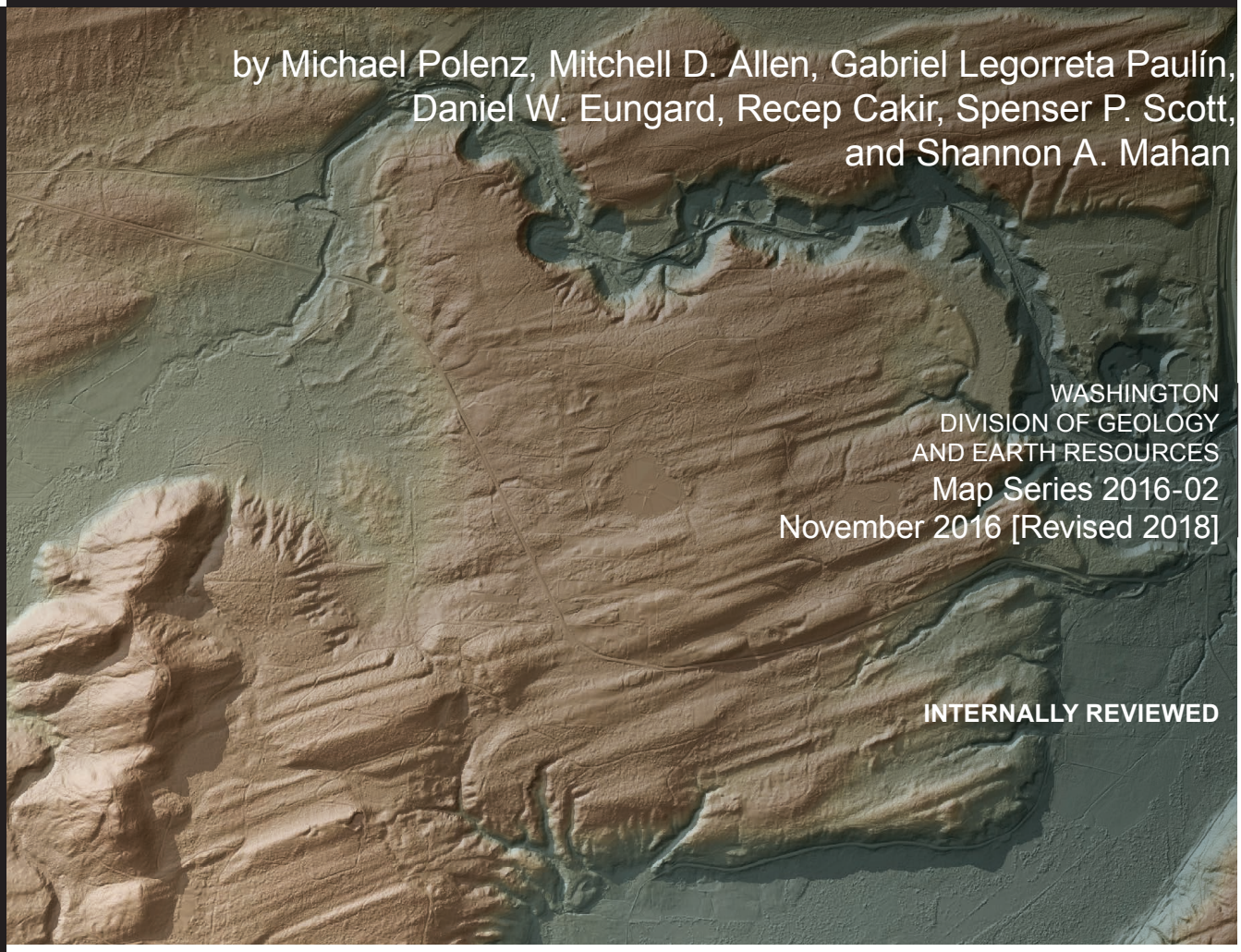

WASHINGTON
DIVISION OF GEOLOGY
AND EARTH RESOURCES
Map Series 2016-02
November 2016 [Revised 2018]

INTERNALLY REVIEWED

WASHINGTON STATE DEPARTMENT OF
NATURAL RESOURCES
DIVISION OF GEOLOGY AND EARTH RESOURCES

GEOLOGIC MAP OF THE SHELTON VALLEY 7.5-MINUTE QUADRANGLE, MASON COUNTY, WASHINGTON

by Michael Polenz, Mitchell D. Allen, Gabriel Legorreta Paulín,
Daniel W. Eungard, Recep Cakir, Spenser P. Scott,
and Shannon A. Mahan

WASHINGTON
DIVISION OF GEOLOGY
AND EARTH RESOURCES
Map Series 2016-02
November 2016 [Revised 2018]

This geologic map was funded in part by the USGS National Cooperative Geologic Mapping Program, award no. G15AC00248

This publication has been subject to an iterative technical review process by at least one Division geologist who is not an author. This publication has also been subject to an iterative review process with Division editors and cartographers and has been formatted by Division staff.

WASHINGTON STATE DEPARTMENT OF
NATURAL RESOURCES
DIVISION OF GEOLOGY AND EARTH RESOURCES

DISCLAIMER

Neither the State of Washington, nor any agency thereof, nor any of their employees, makes any warranty, express or implied, or assumes any legal liability or responsibility for the accuracy, completeness, or usefulness of any information, apparatus, product, or process disclosed, or represents that its use would not infringe privately owned rights. Reference herein to any specific commercial product, process, or service by trade name, trademark, manufacturer, or otherwise, does not necessarily constitute or imply its endorsement, recommendation, or favoring by the State of Washington or any agency thereof. The views and opinions of authors expressed herein do not necessarily state or reflect those of the State of Washington or any agency thereof.

INDEMNIFICATION

Research supported by the U.S. Geological Survey, National Cooperative Geologic Mapping Program, under USGS award number G15AC00248. The views and conclusions contained in this document are those of the authors and should not be interpreted as necessarily representing the official policies, either expressed or implied, of the U.S. Government.

WASHINGTON STATE DEPARTMENT OF NATURAL RESOURCES

Peter Goldmark—*Commissioner of Public Lands*

DIVISION OF GEOLOGY AND EARTH RESOURCES

David K. Norman—*State Geologist*
Timothy J. Walsh—*Assistant State Geologist*
John P. Bromley—*Assistant State Geologist*

Washington State Department of Natural Resources
Division of Geology and Earth Resources

Mailing Address:
MS 47007
Olympia, WA 98504-7007

Street Address:
Natural Resources Bldg, Rm 148
1111 Washington St SE
Olympia, WA 98501

Phone: 360-902-1450
Fax: 360-902-1785
Email: geology@dnr.wa.gov
Website: http://www.dnr.wa.gov/geology

Publications and Maps:
www.dnr.wa.gov/programs-and-services/geology/publications-and-data/publications-and-maps

Washington Geology Library Searchable Catalog:
www.dnr.wa.gov/programs-and-services/geology/washington-geology-library

Suggested Citation: Polenz, Michael; Allen, M. D.; Legorreta Paulín, Gabriel; Eungard, D. W.; Cakir, Recep; Scott, S. P.; Mahan, S. A., 2018, Geologic map of the Shelton Valley 7.5-minute quadrangle, Mason County, Washington: Washington Division of Geology and Earth Resources Map Series 2016-02, originally published 2016, 1 sheet, scale 1:24,000, 45 p. text. [http://www.dnr.wa.gov/publications/ger_ms2016-02_geol_map_shelton_valley_24k.zip]

Errata: The normalized XRF major element values and unnormalized XRF major element sum values published in the original data supplement were incorrect. This has been corrected. The citation for Prescott and Hutton (1994) was added to the references list. Corrections were made April 17, 2018.

© 2018 Washington Division of Geology and Earth Resources
Published in the United States of America

Contents

Introduction 1
- Location, Purpose, and Scope 1
- Summary of Results 1

Geologic Overview 1
- Regional Geology 1
- Bedrock Units 3
- The Olympia Structure 3
- Quaternary Deposits 4
  - Pre-Vashon Deposits 4
  - Vashon Drift 4
  - Post-glacial Deposits 4
- Treatment of Named Units 4
  - Salmon Springs Drift 4
  - Skokomish Gravel 4
  - Kitsap Formation 5
  - Olympia Nonglacial Sediment (Olympia Beds) 5

Methods 5
- Geologic Mapping 5
- Bedrock Geochronology and Paleontology 5
- Geochemistry of Volcanic Bedrock Samples 5
- Sedimentary Provenance 5
- Quaternary Geochronology, Paleomagnetics, and Pollen Analyses 6
- Detailed Stratigraphic Analyses 6
- Geophysical Data and Analyses 6

Sediment Composition and Provenance 6

Description of Map Units 8
- Quaternary Unconsolidated Deposits 8
  - Post-glacial Deposits 8
- Bedrock Units 18
  - Geochronology 18
  - Biostratigraphy 18
- Unconsolidated Quaternary Units 19
  - Geochronology and Paleomagnetics 19
  - Weathering of Vashon and pre-Vashon Deposits 19
  - Ages of Quaternary Units 20

Paleoenvironmental Interpretation 22
- Bedrock Units 22
- Unconsolidated Quaternary Units 23
  - Paleoenvironment of pre-Vashon Glacial and Nonglacial Deposits, Undivided 23
  - Deposits, Landforms, and Lakes of the Vashon Glaciation (MIS 2) 25
  - Post-Glacial Conditions 26
  - Paleogeographic Considerations 26

Geochemistry 28

Geophysics of the Map Area 30
- Introduction to Data Sources 30
- Geophysical Observations 30
- Implications for Future Investigations of the Olympia Structure 30

Structures in the Map Area 31
- Bedrock 31
- Unconsolidated Deposits 31

Bedding 31
Faulting 33
Folding 35
Interpretation of Structures 35
The Role of Ice Shove on Faults and Folds 35
Local Tectonic Influences 35
Acknowledgments 36
References 36
Appendix A. New Radiocarbon, Luminescence, and $^{40}Ar/^{39}Ar$ Age Estimates 42

FIGURES

Figure 1. Regional geologic map for the Shelton Valley quadrangle 2
Figure 2. Pie charts of provenance types 8
Figure 3. Principal component analyses (PCA) of provenance 9
Figure 4. Annotated photo and schematic diagram of heavily faulted section along Goldsborough canyon 15
Figure 5. Photo of sedimentary interbeds in basalt flows of the Crescent Formation 18
Figure 6. Photo of sub-horizontal interbed of siltstone to very fine sandstone between basalt flows of the Crescent Formation 18
Figure 7. Plot showing increase in amount of weathering with age of sediment. 19
Figure 8. Schematic section of deformed Quaternary deposits along Goldsborough canyon 22
Figure 9. Pollen diagram for six organic-rich sediment samples 24
Figure 10. Pollen samples L3 and L4 are sampled from the same organic-rich sediment section as radiocarbon sample GD2 24
Figure 11. Geochemical characterization of basalt from the Shelton Valley quadrangle. 28
Figure 12. Photo of steep shear zone in pillow basalt flow of the Crescent Formation 31
Figure 13. Stereonet plots for structures measured in the Shelton Valley quadrangle 32
Figure 14. Annotated photo of subvertical SSE-striking fault in subhorizontally bedded Quaternary deposits along Goldsborough canyon 34
Figure A1. $^{40}Ar/^{39}Ar$ step-heating age and K/Ca spectra for site GD9. 45
Figure A2. $^{40}Ar/^{39}Ar$ step-heating age and K/Ca spectra for site GD10. 45

TABLES

Table 1. Summary of new ages, paleomagnetic data, and biostratigraphic analyses from the Shelton Valley quadrangle. 7
Table 2. Geophysical data collection localities, methods used, and depth to bedrock estimates. 7
Table 3. Sample groupings and data sources for compilations of volcanic rocks from western Washington. 28
Table A1. Radiocarbon ages from the map area. 42
Table A2. New infrared stimulated luminescence (IRSL) results from the map area 44
Table A3. $^{40}Ar/^{39}Ar$ ages for sites GD9 and GD10. 45

MAP SHEET

Geologic Map of the Shelton Valley 7.5-minute Quadrangle, Mason County, Washington

Figure M1. Location map for the Shelton Valley quadrangle
Figure M2. Gravity and aeromagnetic gradients in and around the Shelton Valley quadrangle

Geologic Map of the Shelton Valley 7.5-minute Quadrangle, Mason County, Washington

by Michael Polenz[1], Mitchell D. Allen[1], Gabriel Legorreta Paulín[2], Daniel W. Eungard[1], Recep Cakir[1], Spenser P. Scott[1], and Shannon A. Mahan[3]

[1] Washington Division of Geology and Earth Resources
MS 47007
Olympia, WA 98504-7007

[2] Universidad Nacional Autónoma de México
Instituto de Geografía
Ciudad Universitaria, Del Coyoacán
cp 04510, México, D.F.

[3] U.S. Geological Survey
Box 25046, MS 974
Denver Federal Center
Denver, CO 80225-5046

INTRODUCTION

Location, Purpose, and Scope

The Shelton Valley 7.5-minute quadrangle straddles the northern Black Hills and the western Puget Lowland in Mason County, just west of the city of Shelton and six miles south of Hood Canal (Fig. M1). Mapping in this area is a priority because Hood Canal contains national defense infrastructure, Mason County is increasingly populated, and the nearby city of Olympia (Fig. M1) is home to Washington's state government. The Puget Lowland and the nearby Olympic Mountains and Hood Canal are geologically active and ecologically sensitive. Speculations of a northwest-trending 'Olympia structure' from Olympia to the map area and beyond justify more detailed geologic mapping and identification of associated hazards. Water resources are becoming increasingly scarce, and improved geologic understanding is needed to inform private and public resource management. This 1:24,000-scale geologic mapping focused on identifying hazards and improving geologic understanding within the Shelton Valley quadrangle.

Summary of Results

Our map and cross sections add detailed field observations and geological analyses to previous mapping and studies of the area (Carson, 1970, 1980; Molenaar and Noble, 1970; Logan, 1987, 2003; Jones, 1999). Basalt geochemistry and two new high-quality $^{40}Ar/^{39}Ar$ ages support assignment of basalt to the Eocene Crescent Formation. Most surficial sediments are Vashon Drift. Voluminous pebble gravel and diamictons sourced from the Olympic Mountains were deposited in parts of the map area and may include lodgment till. These deposits imply that paleo-topography differed from the modern setting and suggest that ice advances from the Olympic Mountains may have reached the map area. Deformed sediments suggest that faults in the Shelton Valley quadrangle may have been active in the Quaternary. Olympic-sourced sediment and deformation of Quaternary deposits are best exposed along a reach of Goldsborough Creek that we informally refer to as Goldsborough canyon (Fig. M1)

GEOLOGIC OVERVIEW

Regional Geology

The Shelton Valley quadrangle is underlain by early Eocene basalt of the Crescent Formation (Fig. 1). As part of Siletzia, the Crescent Formation and similar rocks in the Washington and Oregon coast ranges have been interpreted as a large oceanic igneous province (varying in thickness from 10 to 32 km) that was rapidly extruded near the margin of North America between 56 and 49 Ma (Irving, 1979; Babcock and others, 1992; Wells and others, 2014); new U-Pb dates suggest a revised timeline between 53 and 48 Ma (Michael Eddy, Massachusetts Institute of Technology, written commun., 2016). Wells and others (1984) and Babcock and others (1992) postulate that extrusion of this thick sequence of subaqueous to subaerial tholeiitic and alkalic basalt resulted from rifting near the margin of North America due to oblique subduction of the Kula and Farallon plates. Wells and others (2014) suggest possible interaction with the Yellowstone hotspot and accretion to North America about 50 Ma. Biostratigraphic analyses on Crescent Formation rocks from the Black Hills south and southeast of the Shelton Valley quadrangle point to an age in the Ulatisian Stage of the Eocene (W. Rau, cited in Globerman and others, 1982; Logan and Walsh, 2004). Latest Eocene to Miocene marine and rare terrestrial sedimentary rocks were deposited after accretion and onlap the Crescent Formation (Fig. 1)(Pease and Hoover, 1957; Snavely and others, 1958; Pratt and others, 1997; Armentrout and others, 1983; Walsh and others, 1987; Dragovich and others, 2002; Wells and others, 2014).

Strain partitioning related to oblique subduction of the Juan de Fuca plate beneath North America has created a structurally complex forearc of the Cascadia subduction zone (Wells and others, 1998; Lewis and others, 2003; Johnson and others, 2004; McCaffrey and others, 2007, 2013). From south to north, Wells and others (1998) describe west-northwest directed translation of the Sierra Nevada block imparting clockwise rotation on the Oregon forearc block to the north, leading to clockwise rotation of discrete crustal blocks and north-south shortening within the Washington forearc south of where it abuts against a relatively fixed Coast Mountains buttress (at

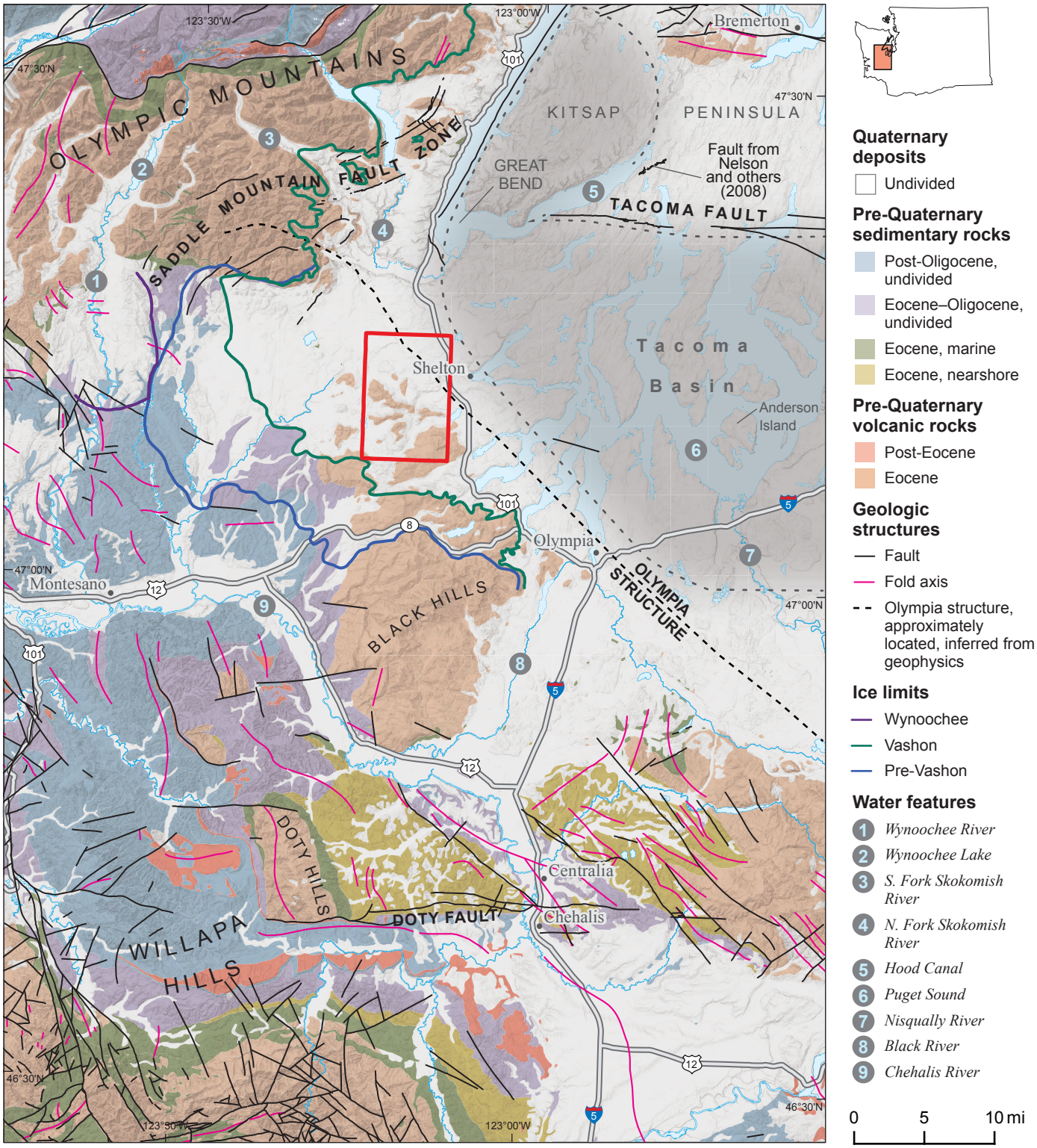

Figure 1. Regional geologic map for the Shelton Valley quadrangle (red outline). Saddle Mountain deformation zone is from Blakely and others (2009). The southern limits of glacial ice are shown with green (Vashon), blue (pre Vashon), and purple (Wynoochee alpine) lines and are modified from Carson (1970) and Logan (1987, 2003). Gray dashed line outlines the margin of the Tacoma basin. Geologic units, faults, and folds are from 1:250,000-scale mapping (Washington Division of Geology and Earth Resources, 2010a). Dashed black line is the Olympia structure, which is approximately located, inferred from geophysics, and modified from Daneš and others (1965), Blakely and others (2009), and Clement and others (2010).

southern Vancouver Island). North–south directed shortening of the forearc in western Washington is expressed as a series of generally east–west trending basins and uplifts (including the Black Hills uplift and Tacoma basin; Fig. 1) separated by reverse faults and folds within the Puget Lowland (Clowes and others, 1987; Johnson and others, 1996; Wang, 1996; Pratt and others, 1997). Northwest-striking structures throughout the Puget Lowland (Gower and others, 1985) may suggest a component of northeast-directed shortening. Steeply-dipping strike-slip faults throughout southwest Washington accommodate the clockwise rotation of discrete tectonic blocks within the forearc south of the Puget Lowland (Wells, 1982; Wells and Heller, 1988; Wells and others, 1998).

Margin-normal compression has contributed to the exhumation of the Olympic subduction complex (Brandon and others, 1998). Immediately west of the Puget Lowland, the Olympic Mountains (Fig.1) are an expression of the Olympic subduction complex. Northeast-trending zones of deformation bounding the Olympic Mountains on the east—and perhaps also farther east beneath the Puget Lowland—include active oblique-slip faults that may be kinematically linked to north–south compressional structures of the Puget Lowland (Blakely and others, 2009; Contreras and others, 2012a,b,c; Mace and Keranen, 2012; McCaffrey and others, 2013). However, Lewis and others (2003) refer to seismogenic strain geometries along the eastern margin of the Olympic Mountains to infer southeast-directed shortening there.

Erosion and deposition of voluminous sediment, mainly by repeated incursions of Cordilleran (continental) ice sheets throughout the Pleistocene, have yielded a stratigraphically complex cover of Quaternary sediment that obscures most structures within the Puget Lowland. The most recent incursion was by the Puget lobe of the Cordilleran ice sheet during marine oxygen-isotope stage 2 (MIS 2)(Morrison, 1991; Booth and others, 2004; Troost and Booth, 2008; Polenz and others, 2015).

Bedrock Units

Prior work within the Shelton Valley quadrangle has identified bedrock exposures as basalt of the Crescent Formation (Molenaar and Noble, 1970; and Logan, 1987, 2003; Walsh and others, 1987), or undivided bedrock (Jones, 1999). Previous radiometric dating of basalts of the Crescent Formation in the northern portion of the Black Hills provides an average age of about 53.1 Ma (Duncan, 1982; Globerman and others, 1982), and is consistent with biostratigraphy in sedimentary interbeds (Globerman and others, 1982; Logan and Walsh, 2004). Paleomagnetic data of Globerman and others (1982) suggest about 29° of clockwise rotation relative to cratonic North America across the Black Hills following extrusion, and Globerman (1981) documented that basalt in the Black Hills is variedly normally and reversely magnetized. Allison (1959), Cady and others (1972a,b), Tabor and Cady (1978a), Glassley (1974, 1976), and closer to the Shelton Valley quadrangle, Blakely and others (2009) divided the Crescent Formation into lower and upper members. Glassley (1974) suggested that the members are tectonically separated, whereas Hirsch and Babcock (2009) advocated a difference in metamorphic grade.

Basalt flows of the Crescent Formation are relatively flat-lying in the Shelton Valley quadrangle and mark the northern end of the Black Hills (Fig. 1). Quaternary sediments conceal all bedrock north of the Black Hills to the foothills of the Olympic Mountains (Fig. M1)(Carson, 1970; Molenaar and Noble, 1970; Tabor and Cady, 1978a,b; Logan, 1987, 2003; Walsh and others, 1987). Moderately southeast-dipping basalts of the Crescent Formation along the Olympic Mountains (Tabor and Cady, 1978a,b) have been interpreted by Brandon and Calderwood (1990) as part of an east-plunging anticline. The transition from the Black Hills uplift to the Tacoma basin northeast of the Black Hills crosses a northwest-trending geophysical lineament that runs through the map area (see *The Olympia structure* below). In the subsurface of the Tacoma basin, younger sedimentary rocks have been inferred to unconformably onlap against a gently northeast-dipping surface of Crescent Formation (Molenaar and Noble, 1970; Pratt and others, 1997; Clement and others, 2010).

The Olympia Structure

A northwest-trending gravity anomaly (Fig. M2; Daneš and others, 1965), an aeromagnetic anomaly approximately coincident with the gravity anomaly (Fig. M2), and 3.5–6 km (2–4 mi) of basalt surface relief between the Black Hills and the base of the Tacoma basin (Pratt and others, 1997; Clement and others, 2010) have inspired inferences of an ‘Olympia structure’ (Daneš and others, 1965; Gower and others, 1985; Brocher and others, 2001; Sherrod, 2001; Magsino and others, 2002, 2003; Van Wagoner and others, 2002; Johnson and others, 2004). The northwest-trending geophysical anomalies separate the relatively flat-lying basalts of the Black Hills from the gently northeast-dipping basalts farther northeast in the Tacoma basin (Figs. M1 and M2)(Pratt and others, 1997; Clement and others, 2010). The Olympia structure has been interpreted as a monocline (Daneš and others, 1965; Pratt and others, 1997; Gower and others, 1985) or a fault propagation fold above a northeast-verging blind thrust beneath the Black Hills (Pratt and others, 1997; Gower and others, 1985; Sherrod, 2001; Clement and others 2010; Jack Odum, USGS, written commun., 2014, 2015, 2016).

Pratt and others (1997) have suggested that the Black Hills uplift is at least in part Eocene in age because Tertiary sedimentary bedrock onlaps onto Crescent basalt west and south of the Black Hills (Pease and Hoover, 1957; Snavely and others, 1958; Walsh and others, 1987). However, the orientation of the geophysical anomalies is also consistent with ongoing northeast-directed compression suggested by a local principal strain orientation that McCaffrey and others (2013) estimate at N66°E.

Late Pleistocene to Holocene deformation of Quaternary sediment along the broader trend of the Olympia structure outside our map area has been documented or inferred by several workers: (1) Clement and others (2010) call on marine seismic sections to infer a zone of northwest-trending strike-slip faults offsetting post-glacial sediment in Budd and Eld Inlets, on trend with surficial lineaments on Steamboat Island Peninsula (see *Geophysics of the Map Area*); (2) Odum and others (written commun., 2014, 2015, 2016) extend this zone of

strike-slip faults in the subsurface to the northwest with a land-based seismic survey across the Steamboat Island Peninsula; (3) slightly southwest of this faulted zone, Odum and others (written commun., 2014, 2015, 2016) also interpret a trough of thicker Tertiary and Quaternary strata bound to the south by a series of south-dipping reverse faults uplifting the Crescent Formation of the Black Hills; (4) subparallel to the Olympia structure, the northwest-striking Lucky Dog (thrust?) fault of Polenz and others (2010, 2011)(Figs. M1 and M2) is expressed as an asymmetric gently southeast-plunging uplift across the late Holocene Skokomish River valley; and (5) evidence for coseismic subsidence about 1,100 years ago in marine inlets that intersect the trend of the Olympia structure supports recent tectonic activity (Sherrod, 2001; Martens and others, 2010).

Quaternary Deposits

PRE-VASHON DEPOSITS

Northern-sourced drift (till and outwash) was deposited in the Puget Lowland due to southward incursions of the Cordilleran (continental) ice sheet during global ice ages. Such incursions are thought to have occurred during even-numbered marine oxygen-isotope stages (MIS)—for discussions of MIS and glaciations see Morrison (1991), Booth and others (2004), and Troost and Booth (2008). Drift of pre-Vashon age (MIS >3) was mapped at the southwest corner of the quadrangle (Carson, 1970) and along the southern flank of Isabella Valley (secs. 1, 2, 11, 12, T19N R4W)(Molenaar and Noble, 1970; Logan, 1987, 2003; Jones, 1999)—see *Treatment of Named Units: Salmon Springs Drift*.

Logan (1987, 2003) and Jones (1999) followed Molenaar and Noble (1970) in mapping the Kitsap Formation of Sceva (1957b) and Skokomish Gravel along Goldsborough canyon, and Skokomish Gravel on both sides of Shelton Valley. Molenaar and Noble also mapped Skokomish Gravel on the south side of Isabella Valley. (See *Treatment of Named Units*.)

VASHON DRIFT

Surficial sediment in the Shelton Valley quadrangle has been previously recognized as mostly Vashon Drift by Robert Carson (1970, 1980, written commun., 2009–2014), Molenaar and Noble (1970), Logan (1987, 2003), and Jones (1999). Vashon Drift in the Puget Lowland consists of till and outwash from an incursion of the Cordilleran (continental) ice sheet during MIS 2 (Armstrong and others, 1965; Easterbrook, 1968; Blunt and others, 1987). For detailed discussion on the timing of MIS 2 see Morrison (1991), Booth and others (2004), Troost and Booth (2008), and Polenz and others (2015). Vashon Drift represents the Vashon Stade of the late Wisconsinan Fraser glaciation of Armstrong and others (1965).

The dominant surficial features within the map area are landforms related to deposition of outwash and till during the Vashon Stade. Booth (1994) noted that deposition of proglacial advance outwash was followed by subglacial erosion and deposition of till. Subglacial landforms consist of linear ridges (fluted uplands) and intervening troughs. At the end of the glaciation, meltwater carved extensive outwash channels across the map area, and ice-dammed lakes filled topographic troughs throughout the Puget Lowland (Bretz, 1910, 1913; Thorson, 1981, 1989; Dethier and others, 1995; Booth and others, 2004). These lakes deposited deltaic and silty sediments. As the ice dams disintegrated, lake levels dropped in stages, leaving behind a series of progressively lower and younger deltas and shorelines at discrete elevations (Bretz, 1910, 1913; Haugerud, 2009; Ralph Haugerud, USGS, oral commun., 2013; Polenz and others, 2012c, 2013, 2015).

POST-GLACIAL DEPOSITS

Except for peat, post-glacial deposits in the map area are minor. Logan (1987, 2003), Jones (1999), and Molenaar and Noble (1970) mapped all post-glacial deposits as Holocene alluvium along parts of Goldsborough Creek, in Isabella and Shelton valleys, and in marshlands near the northeast corner of the Shelton Valley quadrangle.

Treatment of Named Units

We chose not to follow prior usage of some named units in the map area. Our reasons are stated for each unit below.

SALMON SPRINGS DRIFT

Crandell and others (1958) defined the Salmon Springs Drift as two undated pre-Vashon drifts separated by peat, silt, and volcanic ash. Easterbrook and others (1981) assigned the unit a middle Quaternary age, noting that between the drifts at the type section, silt is reversely magnetized and tephra yielded a 0.84 ±0.21 Ma fission track age. The unit was mapped in the Shelton Valley quadrangle by Carson (1970, 1980) and Molenaar and Noble (1970). In light of the specific age assignment we, like Logan (1987, 2003), do not use the unit for undated pre-Vashon drift.

SKOKOMISH GRAVEL

Molenaar and Noble (1970, p. 16) defined the Skokomish Gravel as "stream-laid detritus derived from the Olympic Mountains". In their type section along the south side of the lower Skokomish Valley, Molenaar and Noble (1970, p. 16) identified Vashon advance outwash immediately above Skokomish Gravel and described the latter as 65 m (213 ft) of "oxidized gravels and sands with interbeds of clay and silt" above 24 m (79 ft) of "chiefly buff-colored silt and clay, with two distinctive peat-bearing horizons" and the base of the unit unexposed below sea level. Molenaar and Noble (1970, p. 10, fig. 4, and p. 16) showed the lower, fine-grained part of the unit interfingering with Kitsap Formation and assigned both units to the Olympia 'Interglaciation'(MIS 3—quotes added because MIS 3 is part of the Wisconsinan glaciation of MIS 2–4, and thus not interglacial). We agree with Carson (1979, 1980) and Polenz and others (2010, 2011) that deposits in the Skokomish Gravel type section are not limited to MIS 3 age and include a mix of Olympic and northern sources; we similarly interpret deposits previously mapped as Skokomish Gravel in the Shelton Valley quadrangle as more diverse in age and character and therefore did not map the unit.

KITSAP FORMATION

Sceva (1957a,b) informally named pre-Vashon clay, peat, sand, gravel, and till exposed along Colvos Passage (sec. 21, T22N R2E) as the Kitsap clay member of the Orting gravel. Garling and Molenaar (1965) renamed the Kitsap clay member the Kitsap Formation and—despite the presence of (northern-sourced) till within the type section—defined it as nonglacial. We do not use the unit because we deem this definition inherently conflicted due to the implication that the unit includes both glacial and nonglacial deposits and spans more time than MIS 3.

OLYMPIA NONGLACIAL SEDIMENT (OLYMPIA BEDS)

Armstrong and others (1965, p. 24) defined the Olympia Interglaciation as the "climatic episode immediately preceding the last major glaciation, and represented by nonglacial strata lying beneath Vashon Drift". Hansen and Easterbrook (1974, p. 587) redesignated the period as the "Olympia nonglacial period" during which climate was cooler than the present. Prior mappers referred to time-stratigraphically equivalent units within the map area as the Kitsap Formation. We avoid use of the Kitsap Formation (see *Kitsap Formation* above), and instead apply the unit symbol Qco commonly used for 'Olympia nonglacial deposits' in the Puget Lowland. However, we avoid the label 'Olympia nonglacial deposits' in the map area because our unit Qco includes probable drift of Olympic Mountains provenance in addition to nongalcial sediment. In terms of global climate history (Morrison, 1991), the Olympia nonglacial period corresponds to MIS 3 (Booth and others, 2004; Troost and Booth, 2008). We thus refer to unit Qco and coeval deposits by reference to MIS 3.

METHODS

Geologic Mapping

We identified units from field observations between July 1st and October 29th, 2015. We used thin section analyses, well and boring records, geotechnical reports, geophysical data, prior geologic mapping, geomorphic features identified from lidar, soil maps by the U.S. Department of Agriculture (USDA, 2013), and aerial orthophotos[1] to refine the mapping. We reviewed 1,170 water wells and geotechnical borings within ~1 mi of the Shelton Valley quadrangle; we could precisely locate only 479 and we added these to the DNR subsurface database (http://www.dnr.wa.gov/geologyportal). Locations of 57 wells are shown on the map; these are wells that we identified as best-located and most geologically informative inside the quadrangle. For these 57 wells we transcribed driller's log information and assigned depth intervals to apparent lithology and likely geologic unit in the DNR subsurface database. We used a lidar-based elevation data set with 2-m-grid resolution (http://pugetsoundlidar.ess.washington.edu/) to derive hillshade images, contours, and other products. We adapted methods outlined by Singhroy and others (1992a,b) for LANDSAT satellite image analysis, calibrated by our field observations, to identify surface sediment particle sizes and bedrock character in order to refine our unit boundaries. Edge mismatches with adjacent quadrangles are intentional and based on differences in unit classifications or interpretation.

We used USGS Fact Sheet 2010-3059 for the geologic time scale (USGS Geologic Names Committee, 2010) and the Udden-Wentworth scale (table 5 in Pettijohn, 1957) to classify unconsolidated sediment.

Bedrock Geochronology and Paleontology

Two new $^{40}Ar/^{39}Ar$ dates on basalt (age sites GD9 and GD10), and biostratigraphic (paleontology) analyses from seven sedimentary bedrock sites (age sites GD11–17) are summarized in Table 1; detailed $^{40}Ar/^{39}Ar$ analysis results and analytical details are presented in Appendix A and the Data Supplement; details about biostratigraphy samples are provided in Table 1. Geochronology was performed by Daniel Miggins and staff of the Argon Geochronology Lab at Oregon State University. Biostratigraphy samples were prepared by Ellington and Associates, Inc., for microfossil analysis, and fossil content was analyzed by E. Nesbitt (Burke Museum at the University of Washington). U-Pb analysis on tephra from a sedimentary interbed between basalt flows is in progress (Eddy, written commun., 2016). This sample is collocated with fossil sample site GD14 (Table 1).

Geochemistry of Volcanic Bedrock Samples

Major-oxide and trace-element geochemistry for 16 new basalt samples from the Shelton Valley quadrangle were performed to better define the Crescent Formation in the quadrangle. These analyses are presented in the Data Supplement and figures derived from these data are presented in the Geochemistry section of this pamphlet. The samples were analyzed by ALS Geochemistry, North Vancouver, B.C., Canada. We use geochemistry plots to compare our samples to selected compilations of other volcanic rocks from western Washington (Globerman, 1981; Bowman and others, 2014; Babcock and others, 1992; Philips and others, 1989). Sources and sample groupings are further discussed in Geochemistry.

Sedimentary Provenance

We used clast counts, petrographic review of matrix content, sedimentary attributes (such as bedding style, grain size, and textural changes), and field relations to infer provenance of Quaternary units (Fig. 2) and help determine their depositional setting (glacial, nonglacial, or undivided). We illustrate the strength of these inferences with principal component analysis (PCA) of our clast counts (Fig. 3), including clast counts from active channels of Olympic Mountains drainages north and northwest of the map area. PCA analysis transforms a multivariate dataset into a series of 'principal components' that

[1] Photo series, in order of frequency of use: 2013 3-ft color (National Agriculture Imagery Program 4-band, includes infrared); 2005 18-in. color; 1990–2000 3-ft black and white; 2011 3-ft color (National Agriculture Imagery Program); 2006 18-in. color (National Agriculture Imagery Program).

identify the variance within the dataset. This transformation is performed in such a way that the first principal component explains the greatest amount of variance in the data, the second component explains the next greatest amount of variance, and so forth. Each of the original variables—in this case, the different groups of clast lithology—is then 'loaded' onto the principal component axes. When shown on a two-dimensional PCA plot, these 'loadings' show how the variables are related in the transformed coordinate system. The plot also can define groups of data that might be difficult to identify without the analysis. The clast counts are tabulated in the Data Supplement; pie charts and PCA plots further illustrate these lithologic trends (*Quaternary Unconsolidated Deposits in Description of Map Units*). Weathering trends in Quaternary sediments are discussed in *Ages of Units* and *Weathering of Vashon and Pre-Vashon Deposits*.

Quaternary Geochronology, Paleomagnetics, and Pollen Analyses

Analytical results and locations for five new radiocarbon, two new luminescence, and four new paleomagnetic analyses of Quaternary sediment are summarized in Table 1; detailed results for radiocarbon and luminescence data are presented in Appendix A. Insights into climate conditions prior to the Vashon Stade are provided by pollen analyses for six sediment samples (L1 to L6) from four sites analyzed by Erin Herring (University of Oregon) and interpreted by Dan Gavin (University of Oregon, written commun., 2016). Radiocarbon samples were analyzed by Beta Analytic, Inc. Luminescence samples were prepared and analyzed by Shannon Mahan and Harrison Gray (USGS). Paleomagnetic data were processed by Masoud Mirzaei Souzani and Bernard Housen (Western Washington University).

Detailed Stratigraphic Analyses

Two columnar sections (CS1 and CS2), two schematic site illustrations (Figs. 4 and 8—locations on map shown as D1 and D2) and four photos (Figs. 5, 6, 12, and 14—locations on map shown as P1, P2, P3, and P4) present stratigraphic details for selected locations. A detailed site illustration that includes photographs of site D1 (Fig. 4) is included in the download package as Schematic Diagram D1. To limit map crowding, site data in Columnar Section 2 (age site GD7, paleomagnetic sites M3 and M4, and clast count sample sites C26, C31, C30, and C34) are not shown separately on the map.

Geophysical Data and Analyses

To help constrain the depth to—and thickness of—sedimentary and basalt bedrock beneath Cross Section A we reviewed seismic sections and analyses (Pratt and others, 1997; Odum, written commun., 2014, 2015, 2016), gravity and aeromagnetic data (including data from Richard Blakely, USGS, written commun., 2016), modeling from the southwest margin of the Tacoma basin (Pratt and others, 1997; Odum, written commun., 2014, 2015, 2016; Sammantha Magsino, National Academy of Sciences written commun., 2016), and used Geosoft Oasis-Montaj 4.5 – 2D GM-SYS® software to model gravity and magnetic anomalies. In the modeling, a high-pass filter was applied to target the uppermost 5 km (3.1 mi) of the crust and remove regional gravity anomalies. We used a range of geophysical methods to develop site-specific bedrock depth estimates at eight sites. These methods include:

- Single station, passive seismic, Horizontal-to-Vertical Spectral Ratio analysis (HVSR), using a Tromino ZERO® three-component seismograph (operating range 0.1–64 Hz; http://tromino.eu/prodsel.asp?cat=1&prod=1).
- Multi-sensor single-channel (4.5 Hz) passive seismic survey, using Microtremor Array Measurements (MAM).
- Multichannel Analysis of Surface Waves (MASW) active seismic survey using 4.5 Hz geophones and a 16 lb sledge hammer.
- Ground-Penetrating Radar (GPR) survey to image sediment above a known shallow-basalt surface.
- We used the MAM, MASW, and GPR analyses to calibrate our analysis of HVSR data.

Seven geophysical data collection localities are shown on the map (Table 2); an eighth site (HVSR, GPR, MAM, and MASW) was used to inform Cross Section A but is not shown on the map because it is located at Shelton High School 0.3 mi east of the map area (sec. 12, T20N R4W).

SEDIMENT COMPOSITION AND PROVENANCE

We identified five groupings of sediment provenance in our data (Fig. 2). To decipher provenance, we rely on sand-grain mineralogy (estimated in hand samples and verified and further analyzed by thin-section petrography) and pebble clast counts (Data Supplement). Most surficial sediment in the map area is part of the Vashon Drift (lodgment till, ablation till, and outwash). We refer to this and other sediment that we think was transported into the map area by ice or meltwater from prior incursions of the Cordilleran continental ice sheet into the Puget Lowland as having a 'northern source'.

Alpine ice advances and nonglacial stream transport from the Olympic Mountains also introduced sediment into the map area and are referred to as having an 'Olympic Mountains source'. We refer to a sediment sources of "Black Hills" where we interpreted the sediment as being derived from bedrock exposed in the Black Hills. To characterize Olympic Mountains sources, we sampled five modern stream channels that drain the Olympic Mountains outside the map area. Of these, three drain 'peripheral' rocks and two drain 'peripheral and core' rocks (Fig. 2). We follow Tabor and Cady (1978a,b) in referring to rocks from the Olympic Mountains as 'peripheral' (in the southeastern Olympic Mountains broadly equivalent to Crescent Formation, with minor inclusion of younger sedimentary rocks) and 'core' rocks (in the southeastern Olympic Mountains consisting of sedimentary rock and lesser volumes of basaltic volcanic rocks). Some Olympic Mountains rocks, especially core rocks, are metamorphosed at low temperature and high pressure, up to prehnite-pumpellyite grade (Tabor and Cady, 1978a,b).

Table 1. Summary of new ages, paleomagnetic data, and biostratigraphic analyses from the Shelton Valley quadrangle. Dark gray shading indicates sample in Columnar Section 1; light gray shading indicates sample in Columnar Section 2. See Appendix A for detailed analytical results, sample descriptions, and data compiled from previous studies. Biostratigraphy samples GD11 to GD17 did not yield age-diagnostic constraints and are therefore omitted from Appendix A. Finite radiocarbon dates are given as a calibrated 2σ range (calendar years) to facilitate equivalence to luminescence data and age statements reported elsewhere; infinite radiocarbon dates are given as conventional age (>^{14}C yr BP, in radiocarbon years) and include a 2σ variance against background radiation; luminescence ages are shown with 1σ uncertainty, argon ages with 2σ.

Sample	Unit symbol	Location	Method	Result
GD1	Qpu$_{op}$	sec. 27, T20N R4W	^{14}C	17.690–17.475 ka
GD2	Qc$_{o}$	sec. 14, T20N R4W	^{14}C (AMS)	27.480–27.235 ka
GD3	Qpo	sec. 29, T20N R4W	^{14}C	>43,500 ^{14}C yr BP
GD4	Qc$_{o}$	sec. 15, T20N R4W	^{14}C (AMS)	> 43,500 ^{14}C yr BP
GD5	Qpu$_{op}$	sec. 24, T20N R4W	^{14}C (AMS)	> 49,510 ^{14}C yr BP
GD7	Qc$_{o}$	sec. 15, T20N R4W	IRSL	47.31 ±4.9 ka
GD8	Qc$_{o}$	sec. 16, T19N R4W	IRSL	43.69 ±3.7 ka
GD9	Ev$_{c}$	sec. 24, T20N R5W	^{40}Ar/^{39}Ar age plateau	50.51 ±0.21 Ma
GD10	Ev$_{c}$	sec. 32, T20N R4W	^{40}Ar/^{39}Ar age plateau	50.14 ±0.17 Ma
GD11	Ev$_{c}$	sec. 13, T19N R4W	Fossil content analysis yielded no biostratigraphic constraint	
GD12	Ev$_{c}$	sec. 14, T19N R4W	Fossil content analysis yielded no biostratigraphic constraint	
GD13	Ev$_{c}$	sec. 13, T19N R4W	Fossil content analysis yielded no biostratigraphic constraint—a few diatoms and six recrystallized foraminifera could not be identified to species level	
GD14	Ev$_{c}$	sec. 14, T19N R4W	Fossil content analysis yielded no biostratigraphic constraint— apparent micro- and macrofossils were unidentifiable	
GD15	Ev$_{c}$	sec. 11, T19N R4W	Fossil content analysis yielded no biostratigraphic constraint—contained fossil wood with haloes of quartz	
GD16	Ev$_{c}$	sec. 8, T19N R4W	Fossil content analysis yielded no biostratigraphic constraint—burrows with quartz eluded identification; cylindrical calcite identified in the field as unspecified macrofossils eluded sampling	
GD17	Ev$_{c}$	sec. 4, T19N R04W	Fossil content analysis yielded no biostratigraphic constraint. Calcite cement prevented extraction and identification of foraminifera that were clearly observed in thin section; a tubular, possible trace? fossil eluded sampling	
M1	Qc$_{o}$	sec. 15, T20N R4W	paleomagnetic	normal
M2	Qpu$_{op}$	sec. 24, T20N R4W	paleomagnetic	normal
M3	Qga	sec. 15, T20N R4W	paleomagnetic	normal
M4	Qc$_{o}$	sec. 15, T20N R4W	paleomagnetic	normal

Table 2. Geophysical data collection localities, methods used, and depth to bedrock estimates.

Site	Depth to bedrock (ft)	Type of bedrock	Methods	Location
GP1	272	basalt	HVSR (two measurements)	sec. 22, T20N R4W
GP2	269	basalt	HVSR (one measurement)	sec. 18, T20N R4W
GP3	>476	basalt	HVSR (four measurements) GPR (two lines) MAM (one line) MASW (one line)	sec. 19, T20N R4W
GP4	299	basalt	HVSR (one measurement) GPR (one line) MAM (one line) MASW (one line)	sec. 17, T19N R4W
GP5	476	basalt	HVSR (two measurements) GPR (one line) MAM (one line) MASW (one line)	sec. 34, T20N R4W
GP6	197	basalt	HVSR (two measurements) GPR (three lines)	sec. 3, T19N R4W
GP7	>148	basalt	HVSR (one measurement)	sec. 12, T19N R5W
Shelton High School	614 909	sediment basalt	HVSR (two measurements) GPR (one line) MAM (one line) MASW (one line)	sec. 12, T20N R4W

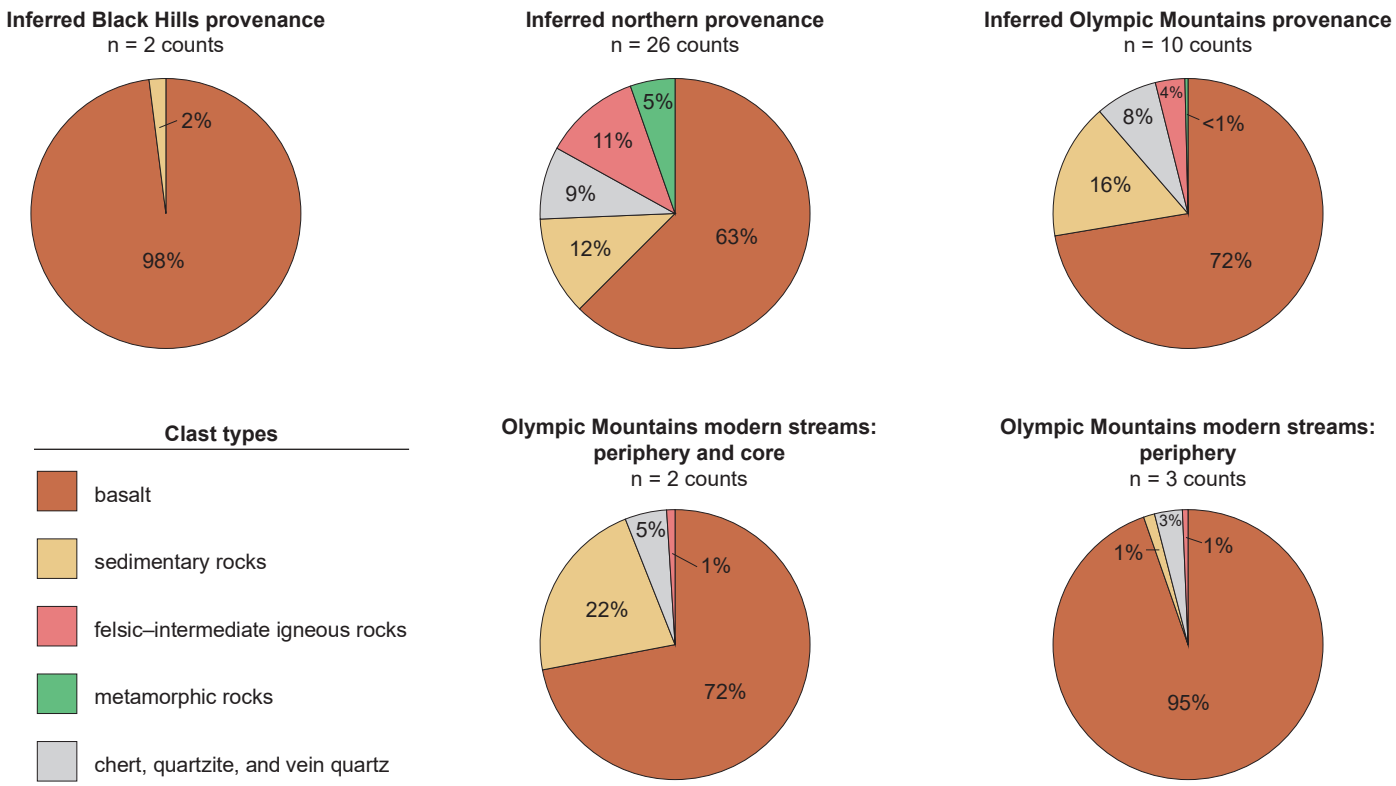

Figure 2. Pie charts of provenance types from 43 clast count samples show an overwhelming amount of basalt. The high percentage of basalt was one of the reasons we undertook a principal component analysis of these data. Percentages are rounded to nearest whole number. n=number of samples for each plot.

Although sedimentary provenance is central to our recognition of geologic context and origin of Quaternary deposits, map units tend to mix these groupings. For instance, modern alluvium in the map area (units Qa, Qaf) is mostly deposited by small streams and sourced from nearby older sediments; sand mineralogy and pebble content are variously of northern, Olympic Mountains, Black Hills, or mixed character.

Principal component analysis of our clast counts (Fig. 3), weathering trends (see *Weathering Vashon and Pre-Vashon Deposits* below), and consideration of clast counts from active channels of Olympic Mountains drainages north and northwest of the map area gave us added confidence in our inferences of provenance.

DESCRIPTION OF MAP UNITS

Quaternary Unconsolidated Deposits

POST-GLACIAL DEPOSITS

Post-glacial sediment locally covers drainages and fills closed depressions. It is in most instances readily separated from older sediment because it lacks the compaction that typically resulted from overriding glacial ice. However, the record of glacial overriding is difficult to recognize in some well-sorted Vashon or older sediment with well-rounded particles because such deposits can be largely incompressible.

We separate post-glacial deposits into Holocene units and Pleistocene to Holocene units because the onset of the Holocene at 11.7 ka (USGS Geologic Names Committee, 2010) does not coincide with the end of the Fraser Glaciation, which we estimate occurred in the map area between 15.8 and 15.3 ka (see *Post-Glacial Conditions*).

Holocene Nonglacial Deposits

af **Artificial fill**—Major road fill along US 101, historically placed to elevate the land; may locally be engineered, as in sec. 12 (T20N R4W)(Rodney Finkle, Washington State Department of Transportation, written commun. to A. H. Walley, 1992). Maximum unit thickness is 60 ft (south of Goldsborough Creek). The unit excludes areas where we chose instead to illustrate the underlying geology and fill areas that appear less voluminous than the polygons shown.

ml **Modified land**—Cobbles, pebbles, sand, silt, boulders, clay, diamicton, and organic matter; locally derived but redistributed to modify topography; underlying units exposed in some areas; we show unit ml where fairly extensive and thick enough (>5 ft) to be geotechnically significant; we exclude roads and pits where underlying units can be readily identified, fill areas appear minor, or excavation exposes the same unit as the surrounding surface, or where underlying units were deemed more significant than surface modification; these exclusions limit the unit to two mining areas—one near the southwest map corner, where excavation exposed underlying Vashon advance outwash, and one at the east end of Goldsborough canyon, where mining continued to modify the land during our field work, and historic

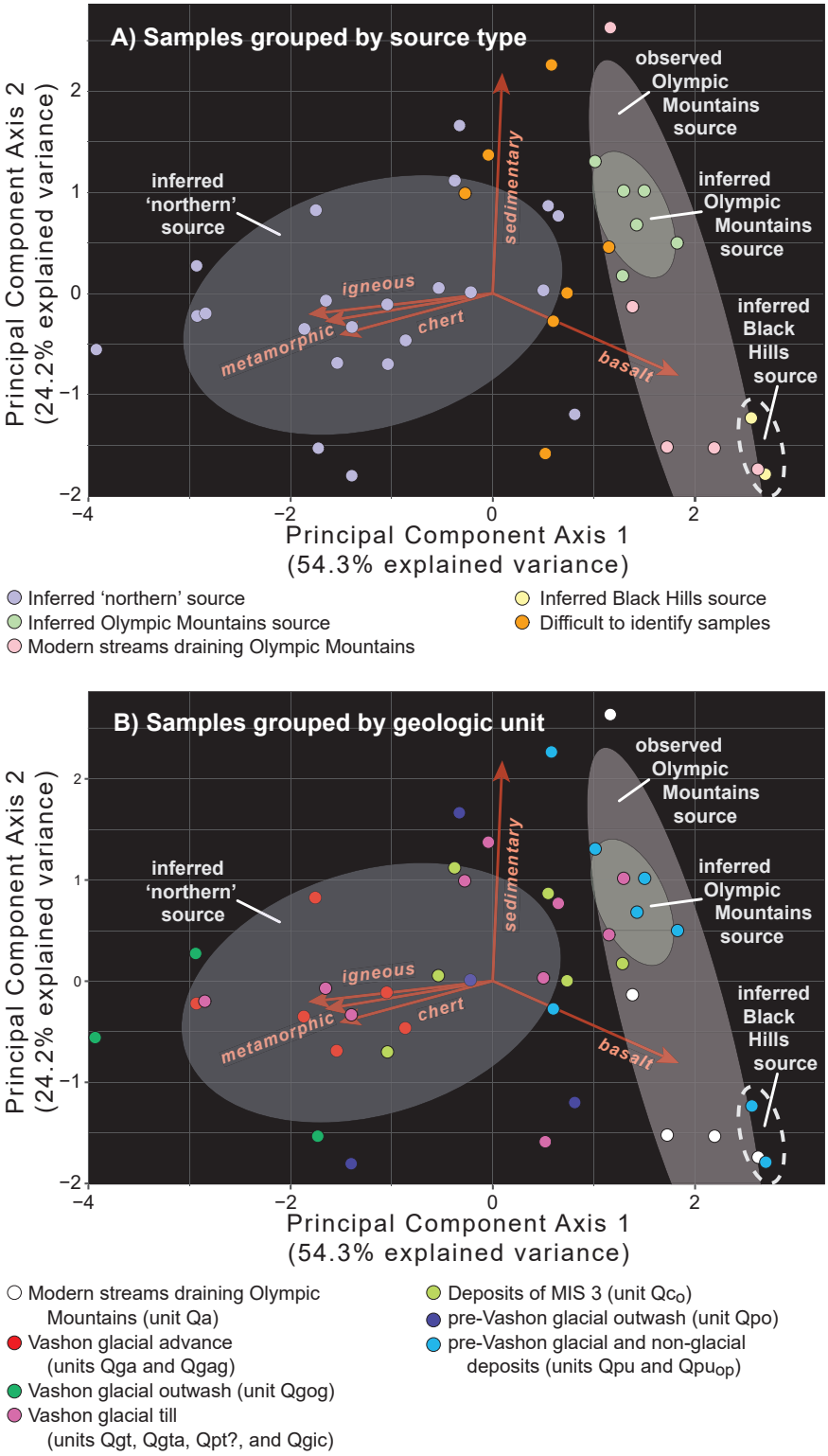

Figure 3. Principal component analyses (PCA) of provenance. We used the results from 43 clast counts to demonstrate that field assessment of provenance based on lithologic differences among clast lithologies in the Shelton Valley quadrangle is generally valid for units that did not intermix with existing deposits (such as till at the base of a glacier or fluvial systems during MIS 3). Red arrows indicate 'loadings' of the principal components into the x-y axes of the plot; line length indicates the relative 'strength' of the component in discriminating the data. Provenance regions on the PCA plot were defined by the 1σ (68.3%) confidence region for clast count samples with an unambiguous provenance. Fields for the inferred Black Hills and observed Olympic Mountains sources had too few data points to define probability fields; those fields are shown schematically. A) Samples grouped by their inferred provenance. Data are tightly grouped within the inferred Olympic Mountains source (n=6) but more scattered in the inferred northern source (n=22). Seven of 37 samples proved difficult to assign to a particular provenance and were not used to define provenance regions; they largely fall near the edges of the regions. B) Samples grouped by their geologic unit; provenance regions are the same as in part A. Note that glacial advance and outwash units are the 'most northern' whereas glacial till, deposits of MIS 3, and pre-Vashon outwash are the most varied.

removal of a dam involved major earth movement and river channel engineering (Garrison, 2007).

Latest Pleistocene to Holocene Nonglacial Deposits

Qp **Peat**—Organic and organic-rich sediment; includes peat, gyttja, muck, silt, and clay; typically in closed depressions; unit thickness in most instances unassessed—we suspect several tens of feet in Isabella and Shelton valleys, in the broad valley of Goldsborough Creek east of Little Egypt Valley, and perhaps also in Little Egypt Valley; mapped in wetland areas and distinctly flat-bottomed depressions; also mapped based on prior work (Rigg, 1958; U.S. Department of Agriculture, Natural Resource Conservation Service, Soil Survey Staff, 2013 to 2014), spectral analysis of LANDSAT data, and (or) where infrared and color aerial photos suggest its presence.

Qls **Landslide deposits**—Cobbles, pebbles, sand, silt, clay, boulders, diamicton, siltstone, and sandstone in varied amounts within areas of mass-wasting; clasts angular to rounded; unsorted; generally loose, jumbled, and unstratified, but locally retaining primary bedding and compaction. Unit thickness varies throughout the map area with an inferred minimum thickness of about 10 ft along a stream channel (sec. 13, T19N R4W). Absence of a mapped slide does not imply absence of sliding or hazard. Many slide areas are unmapped where too small to show at map scale, or because steep slopes, lakes, or streams have dispersed their deposits. Mass-wasting features that are not confidently recognized as landslides are shown as unit Qmw. Some slide areas include exposures of underlying units.

Qmw **Mass-wasting deposits**—Cobbles, pebbles, sand, silt, clay, boulders, or diamicton, in varied amounts; typically loose; generally unsorted; locally stratified; mapped mostly along colluvium-covered or densely vegetated slopes that are potentially or demonstrably unstable; locally includes alluvial fans, debris fans, landslides too small to show separately or those that could not be confidently mapped, and denuded slopes that may expose undisturbed substrate. Unit thickness varies throughout the map area with an inferred maximum thickness of about 10 ft along an incision of the modern drainage (sec. 14, T19N R4W). Absence of a mapped mass-wasting deposit does not imply absence of slope instability or hazard.

Qa **Alluvium**—Sand, pebbles, silt, clay, peat, and cobbles along active or abandoned stream channels and on flood plains; clasts and matrix generally gray and fresh, but in some exposures stained brown by organic matter or weathered to orange brown and iron-stained red; loose; clasts typically well rounded and moderately to well sorted; stratified to massively bedded; derived from local sources and deposited in streams and on flood plains. Maximum unit thickness of 21 ft suggested from well report of borehole W22 (sec. 20, T20N R4W). Unit Qa was mapped where post-glacial deposition is ongoing or inferred, but it resembles and likely includes some relict alluvium (mapped as unit Qgo where inferred to be of Vashon age).

Qaf, Qoaf **Alluvial fan deposits**—Pebbles, sand, silt, cobbles, and boulders, in varied amounts; gray to brown; loose; moderately to poorly sorted; stratified to poorly stratified; derived from local sources and deposited in concentric lobes where streams emerge from confining valleys; morphology in most cases suggests 10 to 40 ft thickness. Deposition at the base of hillslopes commonly sudden, hazardous, and associated with significant storm events. Unit Qoaf is relict and mapped where alluvial fans are sourced from valleys that lack active channels, or streams are too incised to add sediment to the fan surface. In many deposits of units Qaf or Qoaf, much or most of the fan volume likely is of (late) Vashon age (see *Glacial Recession*).

PLEISTOCENE GLACIAL AND NONGLACIAL DEPOSITS

Vashon Drift of the Fraser Glaciation

Deposits of the Fraser Glaciation in the map area are limited to deposits of the Vashon Stade because the map area is located at the southwest margin of the Fraser-age advance of the Cordilleran ice sheet into the Puget Lowland—farther south than the geographic extent of earlier and later stades. We found no evidence for a Vashon-age Olympic ice advance into the map area and assigned sediments from earlier Olympic ice advance(s) to MIS 3 or earlier periods.

Qgo **Vashon recessional outwash**—Cobble and pebble gravel, sand, and occasional silt and clay; mostly quartzo-feldspathic, with high-grade metamorphic, metasedimentary, plutonic, and basalt clasts of uncertain provenance locally supplemented by additional basalt clasts from Crescent Formation within or near the map area; mostly brown-gray where fresh, brown, red, and yellow where iron-stained from weathering; mostly moderately sorted and bedded; sand and clasts are typically northern-sourced. Field observations suggest a minimum thickness of 8 ft along the southern margin of Shelton Valley (sec. 35, T20N R4W). Well records for borehole W47 suggest a thickness of 60 ft (sec. 3, T19N R4W). Unit Qgo forms gently sloping to flat terraces. Some of the unit was apparently deposited as kames on the south side of Shelton Valley and both sides of Isabella Valley. Elsewhere in the same valleys the unit was deposited into ice dammed lakes and in small fluvio-deltaic complexes that locally extend just upslope of former lake shores (see also *Glacial Lakes and Shorelines*). Elsewhere in the map area the unit mostly forms broad fluvial valley floor surfaces. Unit Qgo is distinguished from similar but more recent alluvium (units Qa, Qoa) by better sorting of most exposures (especially of subunits Qgog, Qgos, and Qgof) and field relations that imply deposition late during the Vashon Stade. Unit Qgo was deposited by glacial meltwater, usually with a high rate of sedimentation. Undivided unit Qgo was mapped where the deposits are texturally varied or where exposures were insufficient to identify a dominant grain size; we suspect that it is mostly cobble gravel in Goldsborough canyon. Subdivided into:

Qgog **Vashon recessional outwash, gravel**—Cobble and pebble gravel, in most exposures with coarse-sand matrix; brown and (or) gray where fresh, commonly weathered to orange-brown or red; loose; clasts subrounded to rounded and well sorted; clasts and sand mostly northern-sourced. Many exposures of the unit are cross-bedded or contain cut-and-fill structures. The unit was

deposited mostly in broad outwash channels. Unit thickness proved difficult to constrain within the quadrangle, but exposures of the unit farther northeast in the Skokomish Valley and Union quadrangles mostly reveal 10 to 50 ft of section, and geomorphic relations there suggest thickness may locally exceed 100 ft (Polenz and others, 2011). Unit Qgog is mostly pebbly south of Lost Lake along the western map edge, and in a small (hanging) valley southeast of Shelton Valley (sec. 36, T20N R4W). The unit is mostly cobbly and locally concealed beneath alluvial fans (unit Qaf) or peat (unit Qp) in extensive outwash flats in the northern third of the Shelton Valley quadrangle.

Qgos **Vashon recessional outwash, sand**—Sand and some beds and lenses of pebbles, silt, and clay; gray to pale brown; clasts moderately to well rounded; moderately to well sorted and stratified; loose and generally less compact than outwash sand that has been overridden by glaciers (mainly units Qgas and Qpo); bedding planar to gently cross-bedded; sand and clasts typically northern-sourced. Most exposures and well records suggest about 10 ft unit thickness; maximum observed thickness is 20 ft west of Gosnell Creek, where the unit drapes a slope from about 200 to 450 ft elevation (see *Glacial Lakes and Shorelines*). Unit Qgos was mostly deposited in lakes but may include some overland sheet flow deposits.

Qgof **Vashon recessional outwash, fine-grained**—Vashon recessional outwash, fine-grained—Silt, clay, and mixtures of both, in some exposures ranges to fine sand and (or) contains dropstones, usually of northern provenance; pale gray to light-green gray; loose and soft; planar bedded or massive. Maximum thickness of about 163 ft suggested from borehole W36 in Shelton Valley (sec. 27, T20N R4W). Unit Qgof resembles unit Qpf but is loose and tends to be paler in color.

Qgod **Vashon recessional glacial delta deposits**—Vashon recessional glacial delta deposits—pebble gravel, sand, and silt; gray to pale brown; soft and loose to slightly stiff and cohesive; moderately sorted; contains pebbly to sandy topsets and foresets with sandy to silty bottomsets of relict glacial lake deltas. We observed 10 to 15 ft of topset beds above at least 60 ft of foreset beds in a gravel pit at the west end of the Shelton delta (Fig. M1)(secs. 13, 14, 24, T20N R4W—units Qgod and ml)(Bretz, 1910, 1913; Thorson, 1981; Polenz and others, 2011). The upper 40-ft section of a delta at the north side of Isabella Valley (sec. 1, T19N R4W) is partly kettled and reveals southeast-directed paleocurrents. Sand and clasts in unit Qgod are mostly northern-sourced. A unit thickness of at least 110 ft is inferred from surface morphology in the delta at the north side of Isabella Valley. The gravel pit at the west end of the Shelton delta exposed at least 75 ft of section within the unit. Relief within a gravel mine in the same area suggests that unit thickness may exceed 140 ft. The ice-dammed lakes documented by these deltas are further discussed below in *Glacial Lakes and Shorelines*.

Qgic **Vashon ice-contact deposits**—Diamicton (melt-out till, flow till, poorly compacted or isolated exposures of lodgment till, and "sub-glacially reworked till" as described by Laprade, 2003), pebble and cobble gravel, sand, lacustrine mud, and isolated boulders; pale- to ash-gray, tan, or brown; commonly slightly weathered; loose to compact; poorly to well sorted; massive to well stratified; sand and clasts typically northern-sourced. Exposures along the southern margin of Isabella Valley are about 30 ft thick (sec. 1, T19N R4W); borehole W31 (sec. 25, T20N R4W) suggests a maximum thickness of 65 ft. Unit Qgic was deposited by ice and meltwater, mostly beneath, within, or on ice late in the Vashon Stade. The unit commonly coincides with landforms associated with stagnant ice near the end of glaciation, such as kettles, hummocky topography, topographic ripples and disrupted surfaces on or between flutes, eskers, and subglacial or subaerial outwash channels. Where such landforms are present, lodgment till is commonly absent or only a few feet thick. Unit Qgic also includes apparent kame deposits, such as on the south side of Isabella Valley between geochemical sites G8 and G13, and glaciolacustrine drift, such as at photo site P1 (see additional discussion of site below). Unit Qgic locally contains over-steepened beds and isoclinal folds that developed due to sub-ice flow dynamics, and collapse features that formed due to ice shove or melting of nearby ice. Compared to unit Qgt, till facies in unit Qgic tend to be less compact and, in most exposures, more porous and more friable. Because of this porosity, much of the unit does not form an aquitard or may form a more 'leaky' aquitard than unit Qgt (Polenz and others, 2010). Compared to unit Qgt, till matrix in unit Qgic commonly contains less mud, and deposits tend to be slightly more weathered (or at least surficially iron-stained). For additional discussion of leaky aquitards and landforms and deposits associated with stagnant Vashon ice east and north of the map area, see Haugerud (2009), Polenz and others (2009a,b,

2010, 2011), and Contreras and others (2012a,b,c). Locally subdivided into:

Qgim **Vashon end moraines**—Similar to unit Qgic but specifically interpreted as moraine; previously mapped by Carson (1970). The unit is mostly ablation till at and within 0.6 mi of the southwest map corner where it marks the maximum extent of Cordilleran ice of the Vashon Stade (see *Paleoenvironmental Data and Interpretation*). Farther north along the western map edge, unit Qgim is about 4 mi northeast of the Vashon ice limit (as mapped by Carson, 1970, and Logan, 1987, 2003). We recognize the irregular landforms and varied deposits (eskers, kettles, sub-ice channels, and patchy exposures of till and pebble gravel that each range from loose to compact) as indicative of 'dead' (stagnant) ice because ice movement would have obliterated them, but we do not know if this 'moraine' marks an ice margin.

Qgta **Vashon ablation till**—Unsorted, unstratified, and heterogeneous melt-out deposit of diamicton, sand, silt, clay, and gravel; gray to tan and reddish brown; mostly loose but ranges to compact; sand and clasts typically northern-sourced; appears to form an extensive, more than 5-ft-thick surficial deposit where the unit is mapped but also is nearly ubiquitous elsewhere as 1- to 5-ft-thick surficial veneer atop Vashon-age or older deposits; that veneer locally thickens to 10 ft. Unit Qgta commonly serves as the primary soil parent material because it is looser, more susceptible to weathering, more permeable, and less root-restrictive than the underlying substrate.

Qge **Vashon eskers**—Pebble gravel and sand; gray; loose; clasts moderately to well rounded; moderately to well sorted; hints of bedding observed in one exposure; sand and clasts typically northern-sourced; forms low, elongate, sinuous hills, between 15 and 50 ft high. Preservation of the unit indicates formation beneath stagnant ice because moving ice would have obliterated the distinctive sinuous hills that permit confident mapping of the unit even where subsurface exposures are lacking (as they mostly were in the map area). We mapped unit Qge in fluted uplands near the northeast map corner (secs. 9–11, 15, and 16, T20 R4W) and in a moraine identified by Carson (1970) and Jones (1999) along the western map edge (sec. 36, T20N R5W).

Qgt **Vashon lodgment till**—Matrix-supported diamicton consisting of silt and sand matrix with clay, pebbles, and cobbles, in varied amounts with isolated boulders; sand and clasts are northern-sourced; gray to brown or tan; usually lightly weathered or unweathered except in the basal 2–5 ft, which are commonly more weathered; compact and resembles concrete where well-developed. A surficial veneer of 1–10 ft of loose diamicton (ablation till) usually covers more-dense lodgment till; the upper fringe of lodgment till is commonly hackly or looser than till observed deeper in the subsurface. Unit Qgt is less porous and more dense (better developed as lodgment till) than unit Qgic in most exposures. Some clasts are striated and faceted with subangular or rounded edges. Some exposures include locally sheared and jointed lenses or layers of sand, pebbles, and cobbles. The unit is unsorted and unstratified (but locally banded) and forms a patchy cover, with typical exposures 2–10 ft thick. Except for the surficial veneer of late-glacial melt-out till, unit Qgt was deposited directly by ice at the base of the advancing Cordilleran ice sheet. Unit Qgt caps many fluted surfaces. Lodgment till locally forms an effective aquitard, but its discontinuous distribution, varied thickness, and stratigraphic relationships (in some instances gradational) with more permeable ice-contact deposits and outwash channels suggest that the aquitard is leaky at map scale. We mapped unit Qgt where we observed more cohesive (usually less sorted and less fractured), less porous, and more compact lodgment till development—and typically better development of fluting—than where we mapped unit Qgic. Unit Qgt is typically in sharp, unconformable contact with underlying units. Unit Qgt lies stratigraphically below units Qgta and Qgo and above unit Qga. We included some relatively weathered till exposures, usually within 2–5 ft of the base of the till, with Vashon till (units Qgt or Qgic) because we concluded that much of the weathering was likely inherited when Vashon ice entrained and incorporated pre-Vashon sediment or bedrock (see *Weathering of Deposits of pre-Vashon, Northern-Sourced Glaciations*). The unit may also include some pre-Vashon northern-sourced till because we generally mapped surficial northern-sourced drift as Vashon-age when we were unsure of its age. This is because surficial sediment is more likely to be from the most recent glaciation.

Qga **Vashon advance outwash, undivided**—Sand, pebble gravel, cobble gravel, silt, and clay, in varied amounts, commonly forming a coarsening-upward section; gray to tan; generally compact (see fig. 4 of Polenz and others, 2009b), but commonly cohesionless; clasts typically well rounded and well sorted; mud content is low in sandy or pebbly facies, except in ice-proximal deposits; very thinly to very thickly bedded, with planar beds forming the dominant facies in widespread lacustrine deposits; also includes graded beds,

cut-and-fill structures, trough-and-ripple crossbeds, and foresets, but ranges to structureless; sand and clasts typically northern-sourced. Field exposures provide a continuous 45-ft-thick section of unit Qga at the box canyon hollow north of age site GD1. Borehole W31 (sec. 25, T20N R4W) suggests a thickness of 263 ft along the southern margin of Shelton Valley. Unit Qga was deposited as proglacial, fluvial, deltaic, and lacustrine outwash during the Vashon glacial advance and is northern sourced. Local exposures of oversteepened beds—such as along Goldsborough canyon—suggest that some areas include subglacial outwash. North of age site GD1 we observed a progression from distal lacustrine outwash (laminated silt) that forms a basal perching layer, to mid-section sand and ice-proximal pebble to cobble gravel, to lodgment till. In this area there is evidence of many rapid slope collapses above the basal silt. These events produced more than 50-ft-high box canyon hollows and down-valley debris flows and illustrate a lack of shear strength in the sand and gravel portions during periods of groundwater saturation. Together, these features indicate much more landslide activity than might be inferred from the single, small landslide mapped 850 ft north of GD1. Unit Qga is typically overlain by units Qgt or Qgic along a sharp unconformable contact and overlies units Qc_o, Qpf, Qpu, and Qpu_{op} either conformably or unconformably; where the base of unit Qga was observed, the unit overlies all other units unconformably. Like unit Qgt, unit Qga may include some similar but older deposits. For example, moderate weathering at clast count site C17 (sec. 13, T20N R4W) suggests a possible pre-Vashon age for outwash directly beneath surficial till. Subdivided into:

Qgag **Vashon advance outwash, pebble and cobble gravel**—Cobble and pebble gravel, some sand, silt, and clay; pale gray to gray or yellowish brown in some basalt-rich exposures; mostly clean (<5% silt or clay in matrix) except where ice-proximal (and commonly bordering on diamicton); clasts typically well rounded and well sorted; generally compact (see fig. 4 of Polenz and others, 2009b), but commonly cohesionless and therefore prone to being misinterpreted as loose; thinly to very thickly bedded; contains planar and graded beds, cut-and-fill structures, trough and ripple crossbeds, and foresets, but also locally structureless; clasts typically northern-sourced. Field exposures provide a thickness of 15 ft in bluffs on the north margin of Little Egypt Valley (sec. 14, T20N R4W); borehole W05 on the upland surface to the north suggests a thicknesses of about 64 ft. The unit may include some unrecognized older deposits.

Qgas **Vashon advance outwash, sand**—Sand, pebbly in some exposures, but more commonly planar-interbedded with silt; gray, pale gray or pale brown; generally compact (see fig. 4 of Polenz and others, 2009b), but some exposures may seem loose as they become cohesionless and lose all strength when either dry or saturated (but not when moist); clasts typically subrounded to well rounded and moderately to well sorted; mostly lacustrine and planar-bedded, but elsewhere includes cut-and-fill structures, trough-and-ripple crossbeds, or foreset deltaic beds; mostly quartzo-feldspathic; commonly includes northern-sourced clasts. Unit Qgas was mapped only in Isabella Valley, but localized exposures elsewhere are included within unit Qga or its subunits and indicate the lithology is more widespread. Several wells apparently intersect up to 28 ft of the unit along Cross Section A south of Goldsborough canyon and we included these deposits with unit Qga; well W42 suggests 35 ft of the unit on the south side of Shelton Valley (sec. 35, T20N R4W). Unit Qgas is stratigraphically below units Qgt and Qgic. The unit may include some unrecognized older deposits.

Pre-Vashon Glacial Deposits

Qat? **Pre-Vashon alpine till?, Olympic Mountains-sourced**—Matrix-supported, basalt-rich diamicton consisting of silt and sand matrix with clay, pebbles, and cobbles, in varied amounts; reddish brown to dark brown or dark brownish gray; lightly to severely weathered; compact and resembles concrete where well-developed (commonly referred to as 'hardpan'); clasts occasionally striated and faceted with subangular or rounded edges; unsorted; unstratified (but locally banded); clast lithology mostly basalt, with less-common sandstone, siltstone, and occasional quartz; other rock types are rare. Unit Qat? forms a patchy layer, with typical exposures 2–5 ft thick; maximum observed unit thickness is at least 10 ft. The unit may be 130 ft thick, or it could simply drape the slope, at significant site S1 0.6 mi west of the Matlock Interchange (sec. 23, T20N R4W). We mapped unit Qat? where diamicton was composed of dark brown matrix and mostly basalt clasts—with some sandstone and little or nothing else; we interpret this lithology as indicative of Olympic Mountains clast provenance, likely from the Skokomish Valley (Figs. 1, 2, and 3). At significant site S1, cursory review of 25 mildly weathered clasts identified mostly basalt (15–20 clasts), less common basaltic sandstone, and two clasts of vein? quartz. Unit Qat? is mapped as a line unnit on the northwest side of Shelton Valley (sec. 27, T20N R4W), where

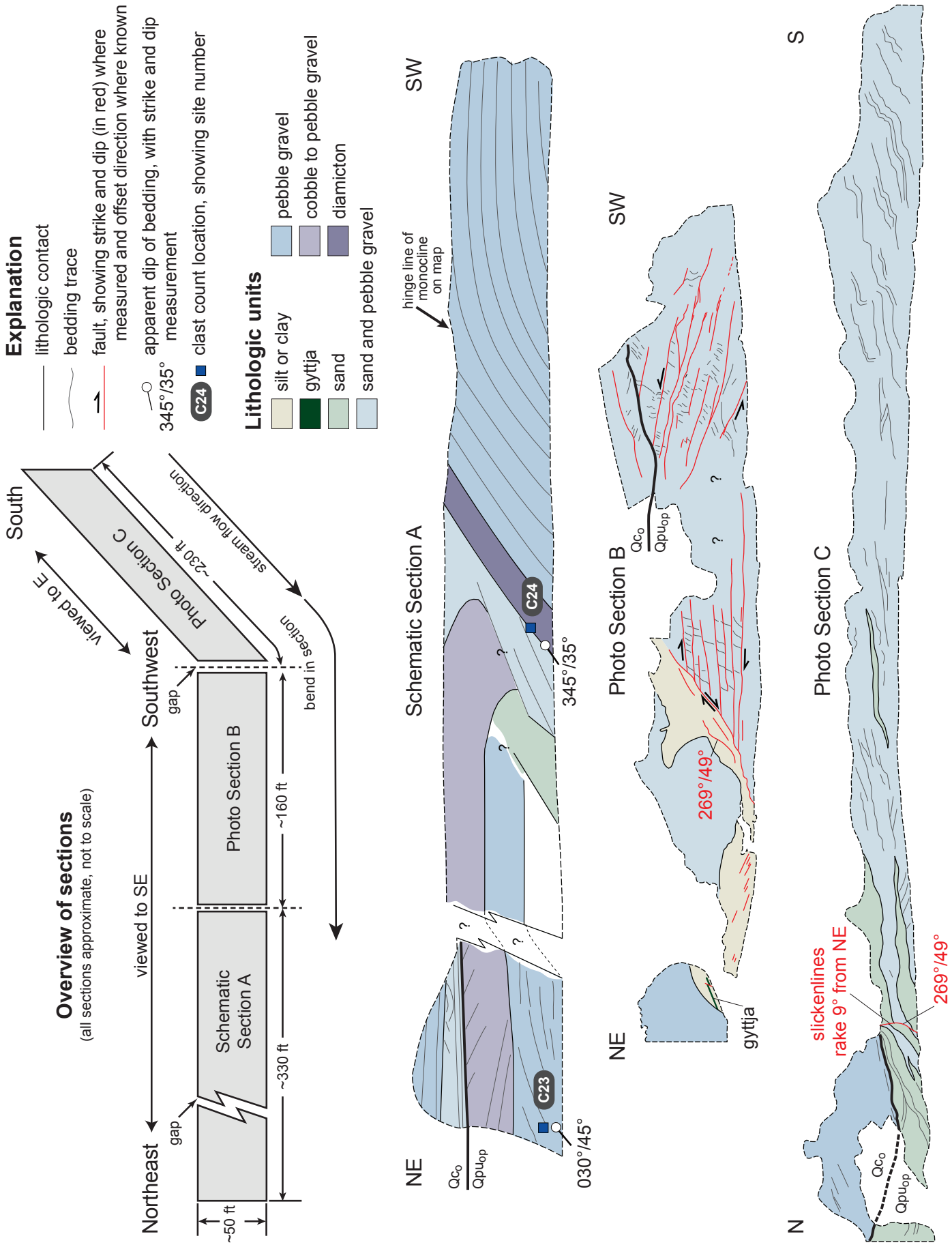
Explanation
lithologic contact
bedding trace
fault, showing strike and dip (in red) where measured and offset direction where known
345°/35° apparent dip of bedding, with strike and dip measurement
C24 clast count location, showing site number
Lithologic units
silt or clay
gyttja
sand
sand and pebble gravel
pebble gravel
cobble to pebble gravel
diamicton
Overview of sections
(all sections approximate, not to scale)
Northeast
Southwest
South
viewed to SE
viewed to E
Schematic Section A
Photo Section B
Photo Section C
gap
~50 ft
~330 ft
~160 ft
~230 ft
bend in section
stream flow direction
Schematic Section A
NE
SW
hinge line of monocline on map
C23
C24
030°/45°
345°/35°
Photo Section B
269°/49°
gyttja
Photo Section C
slickenlines rake 9° from NE
N
S

Figure 4 (facing page). Annotated photo and schematic diagram of heavily faulted section along Goldsborough canyon (site schematic D1 on map). An expanded version of the diagram (*Schematic Diagram D1*) is included as a separate illustration in the download package.

it is exposed near site GD1. Due to map scale, some exposures of unit Qat? were lumped into other units. Examples are along Goldsborough canyon in unit Qc_o at Columnar Section 2, at clast count site C29, and in unit Qpu_{op} at clast count site C24 (Fig. 4). Note that we also mapped tills with similar clast content as northern-sourced at clast count sites C14 (south of Goldsborough canyon) and C36 (Little Egypt Valley) because petrographic analysis of the matrix material at those sites caused us to favor a northern source and we interpreted the apparently Olympic Mountains clasts as scooped up from a nearby substrate. We queried all instances of unit Qat? for two reasons: (1) its Olympic Mountains-sourced clast mixture can also occur where northern-sourced drift has picked up Olympic Mountains-sourced material, especially near the base of a till. Petrographic examination of matrix samples from diamictons with Olympic Mountains-sourced clasts (for example, see C27, Data Supplement) supports this inference in some instances because it revealed ample granitic and metamorphic material. (2) all exposures of unit Qat? could alternatively be debris flow deposits, although we suspect that is not the case. Petrographic examination of matrix samples from diamictons with Olympic Mountains-sourced clasts supports an inference of debris flow origin in some instances because it revealed that matrix particles were generally more rounded than are typically found in lodgment till. Stratigraphic positions of exposures of unit Qat? suggest at least two Olympic ice advances. Weathering of clasts and matrix within some exposures of the unit support an age that is significantly pre-Vashon; minimal weathering of other exposures must be considered in the context of stratigraphic field relations (see *Weathering* discussion, *Quaternary Units* section).

Qpo **Pre-Vashon outwash, northern-sourced**—Pebble gravel, sand, and laminated silt, in varied amounts, locally contains dropstones and diamicton (flow till); gray, light brown, or tan; compact; moderately to well sorted except where unsorted as diamicton; rounded to subangular clasts; silty facies are massive to laminated, sandy facies are crossbedded or massive, and both are locally interbedded with each other and (or) pebble gravel; sand and clasts typically are northern-sourced (but for unexplained reasons include less chert and igneous and metamorphic rocks than Vashon age northern-sourced drift—see Fig. 2). Unit thickness may exceed 250 ft in the southern headwaters of Gosnell Creek (secs. 14–17 and 21, T19N R4W), where exposures of unit Qpo are mostly pebble gravel above 400–440 ft elevation, and mostly silt or sand with dropstones below. This transition suggests a facies change from lacustrine early advance outwash to more ice-proximal and fluvial late-advance outwash. We observed a similar upward-coarsening facies change between 370 and 415 ft elevation up-section of radiocarbon age site GD3. We also observed unit Qpo as pebble gravel above about 250 ft elevation on the north side of Goldsborough canyon (sec. 14, T20N R4W), and as interbedded sand and pebble gravel between 220 and 270 ft elevation on the north side of Shelton Valley (secs. 2 and 11, T19N R4W), whereas laminated silt was observed as high as 440 ft elevation about 1 mi southwest of age site GD3 (sec. 30, T20N R4W). A simple model of a shift from (distal) lacustrine outwash below 400 ft elevation to fluvial advance outwash above fails to account for: (1) the varied elevations of lacustrine and fluvial deposits; (2) the possibility that the unit includes a mix of advance and recessional outwash from multiple Cordilleran ice advances; and (3) possible tectonic land-level changes. Ages from—and weathering in—unit Qpo are discussed below (*Unconsolidated Quaternary Units*). Where unit Qpo is mapped on upland surfaces or directly beneath Vashon Drift, it may include Vashon advance outwash.

Qpt? **Pre-Vashon till, northern-sourced**—Matrix-supported diamicton consisting of silt and sand matrix with clay, pebbles, and cobbles, in varied amounts, with isolated boulders; sand and clasts are northern-sourced; gray to brown or tan; usually lightly or moderately weathered (see below); compact and resembles concrete where well-developed (commonly referred to as 'hardpan'); clasts occasionally striated and faceted with subangular or rounded edges; unsorted; unstratified (but locally banded). Unit thickness is mostly unconstrained because unit Qpt? was observed only in small patchy exposures. At clast count site C14 (sec. 14, T20N R4W) only 3 ft of section was exposed, and along the channel of an unnamed tributary of Goldsborough Creek (sec. 21, T20N R4W) no more than 1.5 ft of the unit was exposed at any one site. Unit Qpt? was deposited directly by glacial ice of the Cordilleran ice sheet. Some exposures include locally sheared and jointed lenses or layers of sand, pebbles, and cobbles. Unit Qpt? was not observed in direct contact with underlying units and is mapped beneath units Qgic or Qgo (and subunits). In all cases, our identification of unit Qpt? is queried because we did not observe other pre-Vashon deposits above the unit and weathering characteristics alone suggest—but fall short of demonstrating—a pre-Vashon age. One exception may be an isolated, 3 ft-tall roadside exposure of atypically dark reddish-brown, apparently northern-sourced till downslope—but not necessarily downsection—of pre-Vashon Olympic Mountains-sourced gravel at clast count site C32 (sec. 25, T20N R4W). That till exposure was included in unit Qpu_{op} because the exposure was localized and isolated, its stratigraphic relation to the nearby upslope exposure

of Olympic Mountains-sourced gravel at C32 remains uncertain, and we have not excluded the possibility that the apparently northern character of this till could be inherited where ice from the Olympic Mountains overrode and picked up sediment from a possibly pre-existing northern-sourced drift. We mapped unit Qpt? in an unnamed tributary of Goldsborough Creek (sec. 21, T20N R4W), where we systematically observed more-advanced weathering of clasts and matrix than usually observed in Vashon Drift; we queried the assignment because we concluded that the weathering analysis alone did not provide compelling evidence of pre-Vashon age. Our mapping of unit Qpt? at clast count sample C14 (sec. 14, T20N R4W) is similarly based on weathering. At this site a broad range of weathering in clast and matrix suggests a pre-Vashon age for surficial till—that could not be definitively differentiated from Vashon till with incorporation of older particles from a nearby substrate. At significant site S2 (sec. 11, T19N R4W), an isolated patch of saprolitized diamicton is likely till and the severity of weathering suggests pre-Vashon age, consistent with prior mapping of pre-Vashon drift in this area (Logan, 1987). However, we did not observe exposures that would justify its larger extent on the 1:100,000-scale map.

Pre-Vashon Glacial and Nonglacial Deposits, Undivided

Qco **Pre-Vashon deposits of MIS 3 (equivalent to the Olympia nonglacial interval)**—Pebble gravel, and less-voluminous sand, silt, clay, diamicton, peat, and detrital wood; light brown, brown, gray, or dark gray; compact and locally stiff; moderately well sorted (except where diamicton); planar bedded, crossbedded, or massive. Diamicton is interpreted as debris slurries into lakes, but also includes possible lodgment till from the Olympic Mountains—see also unit Qat?. Clast content and petrographic analysis of sand (and silt) indicate that unit Qco in the Black Hills—like the undated equivalent unit Qpuop—is locally reworked from northern-sourced pre-Vashon drift. North of the Black Hills, unit Qco is mostly sourced from the Olympic Mountains, and fewer exposures contain northern-sourced clasts and grains. For example, deposits at GD7 and clast count C31 (both in Columnar Section 2) and GD8 (clast counts C21 and C22) contain enough quartz grains and diagnostic northern-sourced material to suggest northern provenance—but not enough to exclude a mix of northern and Black Hills or Olympic Mountains sources. The maximum observed thickness of unit Qco is 120 ft within Columnar Section 2 in Goldsborough canyon. Unit Qco closely resembles unit Qpuop but is mapped separately where age-control data suggest an MIS 3 age. Unit Qco includes some deposits mapped by Schasse and others (2003) as unit Qpgo east of the Shelton Valley quadrangle, and some deposits mapped as Skokomish Gravel by Molenaar and Noble (1970).

Qpf **Pre-Vashon sediment, fine-grained**—Silt, clay, and mixtures of both, ranges to fine sand in some exposures; pale-gray to dark-gray and brown; dense and hard; planar bedded or massive. A minimum thickness of 11 ft is observed slightly upstream of Goldsborough canyon (sec. 15, T20N R4W). Well records suggest thicknesses of 185 ft beneath Little Egypt Valley (W14—sec. 18, T20N R4W), 192 ft beneath Shelton Valley (W35—sec. 27, T20N R4W), and up to 260 ft beneath the upland surface about 0.5 mi north of Shelton Valley (W27—sec. 26, T20N R4W). Dropstones of varied lithologies suggest at least some deposits were lakes dammed by Cordilleran continental ice (for example at secs. 15, 21, and 22, T20N R4W). Unit Qpf includes undated silt and clay directly beneath Vashon Drift and thus may include Vashon advance outwash (equivalent to the Lawton Clay); however, at least some exposures of unit Qpf are of pre-Vashon age. For example, a radiocarbon-infinite date at age site GD3 (sec. 29, T20N R4W) suggests a pre-Vashon age for associated lacustrine sediment, although at that particular site these sediments are interbedded with pebble gravel and were therefore included with the texturally less restrictive unit Qpo.

Qpu **Pre-Vashon sediment, undivided**—Pebble gravel, sand, silt, clay, diamicton, organic sediment, and boulders, in varied amounts; color and weathering varied; compact; varied grain size, rounding, sorting, and bedding. Unit Qpu is mapped where age, paleoenvironment, and provenance were poorly known or too diverse to map separately; more than 300 ft of the unit is inferred along Cross Section A. Although the unit mostly includes pre-Vashon deposits, it may contain some Vashon advance outwash and (or) recessional outwash where boreholes and driller logs do not indicate degree of compaction. Locally subdivided into:

Qpuop **Pre-Vashon sediment of mostly Olympic Mountains provenance, undivided**—Mostly pebble gravel, ranging to sand, diamicton (including some till), silt, clay, and peat; reddish brown to tan or gray; gravel matrix typically sandy, and in some exposures suffused with and (or) weathered to clay; compact; moderately sorted in most exposures, but ranging to poorly or well sorted. Fresh clasts can be found in the unit, but overall the weathering is varied and exceeds that of the overlying Vashon-age deposits; in some exposures all clasts are saprolitized and there is a matrix of residual and (or) illuvial clay. Most exposures reveal planar horizontal lake beds or fluvial crossbeds. Beds are commonly tilted or post-depositionally distorted,

as at site D1 along Goldsborough canyon (Fig. 4). Clasts in the unit are mostly basalt with less abundant sandstone, suggesting an Olympic Mountains provenance, but some exposures include plutonic and metamorphic clasts indicative of northern-sourced glacial deposits. Such northern drift was included with unit Qpu_{op} where map crowding did not permit separate display. An example is northern-sourced till downslope of clast count site C32 (sec. 25, T20N R4W). We infer that the sediments at both C32 and C33 (sec. 35, T20N R4W) are sourced from the Black Hills based on the prevalence of basalt clasts at the expense of all other lithologies. Unit thickness exceeds about 40 ft along the north slope of Goldsborough canyon (sec. 14, T20N R4W). Well records suggest a thickness up to 197 ft beneath the upland surface at the southern margin of Shelton Valley. The unit is exposed in Goldsborough canyon and in the slopes of Shelton Valley. The unit includes deposits mapped by Schasse and others (2003) as unit Qpg_o east of the Shelton Valley quadrangle, and deposits mapped by Molenaar and Noble (1970) as Skokomish Gravel or as Kitsap Formation at and near radiocarbon infinite age sites GD2 and GD6. Our map shows GD6 within unit ml because sometime after John Noble had obtained this date, dam removal triggered significant land modifications (Garrison, 2007). Our usage of unit Qpu_{op} generally follows that of Polenz and others (2010, 2011); some of the more-weathered exposures of the unit along Goldsborough canyon may correspond to their sub-unit Qpu_{opl}.

Tertiary Volcanic and Sedimentary Bedrock

ΦEm **Undifferentiated sedimentary rocks (Eocene to Oligocene)(Cross Section A only)**—Sandstone, siltstone, mudstone, and conglomerate, in varied amounts; inferred in Tacoma basin above volcanic rocks of the Crescent Formation because Eocene to Oligocene marine sedimentary rocks have been mapped up-section of Crescent Formation near the map area (Molenaar and Noble, 1970; Logan, 1987, 2003; Tabor and Cady, 1978a; Walsh and others, 1987; Dragovich and others, 2002; Polenz and others, 2012a; Snavely and others, 1958; Pease and Hoover, 1957). Inference of similar rocks in the Tacoma basin is further supported by interpretations of seismic sections and other geophysical measurements 5–10 mi east of the map area (Pratt and others, 1997; Magsino, written commun., 2016; Odum, written commun., 2015, 2016, Clement and others, 2010). In addition, our own analysis of new seismic measurements adds support for the presence of sedimentary bedrock, albeit at poorly constrained depth, at the northeast end of Cross Section A (Table 3; Cross Section A). Significant changes in the depth to bedrock over a short distance are illustrated by a 752-ft-deep water well located 0.9 mi southeast of cross section endpoint A'. This well does not reach bedrock (sec. 7, T20N R3W; Washington Department of Ecology ID nos. 34035 and 274273), whereas our seismic measurements at Shelton High School 0.7 mi southeast of cross section endpoint A' (sec. 12, T20N R4W) reveal strong seismic velocity contrasts at 384 ft below the surface and 909 ft below the surface. We interpret this as evidence that sedimentary rock is present above basalt and shallower than suggested by the nearby well. The contrast in bedrock elevation between the well and the seismic velocity site suggests that the sedimentary rock surface is more uneven than shown along the cross section. We speculate that the sedimentary rocks are marine and Eocene to Oligocene in age because such rocks were mapped at the nearest sedimentary rock exposures upsection of Crescent Formation in the western Puget Lowland (Polenz and others, 2012a), but we note that Eocene to Miocene nearshore and nonmarine sedimentary rocks are present south of the Black Hills (to the east of the Doty Hills)(Pease and Hoover, 1957; Snavely and others, 1958), and locally at the southeastern margin of the Puget Lowland near the Nisqually River (Walsh and others, 1987).

Ev_c **Crescent Formation basalt (early to middle Eocene)**—Mostly aphanitic basalt; pillows or massive to columnar flows with plagioclase and pyroxene phenocrysts commonly visible in hand sample; rare minor interbeds of sandstone or siltstone and small pockets of sandstone or siltstone between basalt pillows; at least one siltstone bed contains a tuff layer at fossil sample site GD14 (Fig. 5); sedimentary interbeds commonly brecciated during deposition of overlying basalt (Fig. 6); basalt is medium to pale gray and dark gray where fresh; weathers gray and medium yellow-brown to reddish brown. In thin section, basalt groundmass is mostly cryptocrystalline. Phenocrysts are 35–50% plagioclase and up to 45% pyroxene. Less common constituents are glass (up to 37%), opaque minerals (3–10% in most samples), and zeolites. Basalt within the map area crops out in the southern two thirds of the Shelton Valley quadrangle, where the Black Hills form approximately 1,000 ft of relief. Basalt is inferred farther north, based on gravity data (see *Geophysical Observations*). We also used seismic data to inform our estimates of depth to basalt along Cross Section A (site GP1 and at Shelton Valley High School; Table 3) and along Cross Section B (sites GP4 and GP5; Table 3). An early Eocene age for unit Ev_c in the Black Hills is supported by several $^{40}Ar/^{39}Ar$ dates, including

Figure 5. Photo of sedimentary interbeds in basalt flows of the Crescent Formation (photo site P2 on map). Very thin bed of tuffaceous siltstone in 4- to 20-ft-thick siltstone and minor very fine sandstone. Tuffaceous bed is approximately 6 in. below the base of the overlying basalt flow. In thin section, pyroclasts consist largely of crystal ash (potassium feldspar, plagioclase, biotite, hornblende, and muscovite) with sparse lithic ash. Zircons from the tuffaceous bed were analyzed for U/Pb CA-IDTIMS geochronology by Mike Eddy (MIT, written commun., 2016).

Figure 6. Photo of sub-horizontal interbed of siltstone to very fine sandstone between basalt flows of the Crescent Formation (photo site P4 on map). Thickness of the sedimentary rock averages 2 ft. but locally ranges up to 4 ft. Local thickening occurs along discrete undulating shear planes; we interpret this as the product of deformation due to loading and shear during deposition of the overlying basalt flow.

two new analyses (this study), and by a new U-Pb age discussed below in *Ages of Units*.

AGES OF UNITS

Bedrock Units

GEOCHRONOLOGY

We present two new $^{40}Ar/^{39}Ar$ ages from the north end of the Black Hills within the Shelton Valley quadrangle. GD9 yielded an age of 50.51 ±0.21 Ma and GD10 50.14 ±0.17 Ma (Tables 1 and A3). Both ages were performed by Oregon State University and analyzed basalt groundmass. A preliminary age estimate by U-Pb CA-ID-TIMS (Uranium-Lead chemical abrasion-isotope dilution-thermal ionization mass spectrometry) of zircon from tuff in a sedimentary interbed at fossil sample site GD14 (Fig. 5; Table 1) is ~49.7 Ma and will be separately published. This age is consistent with (but more precise than) the above $^{40}Ar/^{39}Ar$ ages (Eddy, written commun., 2016). Micro- and macrofossils from GD14 have so far eluded identification. The new dates from the map area are slightly younger than (but broadly consistent with) an early Eocene age of unit Ev_c in the Black Hills south of the map area, which is well established by $^{40}Ar/^{39}Ar$ dates between 50.9 and 55.6 Ma (Duncan, 1982; Globerman and others, 1982; Babcock and others, 1994; Czajkowski, 2014).

BIOSTRATIGRAPHY

Seven samples of minor sandstone and siltstone from between basalt pillows—or as interbeds between basalt flows—within

the Crescent Formation (age sites GD11 to GD17) did not yield biostratigraphic age constraints (Elizabeth Nesbitt, Burke Museum, written commun., 2016), although fossils were observed at several sites (Table 1).

Unconsolidated Quaternary Units

New dates from the map area proved valuable for evaluating ages and paleoenvironmental associations of map units, but they did not constrain the timing of transitions between paleoclimatic periods, nor the timing of transitions between our map units. We interpret the ages of Pleistocene glacial and nonglacial periods in the Puget Lowland by reference to global proxies for glacial and interglacial intervals and age estimates from within and outside the map area. The timeline remains tentative and is summarized in Morrison (1991), Booth and others (2004), and Troost and Booth (2008). Ages of MIS 3 (the 'Olympia nonglacial interval') and older periods are defined by reference to global changes. Age analyses from the end of the Pleistocene are more abundant, and since transitions between nonglacial and glacial settings are regionally time-transgressive, these data can justify local adjustments to interval boundaries (see *Ages of Quaternary Units* below).

We attributed the stratigraphically highest deposit of northern-sourced glacial drift to the Cordilleran ice sheet during the Vashon Stade of the Fraser Glaciation (MIS 2), except where local ages or weathering suggested an older age for surficial drift.

GEOCHRONOLOGY AND PALEOMAGNETICS

Four paleomagnetically normal analyses favor ages of less than 780 ka for the sediments in the map area (Table 1; Bernard Housen, Western Washington University, written commun., 2016). Of these samples, only M2 (unit Qpu_{op}; sec. 24, T20N R4W) is from sediments not otherwise constrained to MIS 3 or Vashon age (units Qc_o and Qga). Two luminescence ages (GD7–8) and two finite radiocarbon ages (GD1–2) support an MIS 3 age for unit Qc_o (see *Ages of Quaternary Units* below). GD1 is mapped within unit Qpu_{op}; the stratigraphic context of that decision is explained below in *Paleoenvironmental Interpretation*.

Four radiocarbon-infinite dates (age sites GD3–6) support pre-Vashon ages for their host sediments but do not help separate sediments of MIS 3 age from older deposits (Table A1). Pre-Vashon ages elsewhere in the map area are inferred based on stratigraphic constraints or weathering (see below).

WEATHERING OF VASHON AND PRE-VASHON DEPOSITS

We observed that many pre-Vashon deposits in the map area are noticeably weathered and therefore used clast weathering (and petrographic examination of matrix material) to help assess relative ages of Vashon and older deposits (Fig. 7; tabular data in Data Supplement). Clast counts from modern stream channels provide added context.

Despite considerable (and expected) overlap in the amount of weathering (Fig. 7), the clast counts reveal systematic weathering trends, from least weathered (left side of plot) to most weathered (right side of plot). Unit Qpu is absent

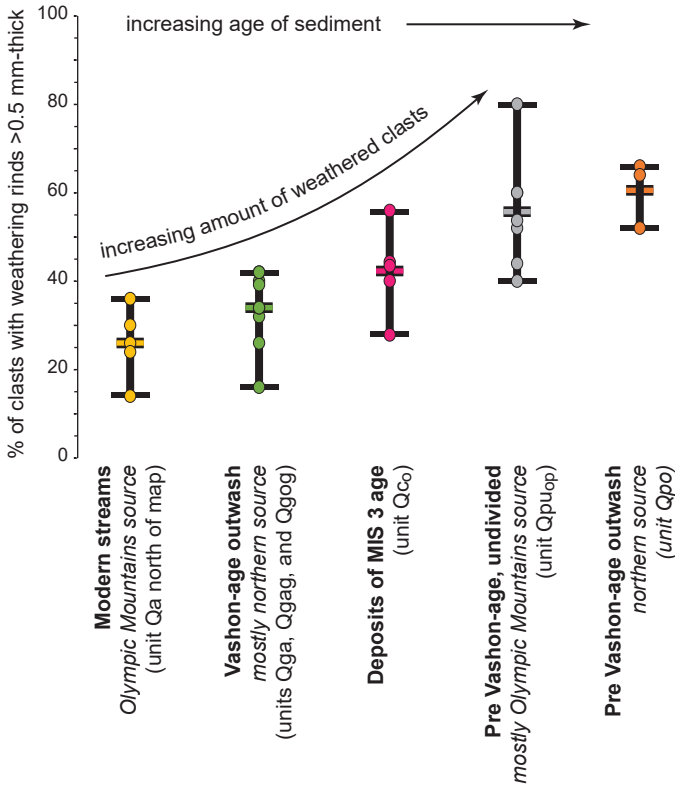

Figure 7. Plot showing increase in amount of weathering with age of sediment. Black bars indicate range of data for each grouping of units; colored dots show actual weathering of each clast count sample; colored bar indicates average weathering. 0.5 mm weathering rind thickness (Y axis) serves as proxy for more detailed criteria used to assess clast weathering—see footnotes to clast weathering tabular data in Data Supplement. Plot excludes clast counts from diamictons because, due to high matrix density (and thus low permeability), we expect diamictons to be less susceptible to weathering than fluvial deposits, and because we observed that weathering of many clasts in some diamictons does not represent the age of the deposit because the diamictons incorporated clasts from older Pleistocene deposits and thereby inherited weathering (see *Weathering of Vashon and Pre-Vashon Deposits*).

from the clast counts—in part because by counting clasts, we usually gained a clearer sense of provenance and age and were then able to assign a more specific unit. However, conceptually, unit Qpu includes all other map units older than Vashon till, and we would expect weathering data from the unit to be correspondingly varied.

Weathering of Glacial Deposits

Pre-Vashon Northern-Sourced Glacial Deposits

We tentatively interpret some—but not all—relatively strongly weathered exposures of northern-sourced till as pre-Vashon unit Qpt based on relatively advanced weathering of clasts and matrix. A pre-Vashon age was inferred for glacial outwash (unit Qpo) on the basis of considerable clast weathering at clast count sites C18 (north side of Goldsborough canyon) and C6 and C7 (southern headwaters of Gosnell Creek, sec. 21, T19N R4W), and moderate clast weathering at C9 (southern headwaters of Gosnell Creek, sec. 15, T19N R4W). Weathering among all clast counts from unit Qpo exceeds that of any clast count from Vashon outwash (Fig. 7). This is consistent with our

suspicion that MIS 4 (Possession Glaciation) ice of northern provenance did not reach the map area and pre-Vashon glacial deposits date to MIS 6 or earlier.

Pre-Vashon Olympic Mountains-Sourced Glacial Deposits

Weathering of unit Qat? is varied. Clasts in unit Qat? are unweathered or minimally weathered at and upslope of significant site S1, 0.6 mi west of the Matlock Interchange. Weathering is more advanced near the top of the same till. Cursory observation of till near age site GD1 northwest of Shelton Valley suggests moderate weathering. Clasts and matrix at C26 (Columnar Section 2) are lightly weathered. Clasts and matrix at C24 (Fig. 4) are lightly weathered. A more weathered exposure of unit Qat? may be present west of Shelton Valley at significant site S3 (sec. 33, T20N R4W), where a small excavation surrounded by surficial till that we mapped as unit Qgt revealed weathered till matrix with clasts that suggest an Olympic Mountains provenance.

Pre-Vashon Undivided Glacial and Non-glacial Deposits

Among undivided pre-Vashon glacial and nonglacial deposits, we obtained clast counts from units Qpu_{op}, and Qc_o (Data Supplement). The clast counts document varied weathering that is on average more advanced than in either modern alluvium or Vashon Drift (Fig. 7). The separation from modern alluvium and Vashon Drift is understated in Figure 7 because our undivided units include some deposits that were so weathered that we did not attempt to count clasts because they were rotten and their original lithologies were beyond recognition; this was the case south of the active channel in Goldsborough canyon, 260 ft northwest (upstream) of photo site P1. Figure 7 also reveals considerable overlap between units Qc_o and Qpu_{op}.

Vashon Glacial Deposits

In general, Vashon Drift is only slightly more weathered than modern alluvium (Fig. 7). We mapped some relatively weathered till exposures, usually within 2–5 ft of the base of the till, as Vashon till (units Qgt or Qgic) because we concluded that most of their weathering was likely inherited when Vashon-age ice incorporated nearby substrate of pre-Vashon sediment or bedrock. For instance, at clast count sites C10 and C11, Vashon lodgment till can be seen to have a decidedly northern-sourced clast content near the upland surface (C10), whereas a progressively more basalt-rich—and weathered—clast content is found closer to the base of the apparently same till (C11). However, petrographic examination of the till matrix revealed mostly light weathering of particles near the till surface, whereas near the base of the till, weathering was on average more advanced—but bimodal, with lightly weathered particles (inferred to be northern-sourced material of Vashon age) and strongly weathered particles (inferred to be derived from nearby substrate of weathered regolith and bedrock), with few moderately weathered particles.

Our inference of inherited weathering by enrichment of the till with locally derived (previously weathered) substrate material is strengthened by the observation that in the basal till at C11, 44 of 50 clasts were basalt, among which 28 were moderately weathered or rotten, whereas near the surface at C10 only 28 of 50 clasts were basalt, and 17 of those were at most lightly weathered. These observations are consistent with introduction into the basal till of previously weathered basaltic material from substrate beneath the ice. Similar inferences have been made elsewhere in the western Puget Lowland (Carson, 1980; Polenz and others, 2012a,c).

Although we are confident of this pattern overall, we caution that for most exposures, the inferences are not compelling, and the presence of some inherited weathering among Vashon-age deposits lessens distinctions between exposures of basal Vashon till, pre-Vashon till, and Olympic Mountains-sourced till. Where we did identify unit Qpt?, it was mainly because we observed degrees of weathering in the unit to be more evenly scattered and therefore inferred to be in-situ, instead of the bimodal pattern noted above as indicative of incorporation of pre-weathered particles. Bimodal weathering was also observed and similarly interpreted in some exposures of outwash, such as at C17.

AGES OF QUATERNARY UNITS

Pre-Vashon Northern-Sourced Glacial Deposits

We attribute northern-sourced pre-Vashon sediment to Cordilleran ice advance(s) during or before MIS 6. A key location for this assertion is in the headwaters of Gosnell Creek where a section of re-worked northern-sourced sediment rises to greater than 400 ft elevation. In this location, luminescence age GD8 (43.7 ±3.7 ka) suggests deposition during MIS 3, and the deposits there are thus mapped as unit Qc_o. Clasts and matrix grains at the site indicate a northern glacial provenance, but Cordilleran ice did not advance into the Puget Lowland during MIS 3. In order to deposit the sand and pebble gravel observed at and up-section of GD8, glacial ice likely would have advanced onto the northeastern peripheral slopes of the Black Hills in the Shelton Valley quadrangle to an elevation greater than about 400 ft. Because luminescence dates are approximate, a Possession age (MIS 4—Booth and others, 2004; Troost and Booth, 2008) instead of an MIS 3 age merits consideration for the deposits. However, we deem Possession-age outwash unlikely because: (1) the dates are more suggestive of MIS 3; (2) we do not know of any compelling record of Possession-age ice advancing farther south than the latitude of Tacoma—approximately equivalent of the northern map boundary of the Shelton Valley quadrangle (Lea, 1984; Troost, 1999; Kathy Troost, University of Washington, oral commun., 2016); and (3) MIS 4 corresponds to a relatively weak peak in the global oxygen isotope curve. Thus, in order to explain the apparently voluminous pre-Vashon northern-sourced outwash in the headwaters of Gosnell Creek and the MIS 3 age, we suggest that an earlier ice advance (MIS 6 or older) initially deposited the northern-sourced sediment which was locally reworked into unit Qc_o during MIS 3. We similarly infer that northern-sourced sediment of MIS 6 or older age was reworked into the MIS 3-age deposits of unit Qc_o at GD7 (47.3 ±4.9 ka) and elsewhere in Goldsborough canyon. An MIS 6 or older age for pre-Vashon glacial sediment in the map area is consistent with our observation that this sediment is generally more weathered than Vashon Drift (Fig. 7; see *Weathering of Glacial Deposits*).

There is a case for possible Possession-age outwash in the map area below 200 ft elevation (the approximate elevation of the delta-front slope break at the Shelton delta of glacial Lake Russell—see *Glacial Lakes and Shorelines*). The rationale is that proglacial streams and ice-dammed lakes of MIS 4 would, like Lake Russell, have drained south to the Chehalis Valley via Olympia (southeast of the Shelton Valley quadrangle) unless pre-Vashon land surfaces near Olympia were markedly higher than they are today. If correct, southward drainage implies that: (1) northern-sourced drift of MIS 4 age is unlikely in the Shelton Valley quadrangle above approximately 200 ft elevation; (2) if MIS 4 sediment is present below that elevation, there is a good chance it is lacustrine; and (3) where MIS 4 sediment is fluvial (if anywhere), it would likely be overwhelmed by sediment from the Olympic Mountains, such that it would resemble units Qco and Qpuop. We therefore expect that, except perhaps for unit Qpf below 200 ft elevation, pre-Vashon northern-sourced drift (units Qpo, and where correctly identified, Qpt?) is of MIS 6 (Double Bluff) or greater age.

Age site GD3 (infinite radiocarbon age) samples a detrital wood fragment and is the reason the sediment at that site and in nearby drainages with similar setting and deposits (secs. 29 and 30, T20N R4W) are mapped as pre-Vashon deposits. However, the wood was sampled from a northern-sourced section of glacial outwash capped by surficial till and we cannot rule out that the wood was reworked from an older deposit into Vashon advance outwash.

Pre-Vashon Olympic Mountains-Sourced Glacial Deposits

Unit Qat? is consistently exposed downsection of Vashon Drift, suggesting that it is older. Weathering of clasts and matrix within some exposures of unit Qat? support an age that is significantly older than the Vashon Stade; minimal weathering of other exposures within the unit must be evaluated in the context of stratigraphic field relations. For instance, weathering near the top of Olympic Mountains-sourced till at and upslope of significant site S1 along a road cut 0.6 mi west of the Matlock Interchange suggests a significantly pre-Vashon age for the entire deposit at that site, although clasts lower down in the till at S1 are only minimally weathered. At age site GD1 (Table 1) northwest of Shelton Valley, radiocarbon analysis yielded a late MIS 3 age for nonglacial deposits and may imply a similar age for till exposed nearby; however, the stratigraphic position of the till relative to GD1 is unresolved. Based on cursory observation, moderate weathering of the till at that location suggests that the till may be older than late MIS3. Clasts and matrix at C26 (Columnar Section 2) are lightly weathered. Their stratigraphic position downsection of age site GD7 suggests early MIS 3 or older age. Stratigraphic field relations suggest a pre-MIS 3 deposit of Qat? at C24 (Fig. 4). If till at significant site S3 is Olympic Mountains-sourced (as we suspect), then weathering of matrix and clasts there suggests a penultimate or older Olympic ice advance, equivalent to unit Qapt of Polenz and others (2011, 2012b), or a site where surficial weathering in a till from the most recent (undated) Olympic ice advance into the map area has been (improbably) preserved.

Pre-Vashon Undivided Glacial and Nonglacial Deposits

We mapped undivided pre-Vashon glacial and nonglacial deposits as units Qpu, Qpuop, Qpf, and Qco. Sediment that we could link to an MIS 3 age was mapped as unit Qco. Examples are IRSL age estimates at age sites GD7 (47.3 ±4.9 ka) and GD8 (43.7 ±3.7 ka)(Columnar Sections 1 and 2) and radiocarbon age estimates at GD1 (17.7–17. 5 ka) and GD2 (27.5–27.2 ka; Fig. 8). Sidall and others (2008) placed the onset of the nonglacial MIS 3 period at 60–57 ka and so our spread of ages covers most of MIS 3. The arrival of lacustrine Vashon advance outwash marks the end of the period in the map area, likely at or sometime after about 18 ka (when low-lying parts of the Puget Lowland became submerged beneath proglacial lakes because advancing ice dammed the Strait of Juan de Fuca); the period was fully replaced by Vashon Stade glaciation when Cordilleran ice entered the map area—likely between 17 and 16 ka (between Tacoma and Olympia in fig. 3 of Polenz and others, 2015).

For all other pre-Vashon sediments, age-control data are limited to stratigraphic field relations, four radiocarbon-infinite ages, and implications of clast counts, petrographic analyses, and paleomagnetically normal polarity in four samples.

Age-control data for unit Qpuop do little to constrain the age of the unit; they include radiocarbon infinite analyses at GD2 and GD6 (east end of Goldsborough canyon), and paleomagnetically normal analyses M1 and M4 (Columnar Section 2). Radiocarbon-finite age site GD1 (northwest of Shelton Valley) was included in unit Qpuop because we suspect that the deposit we sampled moved downslope due to mass wasting, and surrounding deposits may be much older. This age does indicate that late MIS 3 deposits are present in this area, however.

Considerable overlap between units Qco and Qpuop in Figure 7 suggests that much, but not all of unit Qpuop may also be of MIS 3 age. Despite this overlap, we separated the less weathered samples of unit Qpuop from unit Qco because: (1) we consider age distinctions based on our clast weathering data to be crude and approximate—insufficient as indicators of similar ages where other suggestions of similar ages (such as stratigraphic equivalence) are missing; (2) some exposures of units Qpu and Qpuop predate MIS 3 because they are stratigraphically below pre-Vashon, northern-sourced drift; (3) our relative-weathering data suggest that some deposits are significantly older than those we mapped as MIS 3 (see *Weathering of Glacial Deposits*), and (4) we know that some sediments are stratigraphically below deposits that we mapped as MIS 3, but we lack constraints on the stratigraphic distance. Units Qpu and Qpf lack age control beyond stratigraphic field relations.

Vashon Glacial Deposits

We generally equate the Vashon Stade of the Fraser Glaciation with MIS 2 (19–17 ka)(fig. 2 in Polenz and others, 2015) but believe that Cordilleran ice of MIS 2 invaded the Puget Lowland somewhat later. An ice-incursion time curve for the Vashon in the Puget Lowland is presented by Polenz and others (2015, their fig. 3) and appears to provide a good estimate of when MIS 2 ice advanced into the map area—likely not before

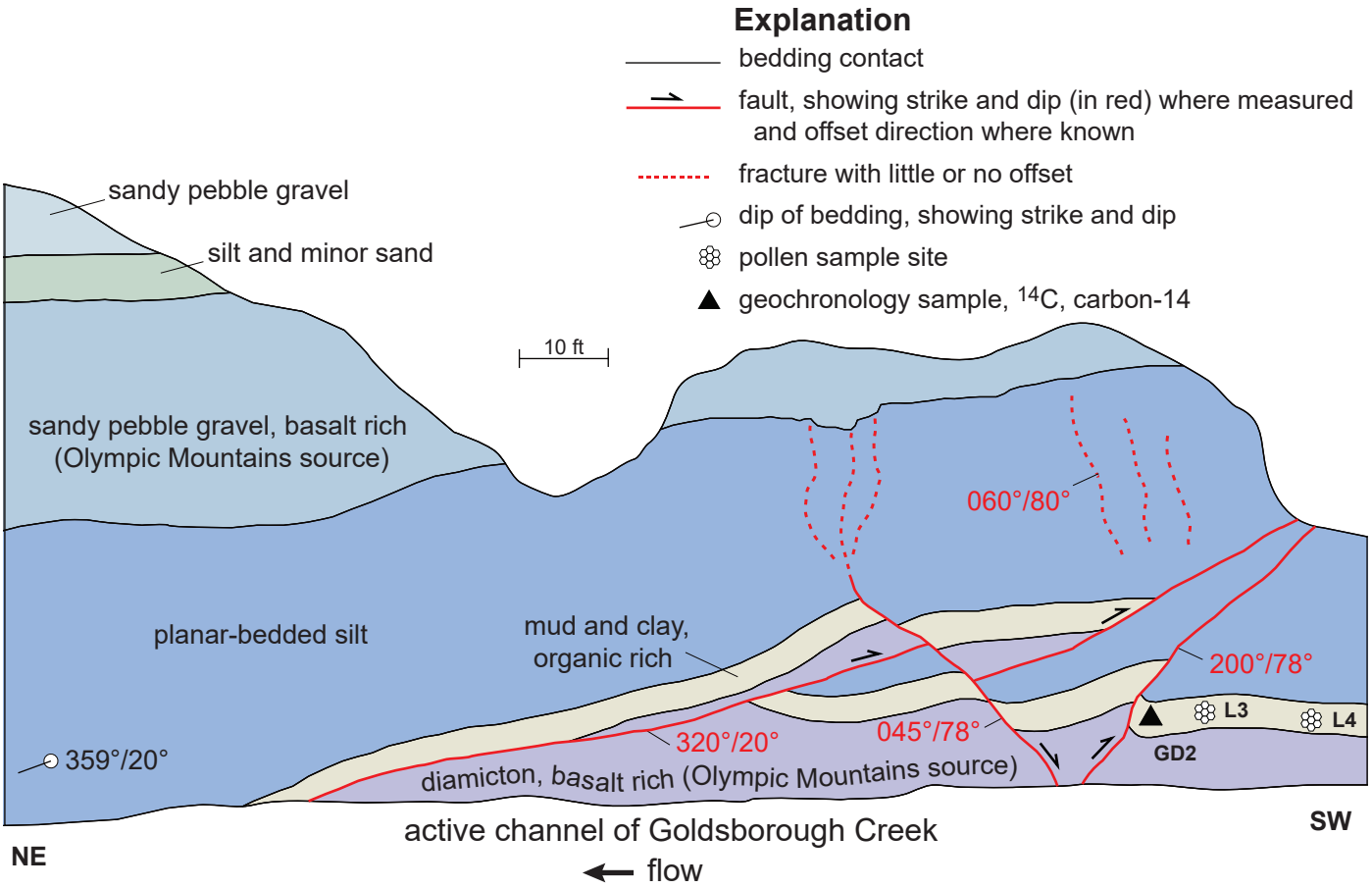

Figure 8. Schematic section of deformed Quaternary deposits along Goldsborough canyon (site D2 on map). Low-angle thrusts and high-angle faults cut and offset these units. Due to map scale, site details are not shown on the map. Deposits are mapped as unit Qc_o based on a 23,030 ±90 ^{14}C year BP age from the organic rich mud (age site GD2). Pollen analysis sample L3 is from organic-rich mud at the same stratigraphic level as age site GD2; pollen analysis sample L4 is from slightly lower in section, at the base of the same organic-rich deposit. Both pollen analyses suggest a cooler than modern climate. The base of outcrop is at 132 ft elevation.

16.5 ka. Advance was shortly followed by retreat, likely sometime between 15.8 and 15.3 ka. The curve suggests to us that outwash lake deposits during Vashon ice advance may have begun to accumulate in low-lying parts of the map area at about 18 ka (or later), and ice may have advanced into the map area about 16.5 to 16 ka, with retreat sometime between 15.8 and 15.3 ka. As Polenz and others (2015) acknowledged, age-control data on the timing of the ice incursion—and especially ice retreat—conflict across the Puget Lowland, and prior workers have suggested earlier ice advance and recession (Anundsen and others, 1994; Porter and Swanson, 1998; Haugerud, written commun., 2012; oral commun., 2015). Our conclusions assume that the ice-incursion time curve of Polenz and others (2015) is accurate and rest on the rationale that: (1) deposition of distal advance outwash in a proglacial lake could have begun when ice arrived at the latitude of Port Ludlow (50 mi north of the Shelton Valley quadrangle) and stopped drainage from the Puget Lowland into the Strait of Juan de Fuca about 18 ka; (2) ice arrived in the Shelton Valley quadrangle sometime after it had passed the latitude of Tacoma about 17 ka and before it arrived in Olympia about 16 ka; (3) ice collapsed quickly across most of the Puget Lowland between 15.8 and 15.3 ka, although some ice patches locally persisted for millennia (Porter and Carson, 1971).

PALEOENVIRONMENTAL INTERPRETATION

Bedrock Units

Fossilized wood from age site GD15 (Table 1) suggests sediment deposition in shallow waters near the shore because the deposition of wood is less likely at greater depth farther offshore. Fossils and other considerations similarly led Logan and Walsh (2004) and Squires and Goedert (1994) to infer shallow water (to possibly subaerial) conditions in the Crescent Formation south and southeast of the Shelton Valley quadrangle. However, vesicle sizes in basalt within the quadrangle are generally smaller than 1 mm, and Compton (1985, p. 278) asserts that such vesicle size implies water depths in excess of 500 m (1,640 ft). Small vesicles, slightly younger ages, and a greater abundance of pillows in basalt in the map area compared to farther southeast in the Black Hills (Logan and Walsh, 2004) could be an indication that the basalt at the north end of the Black Hills is up-section of, and represents deeper marine conditions than, basalt farther southeast in the Black Hills uplift.

Unconsolidated Quaternary Units

PALEOENVIRONMENT OF PRE-VASHON GLACIAL AND NONGLACIAL DEPOSITS, UNDIVIDED

Deposits of Unconstrained Pre-Vashon Age

Units Qpu and Qpf are mainly defined by how little is known about them. Their scattered exposures include both glacial and nonglacial deposits and deposits of Olympic, northern, or mixed provenances. Stratigraphic field relations are mostly inconclusive, although some indicate inclusion of pre-MIS 3 deposits, as noted above.

Unit Qpu_{op} in all aspects except age control resembles unit Qc_o, and much of it may be of that age (see *Ages of Quaternary Units*). The unit also includes deposits for which stratigraphic field relations suggest or require pre-MIS 3 age.

Stratigraphic field relations for pollen sample L6 suggest that it predates deposits that were mapped upslope as unit Qpu. Poorly exposed, weathered till in unit Qpu in this area suggests that it includes pre-Vashon, northern-sourced till. This suggests that pollen sample L6 predates MIS 3. The pollen data from L6 suggest cooler than modern paleoclimatic conditions similar to those recorded by pollen samples L1–L5 (Gavin, written commun., 2016). Pollen samples L1–L5 are discussed below in the context of MIS 3. The arguments presented below for proximity or presence in the map area of Olympic ice advances during deposition of unit Qc_o similarly apply to unit Qpu_{op}.

Radiocarbon sample GD1 from northwest of Shelton Valley yielded a late MIS 3 age but is shown on the map as part of unit Qpu_{op}. A 5-ft-thick section of interbedded silt and gyttja is exposed as a stiff block that yielded the samples for GD1 and pollen samples L1 and L2. The block is fractured, with clastic dikes of soft material, strongly suggesting post-glacial dike emplacement—either due to landslide movement, or due to tectonic activity. We favor the landslide hypothesis. The age and pollen analyses clearly record conditions that prevailed during late MIS 3, but we are uncertain if those conditions are associated with the sample site and its vicinity, or with younger deposits someplace farther upslope. Due to our suspicions of post-glacial downslope movement of the gyttja, we did not want to infer an MIS 3 age for surrounding deposits and therefore mapped the silt and gyttja at the upper end of a downslope polygon of Qpu_{op}.

Pollen samples L1 and L2 suggest cooler-than-modern conditions during deposition of the interbedded silt and gyttja that yielded these samples and age sample GD1; the stratigraphic relationship of these samples relative to a nearby exposure of possible Olympic Mountains-derived till is uncertain, although we suspect that post-glacial mass wasting moved the block of silt and gyttja downslope, and that the possible till is older. The age of the diamicton is not constrained by the date, and the timing of the cooler-than-modern conditions documented by pollen analyses L1 and L2 at age site GD1 relative to an Olympic ice advance suggested by the nearby diamicton is not known.

Deposits of MIS 3

In the Shelton Valley quadrangle, MIS 3 is marked mainly by deposition of Olympic Mountains-sourced pebble gravel (channel deposits) with less-voluminous diamictons, sand, silt, and sparsely scattered lenses of peat. The abundance of thick packets of pebble gravel and relative paucity of low-energy deposits (and especially of organic-rich deposits) suggests that the sediments mostly record episodes of rapid sedimentation and (or?) vigorous sediment flux.

Pebbly diamictons in some exposures were deposited as debris slurries into lakes, but elsewhere may include lodgment till from the Olympic Mountains. One exposure of possible lodgment till is in the active channel of Goldsborough canyon between Columnar Section 2 and C29 (1,150 ft upstream of CS2)(see also units Qc_o, Qat?, and *Faulting: Pre-Vashon Deposits at Photo Site P1*). We interpret these exposures as likely indication of proglacial (to glacial?) conditions in response to Olympic ice advances; this interpretation is consistent with pollen analyses that indicate a cooler than modern climate.

A robust record of MIS 3-age ice advances from the Olympic Mountains and associated pulses of voluminous outwash has been documented on the western Olympic Peninsula (Thackray, 1996, 2001; Thackray and others, 2015; Staley, 2015) and west of the map area on the southern Olympic Peninsula (Jaime Delano, Washington State Department of Transportation, oral and written commun., 2016). MIS 3 ice advances from the southeastern Olympic Peninsula are therefore plausible, and characterization of all MIS 3-age deposits in the Shelton Valley quadrangle as Olympia 'nonglacial' is likely inappropriate. We similarly infer that the undated unit Qpu_{op} is best mapped as undivided glacial and nonglacial because: (1) it may include deposits of MIS 3, (2) some outwash on the western Olympic Peninsula appears to date to MIS 5 (and/or 4?)(Thackray and others, 2015; Staley, 2015), and (3) unit Qpu_{op} is, like unit Qc_o, dominated by pebble gravel and includes possible Olympic Mountains-sourced till, but, unlike unit Qc_o, includes some deposits older than MIS 3. Except for older deposits within unit Qpu_{op}, the MIS 3 age of this record of mostly pebbly, mostly Olympic Mountains-sourced sediment is supported by ages along and near Goldsborough canyon (Figs. 8 and 14; Columnar Section 2).

In the headwaters of Gosnell Creek (and elsewhere in the Black Hills), it appears that MIS 3 was a time of reworking of pre-Vashon, northern-sourced glacial outwash (*Age of Northern-Sourced Glacial Deposits*; Columnar Section 1). We infer that these reworked deposits are confined to narrow valley corridors (Cross Section B) because: (1) outcrops and theoretical considerations of advance outwash deposition suggest that pre-Vashon northern-sourced sediment is voluminous and extensive in the upper Gosnell Creek watershed; (2) relief and headwaters upstream of Columnar Section 1 are small and steep, suggesting that nonglacial periods would be mostly erosional. Consequently, fluvial channel redeposition of the pre-Vashon northern-sourced glacial sediment would be neither voluminous nor extensive. Nonetheless, we favor MIS 3-age erosion and redeposition at Columnar Section 1 because the luminescence date (GD8) suggests it and three clast counts within the section reveal a systematic down-section increase in weathering (C20–C22, Columnar Section 1)—consistent with initial erosion followed by gradual aggradation.

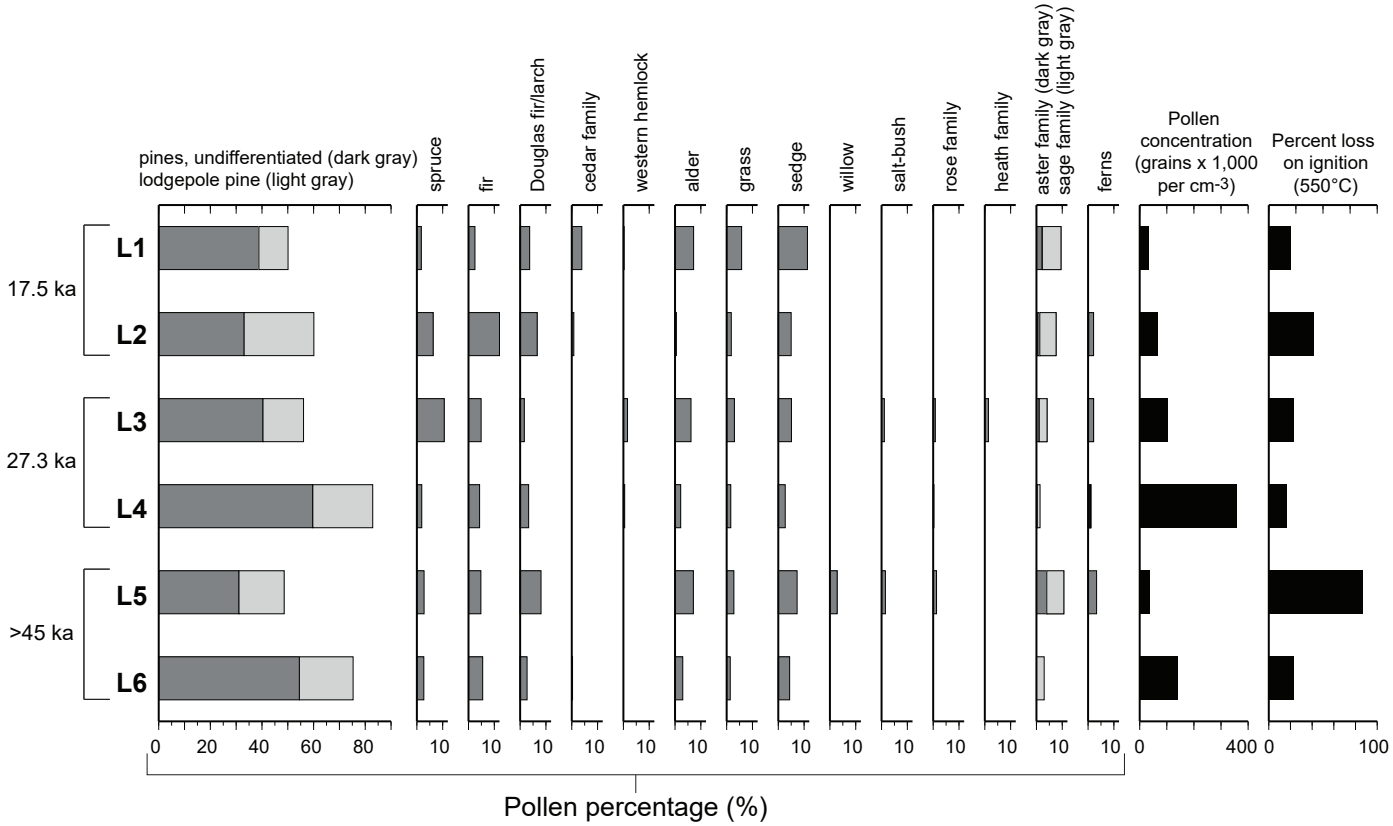

Figure 9. Pollen diagram for six organic-rich sediment samples from the Shelton Valley quadrangle. Two sites each have an upper and lower stratigraphic sample: L1 and L2 are from northeast of Shelton Valley; L3 and L4 are shown in Fig. 8. The ages for these sites are constrained by age site GD1 (at L1) and GD2 (at L3); ages are stated in calibrated calendar years. Sample L5 is identified in Fig. 14 and corresponds to age site GD4; L6 corresponds to age site GD5 at the east end of Goldsborough canyon. This figure plots pollen types with >1% abundance in any sample and is slightly modified from D. Gavin (University of Oregon, written commun., 2016). Pollen analyst Erin Herring, University of Oregon.

Pollen data from the Shelton Valley quadrangle (Fig. 9) document cooler-than-modern conditions that likely include the presence of glacial ice someplace nearby (Gavin, written commun., 2016). Age-control data and stratigraphic field relations strongly suggest that pollen analyses L1–L5 record conditions during MIS 3. The cooler-than-modern conditions documented by these pollen analyses add support to mostly cooler-than-modern MIS 3 paleoclimatic assessments from farther southeast and south (Grigg and Whitlock, 2002), west (Heusser and others, 1999), northwest (Florer, 1972; Heusser, 1972; Heusser and others, 1980; Cong and Ashworth, 1996) and north in Washington (Hansen and Easterbrook, 1974) and British Columbia (Clague, 1978; Alley, 1979; Hebda and others, 2016). However, radiocarbon age GD2—collocated with pollen sample L3 (Fig. 8)—suggests that at least one of our cooler-than-modern peat-forming interludes marks a global warm spell within MIS 3. We infer this because our 27.480–27.235 ka (calibrated 2σ) radiocarbon age estimate coincides with the Dansgaard-Oeschger (brief warm stadial) event 3a from a Greenland Ice Core oxygen isotope record (Fig. 10). Assuming this brief warm stadial, peat-forming event at site D2 also corresponds to a relatively warm (or dry?) spell in the map area, then most of unit Qc$_o$ may be alpine-glacial outwash—as suggested for other reasons above. The coincidence of sample L3 and a global warm spell might explain the contrast of the peat-forming interlude at site D2 with otherwise mostly pebbly exposures of unit Qc$_o$ in Goldsborough canyon.

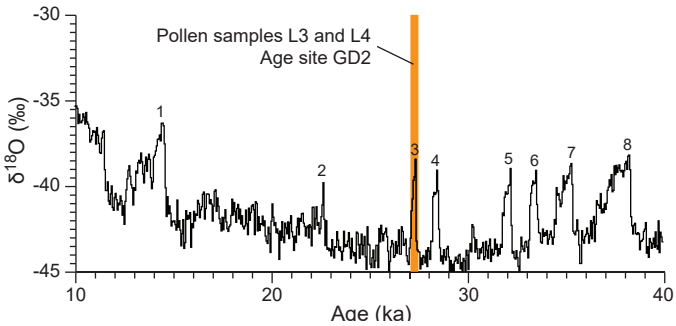

Figure 10. Pollen samples L3 and L4 are sampled from the same organic-rich sediment section as radiocarbon sample GD2 (calibrated radiocarbon age of 27.2–27.4 ka). This indicates deposition of the organic-rich section during a brief warm stadial event that is identified as (Dansgaard-Oeschger event 3) in the North Greenland Ice Core oxygen isotope record. Oxygen isotope record is from North Greenland Ice Core Project members (2004) and annotated numbers indicate Dansgaard-Oeschger events. Figure modified from D. Gavin (University of Oregon, written commun., 2016).

DEPOSITS, LANDFORMS, AND LAKES OF THE VASHON GLACIATION (MIS 2)

Glacial Advance

The Vashon glaciation may have started with inundation of low-lying parts of the Shelton Valley quadrangle by an ice-dammed lake that would have filled the Puget Lowland once Cordilleran ice had advanced to approximately the latitude of Port Ludlow, about 50 mi north of the Shelton Valley quadrangle. This mostly ignores isostatic effects that crustal loading from the advancing ice sheet may have had south of the ice sheet, and it assumes that late MIS 3 geography within the map area included surfaces that were open toward the Puget Lowland at lower elevation than any pathway for lake drainage from the Puget Lowland south to the Chehalis Valley. Widespread advance outwash sand in the map area appears to document such proglacial lake inundation and is represented by unit Qgas below 200 ft elevation in Isabella Valley, and smaller patches of sand, silt, or clay that were lumped into unit Qga, such as on the southern valley wall of Goldsborough canyon. Unit Qpf may also include lacustrine Vashon advance outwash and is found below 150 ft elevation on the southern margin of Shelton Valley and below 225 ft elevation along Goldsborough Creek just upvalley of Goldsborough canyon.

Once Vashon ice approached or entered the map area, proximal outwash graded upward into coarser and less-sorted fluvial deposits, with pebbly to cobbly outwash of unit Qgag ranging in elevation from 90 ft at the south side of Shelton Valley (secs. 25, 35, and 36, T20N R4W) to broad valley floor fills that extend up to at least 525 ft elevation east of Lost Lake (secs. 5–8, T19N R4W).

Glacial Maximum

The Shelton Valley quadrangle was entirely overrun by ice during the Vashon Stade (Fig. 1). This is documented by fluted landforms, ridge tops with striated bedrock, patches of till throughout the Black Hills, and absence of the more advanced soil development and deeper bedrock weathering commonly found south of the Vashon ice limit. The southwest corner of the map marks the Vashon ice limit and moraine deposits abound just north of there in the Shelton Valley quadrangle. We observed multiple exposures of basaltic saprolite and distinctly more advanced soil development just outside of the quadrangle within 800 to 2,500 ft south and southeast of the southwestern map corner. This places our assessment of the Vashon ice limit within 2,500 ft or less of prior assessments (Carson, 1970; Logan, 1987, 2003).

We interpret the large broad valleys in the map area as a product of sub-ice erosion—mainly by subglacial meltwater—as envisioned by Booth (1994). These features are notable in Isabella and Shelton valleys, and the valley of Goldsborough Creek in, south of, and east of Little Egypt Valley (secs. 18–20, 28, and 29, T20N R4W and secs. 24–25, T20N R5W). We infer that Goldsborough canyon was also present as a landform beneath the ice, and post-glacial erosion of the canyon was correspondingly limited. Evidence for this inference is provided by drapes of surficial till (mapped as unit Qgic) that extend from the upland surface north of Goldsborough canyon down into the canyon (secs. 14 and 15, T20N R4W), and from disjointed patches of till elsewhere in the valley floor (such as at the top of the section illustrated by Figure 14).

Glacial Recession

Unit Qgim along the western map edge marks areas where stagnant ice may have formed an ice margin. At the southwest map corner, we interpret unit Qgim as a terminal moraine that marks the maximum Vashon ice extent. Farther north, unit Qgim is about 4 mi northeast of the Vashon ice limit as mapped by Carson (1970) and Logan (1987, 2003), and we do not know if this "moraine" marks an ice margin (see description of unit Qgim). Farther east, scattered sub-ice landforms and associated deposits also document stagnant ice, although less dramatically. These include eskers at the western and southern fringe of well-developed flutes amid unit Qgic near the northern map boundary (sec. 10, T20N R4W). Fluted surfaces elsewhere (such as in secs. 26 and 27, T20N R4W) are locally disrupted by channels that we interpret as subglacial meltwater drainage conduits like those noted on the Kitsap Peninsula by Haugerud (2009) and Polenz and others (2009b)—features that moving ice would have obliterated. In the vicinity of the northwest corner of the quadrangle, fluted surfaces with some eskers appear to be kettled and surficially draped with outwash that reveals relict channels cutting across flutes, paradoxically without obliterating the fluted landforms. Instead, the channels follow the fluted surface morphology up and down across individual flutes—see Polenz and others (2010). We would ordinarily interpret kettles, and especially eskers, as evidence of stagnant ice but have been unable to explain how loose, surficial outwash channel landforms and deposits could be superposed across the fluting without obliterating the fluted landforms. We speculate that the outwash may have been subaerially deposited on a thin (and probably patchy) residual ice sheet that smoothed out and allowed for preservation of the underlying flutes, but to our knowledge these features remain unexplained.

Meltwater at the end of the Vashon Stade dissected much of the fluting in the map area and replaced it with a network of braided to meandering channels that are now relict. The channeled surfaces contain a patchwork of recessional outwash (units Qgo, Qgog) and exposures of underlying and more compact advance outwash (unit Qgag), all of which tend to be highly permeable (excessively drained), in contrast to the surrounding glaciated surfaces. In the north half of the map area, the relict channels moved outwash from the southern margin of the Skokomish Valley (Fig. M1) southeast to the Shelton delta (secs. 13 and 24, T20N R4W), albeit not everywhere along a direct pathway: one path follows Winter Creek and the North Fork Goldsborough Creek to their confluence, then runs southwest for 3 mi to Little Egypt Valley before apparently turning, first east, and then northeast, along Goldsborough Creek from where the drainage followed either Goldsborough canyon or (and?) a relict valley between Goldsborough canyon and Sanderson Field. The lowest point along this outwash pathway is about 1.7 mi east of Little Egypt Valley—which implies east-up tilting of the land surface sometime after formation of the outwash channels. The resulting trough explains the

formation of large peat areas and post-glacial deposition of unit Qa east of and in Little Egypt Valley.

Most post-glacial deposition in the map area likely occurred during or soon after glacial recession, when residual ice was still melting adjacent to ice-free areas. At that time, rates of geomorphic activity in at least parts of the Puget Lowland exceeded those in the modern environment (Carson, 1980; Kovanen and Slaymaker, 2004; Polenz and others, 2005, 2006, 2014, 2015), as is typical for periglacial environments (Ballantyne, 2002).

Glacial Lakes and Shorelines

Ice-dammed lakes filled large parts of the Puget Lowland during deglaciation (Bretz, 1910, 1913; Thorson, 1980). In the Shelton Valley quadrangle, lake-deltaic outwash deposits provide evidence for Vashon recessional ice-dammed lakes in at least four areas:

North Side of Isabella Valley

Along the eastern edge of the map area along the north side of Isabella Valley (sec. 1, T19N R4W and sec. 36, T20N R4W), a well-expressed delta-front slope break ranges from 200 to 225 ft elevation. The lower-elevation slope breaks may have been somewhat lowered by kettle-related settling after formation. A small remnant of a marginal terrace exists between 226 and 232 ft elevation along the western fringe of the delta complex. This remnant suggests an earlier and higher lake level. To the northeast and just outside the Shelton Valley quadrangle a kettled surface terminates in a concentric lobe that protrudes eastward into Isabella Valley and morphologically suggests an additional, slightly lower, Isabella Valley lake surface (close to 185 ft).

Both Sides of Shelton Valley

The outwash channel that terminates at the delta complex on the north side of Isabella Valley (see above) extends from that delta westward to Shelton Valley. Map units within the channel include Qgo, Qgof, Qp, and Qaf. The channel is morphologically distinct and slopes gently northwest toward Shelton Valley, where it also terminates, paradoxically, in apparently recessional deltaic? outwash (mapped as unit Qgo). Although the deposits of unit Qgo could alternatively be kame deposits, the northwest-down slope of the channel that connects them to the delta complex in Isabella Valley suggests that the flow direction in this channel might have reversed after formation of the 200–225-ft-elevation Isabella Valley delta. This reversal may be in response to tilting of the landscape due to isostatic rebound as ice loading decreased, with subsequent drainage from Isabella Valley feeding into a lake surface that is well expressed by outwash deposits in three locations around Shelton Valley (included with map units Qgo, Qgos, and Qgod), at about 180 to 200 ft elevation; more subtle slope changes and mid-slope termination of small drainages on the south side of Shelton Valley document that an earlier lake level also reached about 220 ft on the south side of the valley.

West End of Shelton Delta

At the west end of the Shelton delta (secs. 13, 14, and 24, T20N R4W)(Bretz, 1910, 1913; Thorson, 1981; Polenz and others, 2010, 2011) delta-top surfaces are between 200 and 215 ft elevation (mapped north of Goldsborough Creek as units Qgog, Qgod, and ml, and possibly south of Goldsborough Creek as Qgo). These elevations suggest water surface levels between 200 and 210 ft—coincident with the approximately 200 ft water surface level suggested on the margins of Shelton Valley. Based on similar delta-front slope-break elevations, it appears that the Shelton Valley exposures—like the Shelton delta—are an expression of Lake Russell. At least one of the three lake levels documented by the delta complex on the north side of Isabella Valley also corresponds well to the Lake Russell surface level at the Shelton delta. If the above speculation about rebound-related land level changes and tilt are correct, we cannot rule out that all three lake levels at the Isabella Valley delta complex correspond to Lake Russell. A terrace segment west of the Shelton delta slopes northwest, like the channel between Isabella and Shelton valleys, perhaps providing additional evidence in support of west-down tilting during the retreat of Vashon ice. This terrace segment is mapped as units Qgic (south of clast count site C15), Qpt (north of C15) and Qco (west of C15), due to map crowding and scant evidence for outwash deposition on the well-expressed terrace surface. A prominent outwash terrace (unit Qgog) between 180 and 155 ft elevation south of Goldsborough Creek at the Shelton delta may have formed in response to lake-level lowering from Lake Russell to Lake Bretz.

Kettles within units Qgod at the Shelton delta, and on the north side of Isabella Valley, indicate that at least some delta deposition into Lake Russell occurred while ice still partially covered the surface.

West of Gosnell Creek

West of Gosnell Creek unit Qgos extensively drapes the valley side between 200 and 450 ft elevation. Up to 20 ft of lake bed section was observed near the base of the deposit. The elevated upper limit of this deposit implies deposition at least partly into an early local lake.

POST-GLACIAL CONDITIONS

Based on figure 3 of Polenz and others (2015), we estimate that post-Vashon ice-free conditions began sometime between about 15.8 and 15.3 ka (see *Ages of Quaternary Units*). Hillslope erosion and fluvial transport and deposition clearly continue in the modern environment, but we suspect that geomorphic change has been minor compared to when glacial conditions prevailed (Ballantyne, 2002; see also *Glacial Recession*).

PALEOGEOGRAPHIC CONSIDERATIONS

Pre-Vashon geography in and near the map area is mostly unknown but likely differed substantially from the modern landscape. Pre-Vashon sediment north of the Black Hills is mostly Olympic Mountains-sourced. The maximum elevation of pre-Vashon northern-sourced glacial outwash exceeds 400 ft in the headwaters of Isabella Valley (see unit Qpo; Fig. M1).

North of the Black Hills, the modern land surface is mostly lower than that, and pre-Vashon sediment exposures mostly indicate an Olympic Mountains source. This suggests either that not much northern-sourced sediment was deposited in the north half of the map area during pre-Vashon incursions of Cordilleran ice, or that such sediment was subsequently eroded away. Given the abundance of surficial Vashon sediment in the north half of the map area, we favor the latter option.

Ice from the Olympic Mountains likely did not impede deposition of pre-Vashon northern-sourced drift in the north half of the Shelton Valley quadrangle. Research on the timing and sedimentation from Olympic Mountains-sourced alpine glaciations on the west side of the Olympic Mountains may offer some support for extensive erosion of northern-sourced pre-Vashon sediment from the north half of the map area. Thackray (1996, 2001), Thackray and others (2015), and Staley (2015) have suggested that Olympic Mountains alpine glaciations were much more extensive and produced much greater outwash volumes during MIS 3 (and 5?) than during the Vashon ice advance (MIS 2). If their conclusions from the western slope of the Olympic Mountains correlate to the southeast side, then ice from the Olympic Mountains likely also was most influential in the Shelton Valley quadrangle during 'nonglacial' pre-Vashon intervals, such as MIS 3 and MIS 5—and Olympic Mountains-sourced ice did not impede deposition of pre-Vashon northern-sourced drift in the north half of the Shelton Valley quadrangle during northern ice advances, such as MIS 6. Hence, it seems likely that northern drift was first deposited and subsequently eroded prior to deposition of the Olympic-sourced sediment that now abounds in the subsurface. This erosion may have occurred subglacially during Olympic ice incursions into the north half of the map area, or low-lying areas farther east (or west?) permitted streams in the north half of the map area to erode older sediment, much as in the modern environment.

An incursion of ice from the Olympic Mountains into the north half of the map area may explain why northern-sourced sediment, once eroded from the south half of the map area, was proximally re-deposited at relatively elevated sites. An example is at Columnar Section 1, where such re-deposition during MIS 3 is suggested by age site GD8 and weathering data that suggest a record of aggradation with more weathered—and thus older?—MIS 3 deposits lower in the section. If ice from the Olympic Mountains advanced to the northern margin of the Black Hills, it could have dammed drainages in the northern Black Hills and caused aggradation in previously erosional settings, like the location of CS1.

The modern Skokomish River likely did not have an MIS 3 analog. Polenz and others (2010a) presented a 41,710 ±2,320 ^{14}C yr BP age for organic sediment at their locality M906, on the northern valley wall of the lower Skokomish River valley, 4.8 mi north of the Shelton Valley quadrangle at 210 ft elevation (sec. 10, T21N R4W). The sediment appears to be part of a section with alternating flood plain to bog and shallow lacustrine conditions. If the age estimate is accurate, it suggests a mid-MIS 3 paleo-Skokomish Valley floor (and river corridor) close to 210 ft elevation. If the ages from sites GD7 and GD2 in the Shelton Valley quadrangle are likewise accurate, it follows that throughout much of MIS 3, a sizeable Olympic Mountains-sourced river flowed south to the latitude of Goldsborough canyon, where age sites GD2 and GD7 suggest valley floor elevations close to 170 ft (at GD7, Columnar Section 2, Table A2) and 135 ft (at GD2, Table A2). One way to interpret the ages and elevations at GD2, GD7, and M906 (Polenz and others, 2010a) is to imagine a river system that drained from the lower Skokomish River valley south to the Goldsborough Creek basin, which would imply a paleo-geography substantially different from the present. One could alternatively imagine that the North Fork Skokomish River drained to Polenz and others' site M906 while the Goldsborough canyon sites might have been fed by a separate basin that included the South Fork Skokomish River valley, and (or) maybe even the Wynoochee River basin.

For all scenarios, it is not clear by what route any of these rivers drained to the sea. During northern ice advances, ice filled the Strait of Juan de Fuca and drainage from the southern Olympic Mountains would have been southward through the Chehalis River. Salmon fossils have provided evidence for this pattern from the South Fork Skokomish River long before the Vashon Stade (Smith and others, 2007). Present-day landforms and the 35 ft elevation drop from site GD7 east to GD2 tempt us to imagine that north-directed river systems similar to today's prevailed after earlier northern ice advances. Yet there certainly were times that lacked an ancestral equivalent to the modern Hood Canal (Deeter, 1979; Polenz and others 2011, 2012c, 2013, 2015; Contreras and others 2010, 2013, 2014). Therefore, north-directed drainage could have looked quite different than today, and drainage south from the Skokomish River basin to the Chehalis River may also have been viable during nonglacial times—especially in light of the possibility that Olympic-sourced ice advances during 'nonglacial' times like MIS 3 (and earlier equivalents) may have moved Olympic ice as far south as the northern Black Hills and thus radically rearranged the landscape in at least the north half of the Shelton Valley quadrangle.

Our observations of Olympic Mountains-sourced diamictons in the Shelton Valley quadrangle hint at Olympic ice incursions to the edge of the Black Hills—and associated rearrangement of sediments and landforms north of the Black Hills. Some of these Olympic Mountains-sourced diamictons may be tills (see units Qat?, Qc_O, and Qpu_{Op}) of MIS 3 age (for instance, clast count C26 at the base of Columnar Section 2); elsewhere, their age is constrained only to pre-Vashon time. The diamictons include (and may in all instances be) pebbly debris slurry deposits into lacustrine silt, clay, and sand. The mere presence of these lakes may hint at nearby ice (to create lake dams) in a setting that otherwise seems to be filled mostly by pebbly channel gravel. In any case, the modern land-level drop from the 210 ft elevation of Polenz and others' (2010) radiocarbon age site in the lower Skokomish River basin need not correspond to land-level differentials that prevailed during MIS 3. Elevation changes among relict Vashon recessional-lake shorelines along southern Hood Canal suggest that there may have been significant post-glacial relative land-level change(s) between the southern margin of the modern lower Skokomish Valley and areas farther north (Polenz and others, 2012b,c), and

the considerable deformation exposed in Goldsborough canyon adds to the paleogeographic uncertainty. The main message is that pre-Vashon geography in and near the map area likely differed substantially from the modern landscape.

Landforms from Isabella Valley via Gosnell Creek, Lost Prairie, and from there west beyond the Shelton Valley quadrangle (Fig. M1) suggest to us that a subglacially carved valley (resembling the inlets of the Puget Sound) may once have run from Isabella Valley west via Lost Prairie toward the Chehalis River or the East Fork Satsop River. Our geophysical data sites GP2 (Isabella Valley), GP4 (Gosnell Creek) and GP7 (Lost Prairie) all suggest a bedrock surface elevation at or below modern sea level, consistent with the former presence of such a valley. We infer that this valley was excavated sometime before MIS 4 because we interpret the northern-sourced drift on both sides of the valley as older than MIS 4 (see *Age of Northern-Sourced Glacial Deposits*).

GEOCHEMISTRY

Sixteen new geochemical analyses (sites G1–G16) are compared (Fig. 11) to geochemical samples compiled from elsewhere in western Washington. Table 4 explains sample groupings and compilation sources.

The analyses confirm that on a plot of $Na_2O + K_2O$ vs. SiO_2 (Fig. 11A), and on a plot of P_2O_5 vs. TiO2 (Fig. 11D), volcanic rocks from the Shelton Valley quadrangle are relatively tightly clustered within the compositional range of basalt mapped as Crescent Formation elsewhere in Washington. A relatively high iron to magnesium ratio, with low total alkali content ($Na_2O + K_2O$) identifies samples from the quadrangle as tholeiitic (Fig. 11B), consistent with basalt elsewhere in the Black Hills (Globerman, 1981; Logan and Walsh, 2004). In contrast, basalt from the Olympic Mountains ranges from tholeiitic to calc-alkaline. As is the case with basalt of the Crescent Formation elsewhere, trace element content in samples from the Shelton Valley quadrangle resemble E-MORB (enriched mid-ocean ridge basalt) far more than either N-MORB (normal mid-ocean ridge basalt) or OIB (ocean island basalt)(Fig. 11C). The similarity to E-MORBs suggest a possible link to a plume

Figure 11 (facing page). Geochemical characterization of basalt from the Shelton Valley quadrangle. Sources and sample groupings are discussed in Table 3.

A) Total alkali (Na_2O+K_2O) versus SiO_2 diagram indicates Shelton Valley samples are basalt, similar to most of the Crescent Formation; the Shelton Valley samples trend towards low SiO_2 content—a trend not shared by some basalt samples from the Black Hills or the Olympic Mountains. TAS classification diagram of Le Bas and others (1986).

B) AFM (total alkali–FeO–MgO) diagram indicates Shelton Valley samples are tholeiitic and have a restricted compositional range. Boundary line between tholeiitic and calc-alkaline is from Irvine and Baragar (1971).

C) Trace-element diagram shows that Shelton Valley samples are most similar to an enriched mid-ocean-ridge basalt (E-MORB). Trace element content is normalized by C1 Chondrite values from Sun and McDonough (1989). Global average values for E-MORB and N-MORB are from Gale and others (2013) and OIB values are from Sun and McDonough (1989). Shelton Valley samples are shown as an orange region that corresponds to the maximum and minimum values. Lines for the Olympic Mountains and Black Hills are averages. Due to limited trace element data the samples of Globerman (1981) are excluded from this plot. Some uranium values from the Olympic Mountains dataset were anomalously high and were excluded from the plot.

D) Abundances of P_2O_5 and TiO_2 indicate that Shelton Valley samples are mid-ocean ridge basalts and near the upper range of basalt from the Crescent Formation. Other Eocene–Oligocene-age volcanic rocks from adjacent areas of western Washington are shown for comparison. Samples of Globerman (1981) are excluded from this plot because no P_2O_5 was reported.

E) Abundances of Y/Nb and Zr/Nb indicate that Shelton Valley samples are enriched mid-ocean ridge basalt and compositionally restricted. The Shelton Valley samples are also similar to the "upper member" of the Crescent Formation from Babcock and others (1992). Plot is modified from Babcock and others (1992) and values for OIB, E-MORB, and N-MORB are from Sun and McDonough (1989).

F) Abundances of Cr and Y indicate that there was about 23–27% partial melt for Shelton Valley samples. Solid lines represent trends for 30%, 20%, and 15% partial melting (Pearce and others, 1984). Figure is modified from Pearce and others (1984) and Clark (1989).

Table 3. Sample groupings and data sources for compilations of volcanic rocks from western Washington, as grouped in Figure 11.

Sample grouping	Comments	Sources
Shelton Valley	Samples from the Shelton Valley quadrangle.	This study
Black Hills	Samples from the Black Hills and classified as Crescent Formation in referenced sources. Globerman's 30 samples include fewer analyses than samples from this project or other sources and are therefore omitted from some plots. Globerman's samples include (and our "Shelton Valley Crescent" grouping excludes) four samples from the Shelton Valley quadrangle—his samples 10.18 1A, 1B, 1C, and 1G, collected between Isabella and Shelton valleys.	Globerman (1981) Bowman and others (2014)
Olympic Mountains	Samples from the Olympic Mountains and classified as Crescent Formation in referenced sources.	Bowman and others (2014) Dosewallips composite section of Babcock and others (1992)
'Lower' Crescent Formation	Dosewallips composite section samples identified as "lower" Crescent Formation in referenced source.	Babcock and others (1992)
'Upper' Crescent Formation	Dosewallips composite section samples identified as "upper" Crescent Formation in referenced source.	Babcock and others (1992)
Grays River volcanics	Volcanic rock samples from the Grays River area in southwest Washington as defined by Philips and others (1989) and Chan and others (2012).	Phillips and others (1989)
Northcraft Formation	Volcanic rock samples identified as Northcraft Formation in referenced source.	Phillips and others (1989)

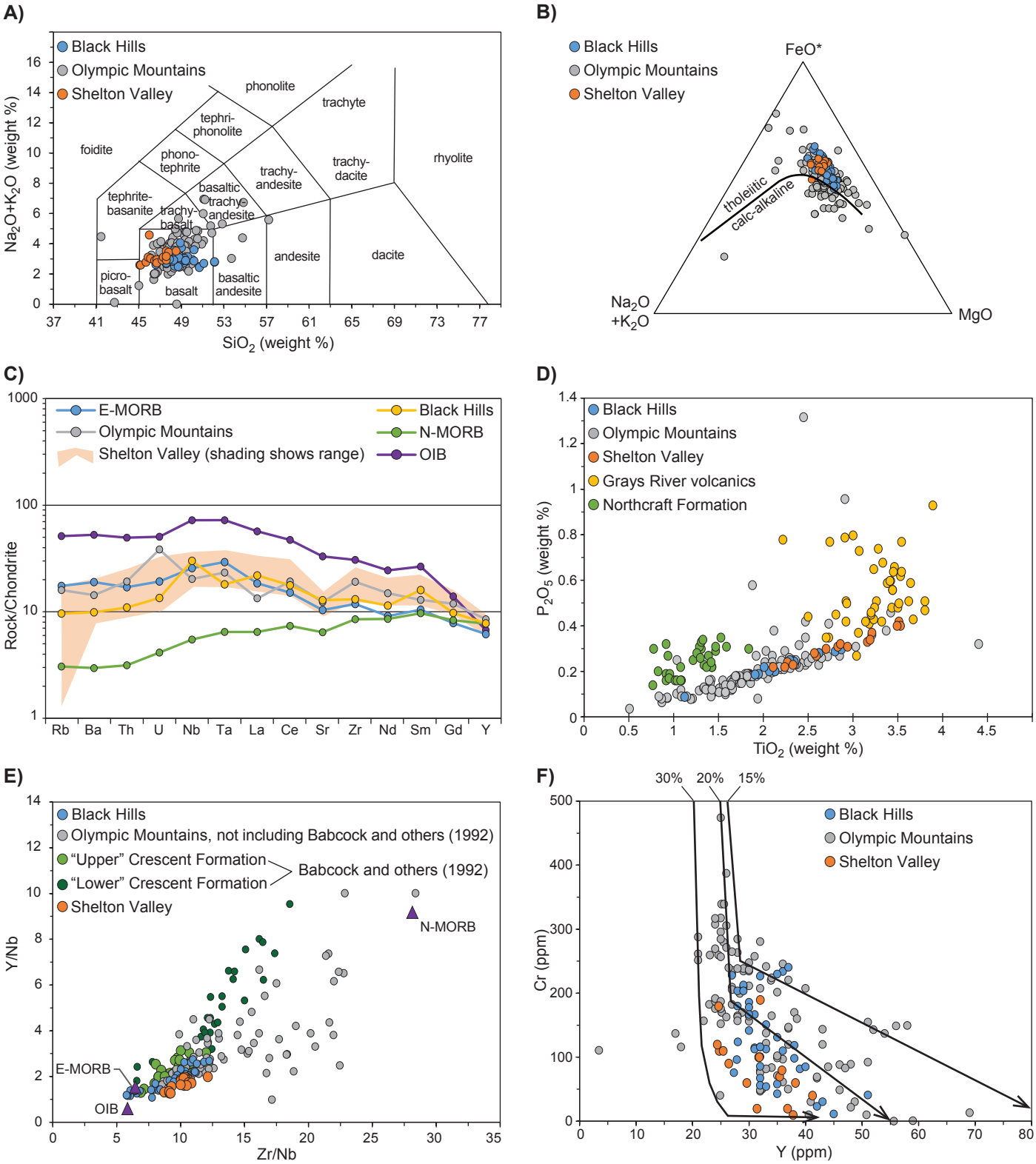

or a slab window, or selective sampling of off-rift melts (low partial melting). Our samples and other Crescent Formation basalts share a well-defined positive linear trend between P_2O_5 and TiO_2 (Fig. 11D). This contrasts with basaltic rocks of the younger, Cascade Mountains-affiliated Northcraft Formation (low TiO_2) found close to the Black Hills southeast of the quadrangle (Walsh and Logan, 2005; Logan and others, 2009). It also differs from high TiO_2 forearc volcanic rocks of Grays River (Phillips and others, 1989; Chan and others, 2012) found south of the Black Hills within the geographic range of the Siletzia province (Wells and others, 2014). A plot of Y/Nb vs Zr/ Nb (Fig. 11E) suggests that basalt in the Shelton Valley quadrangle belongs in the upper Crescent Formation member. This finding resembles the association to upper Crescent Formation that Logan and Walsh (2004) made for basalt in the Summit Lake quadrangle southeast of the Shelton Valley quadrangle.

Babcock and others (1992) further interpreted "variations in Y/Nb and Zr/Nb ratios of the magnitude displayed by the Crescent basalts" as evidence of "source heterogeneities". In that light, the tight clustering of the Shelton Valley samples at the low end of the Crescent Formation range of Y/Nb ratios (Fig. 11E) suggests that Shelton Valley samples share a source that differs from most Crescent Formation rocks elsewhere in Washington. The degree of TiO_2 enrichment is comparable to the younger volcanic rocks of Grays River (Fig. 11D). This TiO_2 enrichment matters for theories about the evolution of Eocene and younger volcanic rocks in the Pacific Northwest; these theories call on either slab windows or plumes as a source of mantle enrichment—see, for example Tepper (2016). A plot of chromium vs. ytrium (Fig. 11F) reveals more than 20 percent partial melting of source material for all but one of our samples, compared to broader scatter, and on average lower degrees of partial melt, among the totality of Crescent Formation samples.

GEOPHYSICS OF THE MAP AREA

Introduction to Data Sources

Efforts to identify active structures beneath the glacial deposits filling the Puget Lowland often include of a mixture of field-based measurements, geophysical surveys, and remote sensing techniques due to extensive Quaternary sedimentation. Local efforts to identify active faulting transect the steep northwest-striking geophysical lineament referred to as the 'Olympia structure' (see *The Olympia structure* above). Previous studies have utilized aeromagnetic, ground-based magnetic, gravity, and marine- and land-based seismic surveys (Fig. M2) in efforts to model the Olympia structure (Pratt and others, 1997; Magsino and others, 2002, 2003; Clement and others, 2010; Odum, written commun., 2014, 2015, 2016).

Geophysical Observations

The strongest supporting evidence for a tectonically significant Olympia structure continues to lie within the overlap of steep northwest-trending gravity and aeromagnetic anomalies bounding the southwest margin of the Tacoma basin (Figs. 1 and M2). A relatively smooth gravity anomaly there suggests a descent of the dense basalts of the Crescent Formation from surficial exposure in the Black Hills northeastward into the Tacoma basin (Fig. M2). The region-scale, northwest-trending aeromagnetic anomaly between the Black Hills and the Tacoma basin broadly coincides with the gravity anomaly, yet the two trends differ markedly at more local scales. Variations between the two data sets may be influenced by inherent differences in the nature of the two data types, specifically the depth profiles they represent, and the lesser data density in the gravity data.

The aeromagnetic anomaly associated with the Olympia structure is symbolized in Figure M2 as a northwest-trending magnetic low (blue trough) in the vicinity of the Shelton Valley quadrangle. This magnetic low is strongly expressed near the Shelton Valley quadrangle but is not continuous elsewhere along the Olympia structure, which is otherwise segmented by smaller east- or northeast-trending anomalies in multiple locations (Clement and others, 2010 and Odum, written commun., 2014, 2015, 2016). One such east-trending anomaly crosses the southeast corner of the Shelton Valley quadrangle. Logan and Walsh (2004), in the Summit Lake quadrangle to the southeast, noted that larger east-trending aeromagnetic anomalies are associated with alternately normally and reversely magnetized basalt and minor topographic lineaments, and these are cut by smaller northeast-trending aeromagnetic anomalies along more significant topographic lineaments and troughs. Prior work supports the local coincidence of normally magnetized basalt with aeromagnetic highs (reds), as opposed to reversely magnetized basalt with aeromagnetic lows (blues)(Globerman and others, 1982; Logan and Walsh, 2004). Bedrock exposures in the Shelton Valley quadrangle mostly correspond to aeromagnetic lows, suggesting that much of the surficial bedrock is reversely magnetized (Fig. M2).

Local seismic surveys along the Steamboat Island Peninsula and nearby marine basins east of the Shelton Valley quadrangle contribute to the mounting evidence in support of a structure related to the geophysical anomalies (Fig. M2). However, these supporting data provide clear evidence only for shallow structures that are speculated to be part of a larger 'Olympia structure' at depth and farther south (as documented in the *Geologic Overview* section above).

The basalt surface elevation also drops from the Black Hills northward. Basalt exposures are absent between the Black Hills and the Olympic Mountains, and gravity data suggest that the basalt surface north of the Black Hills forms a 'saddle' at the (north) western margin of the Shelton Valley quadrangle (Fig. M2). Although wells in this area did not penetrate basalt (all were less than a few hundred feet deep), our seismic data indicate basalt at 269 ft below the surface at geophysical data site GP1 (Table 3), near the 'crest' of the 'saddle'. The basalt surface dips both east to the Tacoma basin and southwest toward the coast. We speculate that the saddle may mark a tectonic boundary because our impression is that basalt flows in the northern Black Hills compared to those in the southeastern Olympic Mountains are marked by gentler dip angles, fewer shears, less internal deformation, and perhaps less alteration. See also *Implications for Future Investigations of the Olympia Structure*.

Implications for Future Investigations of the Olympia Structure

The patterns observed in the aeromagnetic anomaly associated with the Olympia structure may warrant a modified approach for future investigations. Previous efforts to document the Olympia structure have all been transects perpendicular to the northwest-trending geophysical lineament. Yet the aeromagnetic anomaly is segmented in multiple locations, and perhaps the segment boundaries offer evidence for more recently active faulting with a different orientation. This argument is strengthened by the observed association of segmentation of anomalies with the distribution of normal and reversely polarized basalt (i.e. basalt stratigraphy)(Logan and Walsh, 2004). The orientation of the 'saddle' in gravity contours may also suggest a northeast-striking structure that lowers bedrock elevations between the Black Hills and the Olympic Mountains. Zones of deformation along strikes that resemble the northeast-trending

aeromagnetic anomalies have been observed near the map area (Blakely and others, 2009; Mace and Keranen, 2012). If the northwest-trending aeromagnetic lineaments associated with the Olympia structure are in fact segmented along northeast-striking structures, then perhaps future efforts might be better spent along strike of the Olympia structure, specifically where the aeromagnetic data suggest that it is segmented.

STRUCTURES IN THE MAP AREA

Structures in the Shelton Valley quadrangle have largely been masked by deposition and erosion related to repeated Quaternary ice advances into the Puget Lowland. Scattered exposures throughout the map area provide a fragmented view of the degree to which these structures are laterally extensive. We caution that the kinematic analyses of this report relies on relatively few data points, but also note that the Shelton Valley quadrangle and surrounding areas do offer opportunity for additional targeted study of deformation in both bedrock and Quaternary deposits.

Bedrock

Bedding structures and minor faults were observed in basalt of the Crescent Formation in the south half of the Shelton Valley quadrangle (Map Plate and Fig. 12). Gently southwest-dipping to sub-horizontal flow orientations are suggested by sedimentary interbeds, chilled flow-top margins, and flow foliations (Fig. 13A). Landforms observable in the field and from lidar suggest that at least some gently sloping basalt flows are laterally extensive. It remains unclear if the implied gentle flow orientations record primary dips or have been modified by tilting.

Exposures of shears within the Crescent Formation in the map area are sparse and lack evidence for significant vertical offset. These structures are sub-vertical to steeply dipping and strike northeast or northwest (Fig. 13D); slickenlines (where apparent) show a mix of vertical and horizontal motion. Measured structures are often accompanied by sub-vertical concentrated joint sets (Fig. 13E) and surface lineaments on lidar. Although we mapped no faults in the bedrock beyond exposures at individual outcrops, clustering of orientations among structures and alignment of structures with surface lineaments suggest that some faults may be more extensive than outcrop scale.

If structures we measured in bedrock are treated as a conjugate pair, kinematic analysis provides opportunity for rough tectonic interpretations based on classic Andersonian theory (Fig. 13D). Planes to mean vectors for the two groupings of poles to fault planes imply a sub-vertical $\sigma 2$ axis (Fig. 13D). By definition, a sub-vertical $\sigma 2$ axis infers a sub-horizontal plane containing $\sigma 1$ and $\sigma 3$ (at 90º from each other) bisecting the two mean vectors that define the plane. These axes ($\sigma 1$ and $\sigma 3$) plunge gently east-northeast or gently east-southeast. Kinematic axes at these orientations are characteristic of strike slip regimes. We do not know which axis is $\sigma 1$ and which is $\sigma 3$—identifying the preferred orientations requires more kinematic indicators than we measured.

We observed three sub-vertical, unlithified clastic dikes that truncate bedding in either bedrock or Quaternary sediment. Two strike northwest, one northeast (map plate and Fig. 13E). These dikes were observed as 1/8-in. to 2-ft wide planes of sorted and unsorted silt to pea gravel-sized clasts. Their orientations approximate steep northeast- or northwest-striking faults in bedrock.

Unconsolidated Deposits

BEDDING

Goldsborough canyon provides a window into the pre-Vashon Quaternary stratigraphy and structure of the Shelton Valley quadrangle. Quaternary bedding orientations there range from gently southwest to moderately east-northeast dipping (Fig. 13A). Small-scale deformation of these Quaternary deposits is common and locally intense. Along the western

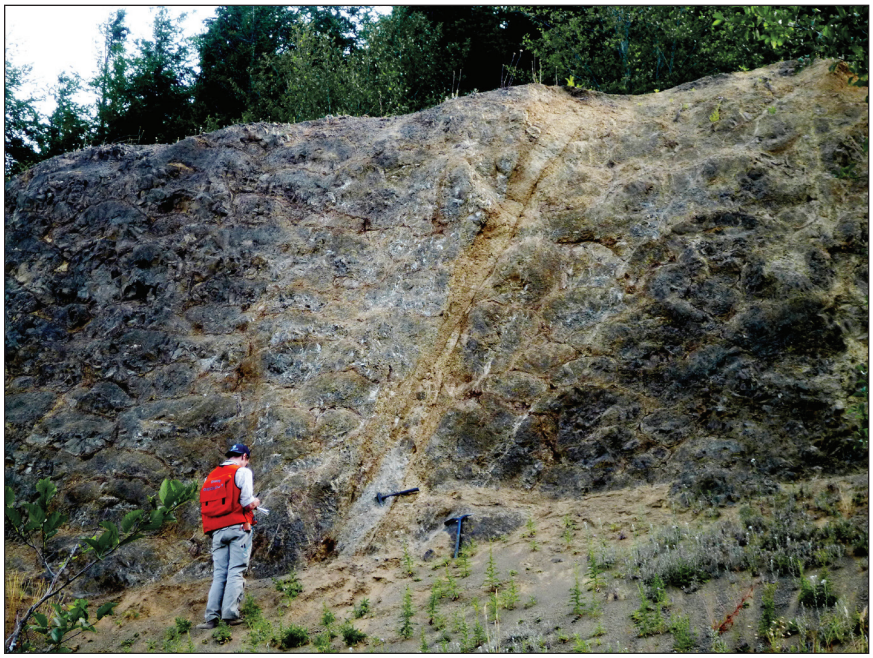

Figure 12. Photo of steep shear zone in pillow basalt flow of the Crescent Formation (photo site P3 on map). Shear zone is 1 ft wide and dips steeply northwest with slickenlines that rake 87° from the southwest. The shear zone truncates pillow boundaries and contains unconsolidated gouge-supported pillow basalt breccia. Well-developed pillows have distinct keels, radial colonnades, chilled margins, and perlitic textures flanking upper pillow margins.

A) Bedding in bedrock and unconsolidated units

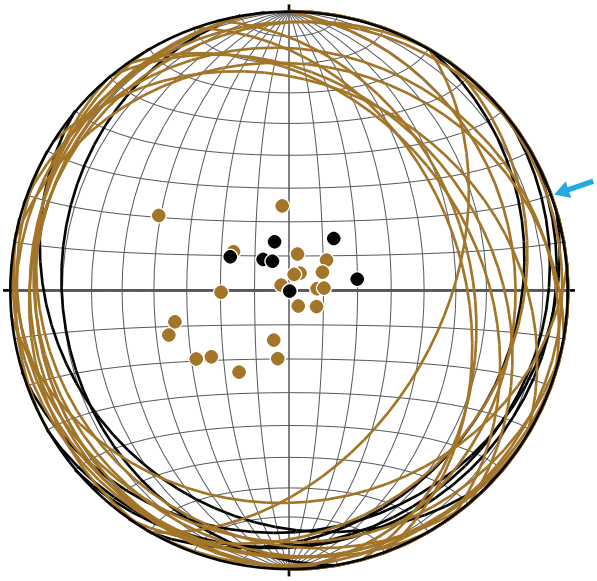

B) Low-angle faults in unconsolidated units

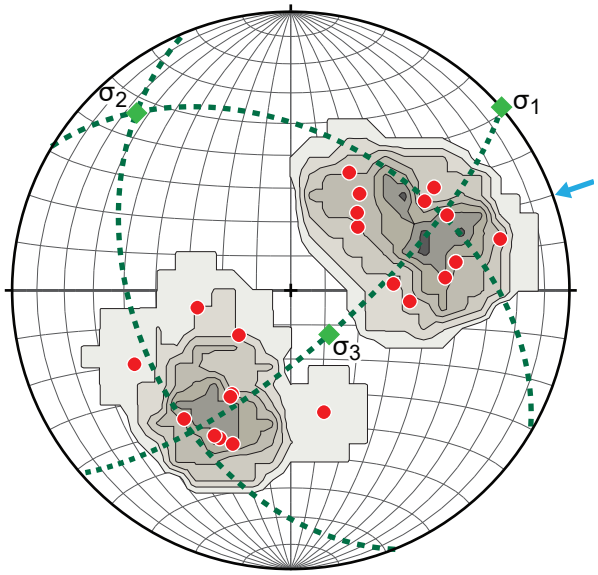

C) High-angle faults in unconsolidated units

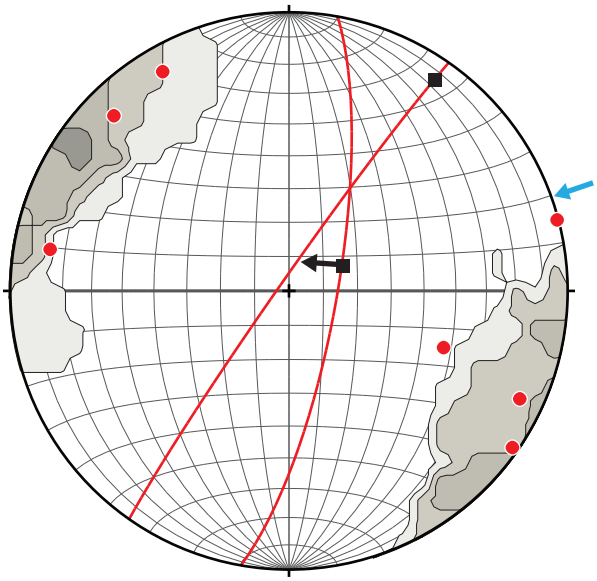

D) Faults in bedrock

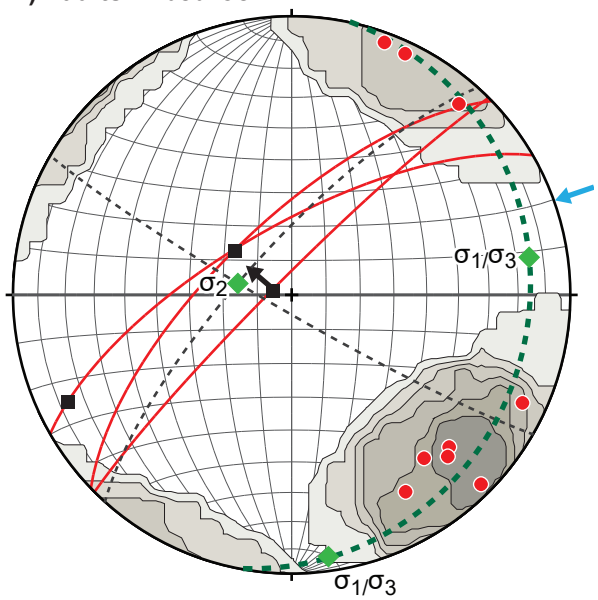

E) Joints and clastic dikes

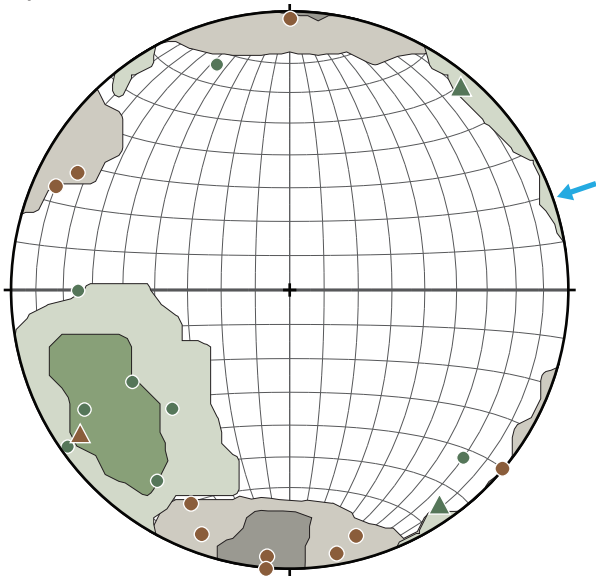

Figure 13. Stereonet plots for structures measured in the Shelton Valley quadrangle. Blue arrows on all plots indicate average ice flow direction (towards ~259°) in the quadrangle. We used Richard W. Allmendinger's 2011–2015 Stereonet © software (Allmendinger and others, 2013; Cardozo and Allmendinger, 2013; pdf file output per 2004© of Toby W. Rush).

A) Bedding planes and poles to bedding for bedrock (black) and unconsolidated units (brown).

B) Kinematic analysis (dashed green girdle and green diamonds) and kamb contours of poles to low-angle faults in unconsolidated units; average fault planes are dashed in black.

C) Kamb contours of poles to high-angle faults in unconsolidated units; slickenlines (and their fault planes) shown in black and red with arrows indicating slip direction.

D) Kinematic analysis (dashed green girdle and green diamonds) and kamb contours of poles to faults in bedrock; average fault planes are dashed in black; slickenlines (and their fault planes) shown in black and red with arrows indicating slip direction.

E) Kamb contour of poles to joints in bedrock (brown) and unconsolidated units (green); poles to clastic dikes shown with triangles.

half of Goldsborough canyon, between localized zones of intense deformation, bedding is generally sub-horizontal to gently dipping. Bedding dips increase with proximity to these deformed zones (Map Plate), and beds form gentle folds with structure-parallel hinge lines. Sites suitable to collect bedding attitudes along the east half of Goldsborough canyon are relatively dispersed but suggest a systematic (?) moderate northeast dip (see *Folding*).

FAULTING

Faulted exposures along Goldsborough canyon are localized within 100- to 200-foot-wide zones of concentrated deformation of older Quaternary units (Figs. 4, 8, and 14). These structures are commonly truncated by younger, sub-horizontal sediments (Fig. 4) of varied ages (ranging from MIS 2 to MIS 3 or older). Two distinct sets of structures in Quaternary deposits are identified along Goldsborough canyon when plotted on stereographic projections: (1) low-angle faults and (2) high-angle faults. Where these two groupings intersect, the low-angle faults are cut by high-angle faults.

Low-angle faults

Low-angle faults in the Quaternary deposits of Goldsborough canyon consist of moderately northeast and southwest-dipping thrusts (Fig. 13B) that display a larger degree of apparent offset compared to high-angle faults. Lithology of the basal deposits associated with the low-angle thrust are often finer grained (clay, silt, and organic-rich mud) than overlying gravel-rich deposits (Figs. 4 and 8). Imbricate thrust faults northeast of the bend in section on Figure 4 appear to rotate the interbedded sand and gravel to near vertical. The vergence of the northeastern set of imbricate thrusts in Figure 4, suggested by folding of beds along the fault planes, is opposite that of the southwestern set. An organic-rich mud and clay layer has about 30 ft of northeast-up throw on a northeast-dipping thrust (Fig. 8) and has a conventional radiocarbon age of 23,030 ±90 yrs BP (GD2). Because this layer is overlain by undeformed deposits related to the Vashon ice advance (16.5–16 ka), the deformation is constrained to between about 23 and 16 ka.

Field observations of the low-angle faults suggest the northeast- and southwest-dipping fault populations are a conjugate set of thrusts and back thrusts. Kinematic analysis of the measured low-angle thrust faults implies a horizontal northeast-trending σ1 (N49°E) and sub-vertical σ3 (Fig. 13B), characteristic of thrust-faulting regimes based on Andersonian theory.

High-angle faults

The high-angle faults in Quaternary deposits of the map area are largely northeast-striking structures, with a mix of sub-vertical and sub-horizontal slickenlines (Fig. 13C). These faults are often associated with similarly oriented concentrated joint sets (Fig. 13E). In Goldsborough canyon the steeply dipping faults splay vertically into minor shears and joints with less offset than the main structure lower in the exposure (Fig. 8). A similar observation of vertically diminishing deformation was also noted in Goldsborough canyon as a steeply northeast dipping plane of open southwest-vergent folds (see *Folding* below) within sub-horizontal strata of unit Qco.

These high-angle faults are in all cases the youngest structures in the Shelton Valley quadrangle. Where the interaction was observed, the high-angle faults always offset the low-angle thrust faults (Figs. 4 and 8). One of these high-angle faults also offsets the lower part of a surficial drift (Fig. 14; site P1 on map) and is therefore interpreted as being of Vashon or younger age (see discussion below), providing the only evidence for faulting as recently as the Vashon ice incursion. It remains unclear if the offset extends to the top of the surficial drift, however.

Deformation of possible Vashon Age in Goldsborough Canyon

We give special consideration to the deposits at photo site P1 along Goldsborough canyon (Fig. 14) because: (1) shearing observed in the Pleistocene deposits there and elsewhere along Goldsborough canyon may be tectonic, and (2) the shearing at P1 offsets drift of apparent Vashon age; if this is correct and the shear is tectonic in origin, this is the youngest faulted deposit recognized in the map area. Due to space constraints, the map plate shows only unit Qco in this part of Goldsborough canyon. At outcrop scale, however, the uppermost deposits appear to be Vashon drift. The following provides stratigraphic context for the site:

Deposits and paleoenvironment at photo site P1

At photo site P1, up to 14 ft of surficial drift consists of till (unit A—above annotated photo, and unit C) and a partly bedded drift (diamicton, silt, and sand) that appears to be glaciolacustrine (unit B). Unit A was mostly inaccessible; we interpret it as directly ice-deposited till. The contact between units A and B appears to be gradational. Unit B is a compact mix of bedded to laminated sand and silt with lenses and bands of diamicton (flow till or lodgment till). Significant particle rounding in matrix material of unit B was observed in thin section and is consistent with a glaciolacustrine setting (as opposed to directly ice-deposited diamicton, wherein we would expect a greater content of angular particles). Unit C is diamicton that resembles unit A. An irregular contact with unit B suggests that it is glaciolacustrine, however.

Pre-Vashon deposits at photo site P1

Below the surficial drift at Figure 14 is 2.5 ft of nonglacial sediment, mostly laminated silt (units D and E in Fig. 14). Gyttja from the upper 8 in. of this 2.5 ft section yielded a radiocarbon-infinite age (GD4) and pollen sample L5. As noted above, pollen analysis documents a cooler-than-modern, possibly periglacial paleoclimate consistent with the late Pleistocene pre-Vashon paleoenvironmental record elsewhere in western Washington. The pollen-based inference of periglacial conditions is consistent with observations that suggest the underlying pebble gravel (unit F) may be glacial. The 2.5 ft of nonglacial sediment overlies 10 ft of basalt-rich pebble gravel with a mud-rich matrix, which forms the base of the exposure shown on Figure 14. At photo site P1 (Fig. 14), this muddy, basalt-rich pebble gravel forms the upper end of a section that

locally ranges from pebble gravel to diamicton and can be laterally traced downvalley to Columnar Section 2; along the way, most of the exposure is best characterized as diamicton that we suspect may have been deposited by debris flow(s) into a lacustrine setting. It appears to range to or interfinger with till, as suggested at the base of Columnar Section 2, where it is shown as unit Qat? just downsection of the MIS 3-aged sand at site GD7. Even if it is not till, the apparently lacustrine character of the pebble gravel may favor association with an ice advance into this part of the map area, as Carson (1970; 1980) has associated ice dammed lakes with pebbly debris flow deposits into lacustrine settings south of the Olympic Mountains, and similar associations are apparent at radiocarbon infinite GD3.

Provenance of surficial drift at photo site P1

A clast count and petrographic examination of matrix material of unit B suggest that the glaciolacustrine drift is northern-sourced. Petrographic examination of the glaciolacustrine matrix revealed that polycrystalline quartz (some with microveins) is common in the matrix. Clasts for clast count C27 (Fig. 14 and Data Supplement) could only be collected within five feet of the base of the drift (within unit B). Three intermediate igneous clasts suggest non-Olympic (for example, northern) provenance, but—atypically for northern-source drift—neither granitic nor high-grade metamorphic clasts were identified. Additionally, a high basalt-clast content (58%), moderate sandstone content (22%), and little overall clast diversity suggest an Olympic Mountains provenance. The abundance of basalt and sandstone clasts at the expense of northern-sourced clasts in the basal part of the drift likely resulted from northern-sourced ice picking up and enriching the drift with Olympic-sourced substrate.

Age of surficial drift at photo site P1

Although we interpret the drift at the top of Figure 14 (units A to C) as Vashon in age, age-control data are not conclusive.

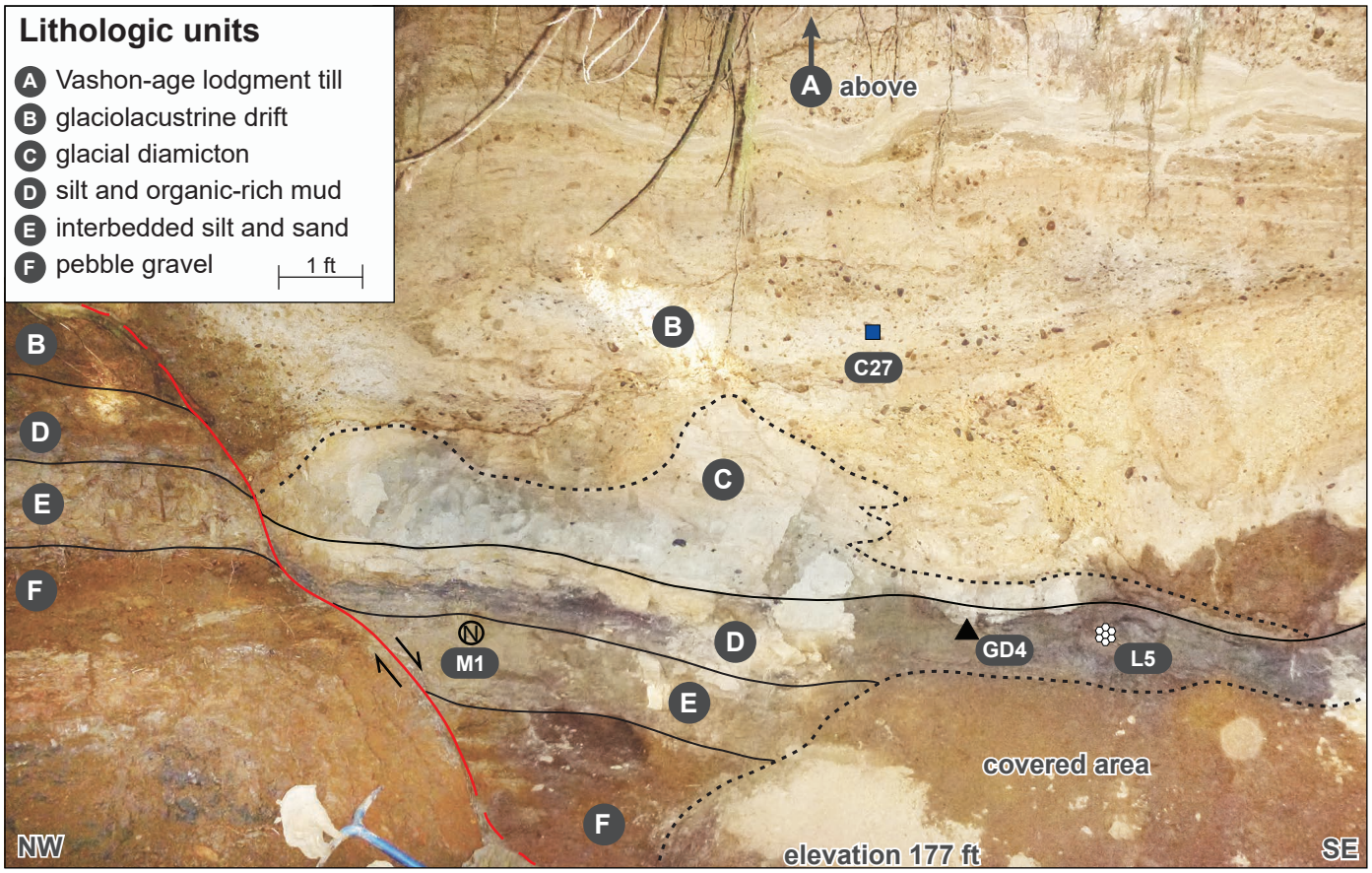

Explanation

bedding contact, short dashed where approximate

fault, showing offset direction

L5 pollen sample site

GD4 geochronology sample, ^{14}C, carbon-14

C24 clast count sample site

M1 paleomagnetic sample site, normal polarity

Figure 14. Annotated photo of subvertical SSE-striking fault in subhorizontally bedded Quaternary deposits along Goldsborough canyon (photo site P1 on map). Due to map scale, site details are not shown on the map (deposits shown as unit Qc_O). The deposits at this site are capped by Vashon lodgment till (unit A; just above top of photo). Poor exposure prevented observation of any deformation in the lodgment till. Units A to C are interpreted as Vashon age. Units D to F are mapped as unit Qc_O based on a >43,500 ^{14}C year BP radiocarbon age from unit D (age site GD4) and the observation that these layers appear to correlate with down-valley age site GD7 (Columnar Section 2; Table A2). Base of outcrop is at 177 ft elevation. Clasts of unit B are northern-sourced and mildly weathered (clast count site C27). Pollen analysis from unit D suggests a cooler-than-modern climate (pollen site L5). Silt beds in unit E have normal polarity (paleomagnetic site M1)..

The matrix and clasts in this drift are only lightly weathered, consistent with a Vashon age. The radiocarbon-infinite age analysis from downsection unit D (GD4) implies that the sediment below the surficial drift pre-dates late MIS 3 time, but the radiocarbon sample does not constrain the age of its host deposit to MIS 3—and therefore also does not constrain the upsection surficial drift to Vashon age (as a finite radiocarbon result would have done). Similarly, the paleomagnetically normal orientation of laminated silt below the gyttja does little to constrain the age of the deposits. Despite these limitations, we deem a pre-Vashon age unlikely for the surficial drift because: (1) The top of the section forms a localized patch of surficial drift that sticks up above the valley floor; field relations allowed us to confidently map other patches of surficial drift elsewhere along the valley floor as Vashon-age unit Qgic. (2) As noted above, the nonglacial deposits below the drift (units D and E) appear to be stratigraphically close to the nearby down-valley age site GD7 (MIS 3-age; Columnar Section 2). If older than Vashon age, the surficial drift would be of MIS 4 (Possession) or greater age, but as discussed above (*Pre-Vashon Northern-Sourced Glacial Deposits*), we deem incursion of Possession-age ice into the map area unlikely. A still-older drift age (MIS 6—Double Bluff) only makes sense if the surficial drift in Figure 14 is stratigraphically much below GD7. While we doubt this, it cannot be ruled out because the only demonstrable element of lateral continuity is the pebbly diamicton beneath the gravel at the base of Figure 14 (unit F). This diamicton can be traced down-valley to clast count C26 in Columnar Section 2 (just below MIS 3-age sand at GD7).

We interpret clast count C26 (Data Supplement) and the sedimentological character of the surrounding diamicton to suggest–but not require–that the upsection deposits shown on Figure 14 and Columnar Section 2 are of similar (MIS 3 and younger) ages, which, if correct, implies a Vashon age for the surficial drift. We favor an MIS 3 age for the basal diamicton based on: (1) the 47 ka luminescence age (GD 7) just upsection in Columnar section 2, although we cannot rule out a larger gap in section between the diamicton and the age; and (2) our suggestions of an Olympic provenance for the diamicton and of MIS 3-age ice advance(s) elsewhere in this part of our map area—and the recognition of vigorous MIS 3-age ice advances elsewhere on the western Olympic Peninsula (Thackray, 1996, 2001; Thackray and others, 2015; Staley, 2015) and southern Olympic Peninsula (Delano, oral and written commun., 2016). These arguments are far from conclusive, but if correct they require a Vashon age for the surficial drift at photo site P1.

FOLDING

A queried northwest-trending monocline is mapped in Quaternary deposits across Goldsborough canyon near Cross Section A. This structure was inferred based on systematic (?) moderate northeast dips of sedimentary deposits within unit Qpu_{op}. These dips were observed at four of five sites northeast of the inferred hinge line, whereas roughly horizontal to gently southwest-dipping bedding was observed southwest of the hinge line. The trend of the hinge line parallels joints and axial planes of open, upright, gentle, inch-scale anticlines and synclines (not mapped) in laminated silt at the intersection of the fold and Cross Section A.

A similarly oriented set of vertically diminishing folds was observed in younger and overall less-deformed deposits of unit Qc_o in Goldsborough canyon about 1,400 ft southwest of the monocline (sec. 22, T20N R4W). At this site we observed a steeply northeast-dipping plane of open southwest-vergent folds within sub-horizontal strata. The folding dies out up-section.

Interpretation of Structures

THE ROLE OF ICE SHOVE ON FAULTS AND FOLDS

Great care must be taken in the interpretation of faulting in areas where glaciers interact with unconsolidated sediments because glaciotectonic structures may form in response to an overriding ice sheet imparting a sub-horizontal compressive stress roughly parallel to the ice-flow direction (Benn and Evans, 1998; Wlodarski, 2014). Sites D1 and D2 along Goldsborough canyon (Figs. 4 and 8) share a similar style of deformation with well-studied glaciotectonic systems (Benn and Evans, 1998; Wlodarski, 2014).

We are unable to rule out glaciotectonics as origin of the deformation we observed in Quaternary deposits. However, we note that northeast-striking high-angle faults found in both Quaternary sediment and bedrock (Figs. 13C and 13D) suggest that they may share a similar cause, and we doubt that glaciotectonic effects would be strong enough to cause the faulting observed in the basalt bedrock. The average local ice-flow direction is about N71°E for the Vashon ice advance within the Shelton valley quadrangle (average of 20 flutes) and is similar to the inferred compressive stress (N49°E) for low-angle faults in the map area. The style of low-angle thrust faults in the map area (Figs. 4 and 8) is also quite similar to that described for glaciotectonic deformation by Benn and Evans (1998) and Wlodarski (2014) in at least three ways: (1) imbricate thrust sheets sole into less permeable deposits and are uncomforably overlain by undeformed drift; (2) there seem to be doubly vergent wedges of imbricate thrust sheets proximal to steeply dipping faults with low convergence angles (section B on Fig. 4), and; (3) low-angle thrust faults are offset by sub-vertical shears (Fig. 8). Seemingly high strain rates (30 ft of low-angle thrust offset between about 23 and 16 ka) implied at site D2 (Fig. 8) are consistent with the short-lived stress environment expected from a glaciotectonic setting.

LOCAL TECTONIC INFLUENCES

The Olympia Structure

This study identified northwest-trending Quaternary and bedrock structures (see discussion above) that may be expected in association with an active Olympia structure. In addition to being oriented similarly to the elusive 'Olympia structure', these features (excluding bedrock structures) are found within Goldsborough canyon, which directly overlies the geophysical lineament (note monocline in Fig. M2 for spatial reference). However, there is no evidence that any of these preferentially oriented structures have been active in the Holocene. Nevertheless, these structures and the monocline mapped in

Goldsborough canyon are likely the strongest evidence for an Olympia structure active in the Quaternary deposits of the map area. A structure of this nature could be expected to contribute to the growth of the Tacoma basin and a fold near this location has previously been proposed as a model for the Olympia structure (Daneš and others, 1965; Pratt and others, 1997; Gower and others, 1985). An Olympia structure active in the Pleistocene is therefore consistent with the available evidence from the Shelton Valley quadrangle; yet we do not show a structure in the bedrock beneath Goldsborough canyon (Cross Section A) because we are unable to rule out glaciotectonics as source of the deformation of the Pleistocene deposits. We note that if the monocline in the Pleistocene deposits at Goldsborough canyon were simply the surficial expression of a corresponding fold in the underlying bedrock, the dip angles in the Pleistocene deposits on the northeast side of the monocline would imply a much steeper bedrock surface slope into the Tacoma basin than is suggested by available data. If the monocline at Goldsborough canyon has a tectonic (instead of glaciotectonic) origin, we would therefore interpret the Pleistocene surficial deformation as response to a controlling structure at depth, likely a northwest-striking thrust.

Northeast-trending deformation

If the most recently active (northeast-striking and high-angle) faults in the Quaternary deposits of Goldsborough canyon are tectonic in origin, they may be related to regional northeast-striking structures previously interpreted as accommodating the partitioning of strain between the Olympic subduction complex and the Puget Lowland (Blakely and others, 2009; Lamb and others, 2012; Mace and Keranen, 2012; see *Regional Geology* above). Geophysical data suggest possible offset of northwest-trending anomalies along northeast-trending lineaments and the range in strike for the high-angle faults (Fig. 13C) approximates the majority of faults measured in the bedrock (Fig. 13D). This relationship may be evidence for activity along bedrock faults at a similar time. If the relation exists, the vertically diminishing strain observed at some of the high-angle faults in unconsolidated units may suggest the propagation of bedrock faults at depth, strengthening the argument that the two sets of structures are kinematically linked. It is also possible that the most-recently active structures observed in the map area are related to the clockwise rotation of discrete structural blocks defined throughout southwest Washington. Although structural interpretations are largely inconclusive at the scale of this project, exposures along Goldsborough canyon offer an opportunity for more targeted efforts to document local structures and add insight into the structurally complex region.

The northwest and northeast-striking clastic dikes (see *Bedrock* structure section above; map plate and Fig. 13E) approximate orientations of near-vertical faults and joints in bedrock and Quaternary sediments (Figs. 13C and D) and are interpreted as either associated with deposition of overlying Quaternary lodgment till, or as expression of steep, northeast- or northwest-striking faulting.

ACKNOWLEDGMENTS

This geologic map was funded in part by the USGS National Cooperative Geologic Mapping Program under award no. G15AC00248. We thank Ken Clark (University of Puget Sound—UPS) for assistance with geochemical sample selection, interpretation, and field work, and Jeff Tepper (UPS) for review and comments on geochemical interpretation; Dan Miggins (Oregon State University) for $^{40}Ar/^{39}Ar$ analysis of igneous rock samples; Dan Gavin and Erin Herring for analysis and paleoenvironmental interpretation of pollen samples; Elizabeth Nesbitt (Burke Museum, University of Washington) for analysis of biostratigraphic samples for fossils and their ages; Masoud Mirzaei Souzani and Bernard Housen (Western Washington University) for paleomagnetic analyses; the Washington State Department of Transportation (WSDOT) for access to geotechnical records and Eric Dingeldein (WSDOT) for his assistance with those records; Richard Blakely (USGS) for aeromagnetic anomaly maps; Jack Odum (USGS) and Sammantha Magsino (National Academy of Sciences) for sharing data and assisting with interpretation of aeromagnetic, gravity, and seismic-section data; Matt Benson (Northwest Geophysics, Inc.) for use of geophysical instruments; and Bob Carson (Whitman College) for sharing field notes and knowledge of geology in the southeastern Olympic Mountains. We thank Peter Polivka (Tetratech), and DGER staff Dave Burris, Ian Hubert, Todd Lau, Kara Jacobacci, and Alex Steely for help with field work. We thank Geosoft Inc. for experimental use of their Oasis-Montaj 4.5 – 2D GM-SYS software for gravity and magnetic modeling. We thank Green Diamond Timber Company for unfettered access to extensive timberlands and logistical assistance with road data, quarry locations, and gates, and other landowners for sharing local knowledge and permitting us to map on their land. Among coauthors, Daniel Eungard spearheaded the geochemical analysis; Recep Cakir and Spenser Scott the geophysical data collection, modeling and inferences; Gabriel Legorreta Paulín processed and interpreted satellite data; Shannon Mahan performed luminescence analysis and substantially contributed to interpretation of Quaternary deposits.

REFERENCES

Alley, N. F., 1979, Middle Wisconsin stratigraphy and climatic reconstruction, southern Vancouver Island, British Columbia: Quaternary Research, v. 11, no. 2, p. 213-237.

Allison, R. C., 1959, The geology and Eocene megafaunal paleontology of the Quimper Peninsula area, Washington: University of Washington Master of Science thesis, 121 p., 1 plate.

Allmendinger, R. W.; Cardozo, N. C.; Fisher, D., 2013, Structural geology algorithms: Vectors & Tensors: Cambridge University Press [Cambridge, U.K.], 289 p.

Anundsen, Karl; Abella, S. E. B.; Leopold, E. B.; Stuiver, M.; Turner, S., 1994, Late-glacial and early Holocene sea-level fluctuations in the central Puget Lowland, Washington, inferred from lake sediments: Quaternary Research, v. 42, no. 2, p. 149-161.

Armentrout, J. M.; Hull, D. A.; Beaulieu, J. D.; Rau, W. W., 1983, Correlation of Cenozoic stratigraphic units of western Oregon and Washington: Oregon Department of Geology and Mineral Industries Oil and Gas Investigation 7, 90 p., 1 plate.

Armstrong, J. E.; Crandell, D. R.; Easterbrook, D. J.; Noble, J. B., 1965, Late Pleistocene stratigraphy and chronology in southwestern British Columbia and northwestern Washington: Geological Society of America Bulletin, v. 76, no. 3, p. 321-330.

Babcock, R. S.; Burmester, R. F.; Engebretson, D. C.; Warnock, A. C.; Clark, K. P., 1992, A rifted margin origin for the Crescent basalts and related rocks in the northern Coast Range volcanic province, Washington and British Columbia: Journal of Geophysical Research, v. 97, no. B5, p. 6799-6821.

Babcock, R. S.; Suczek, C. A.; Engebretson, D. C., 1994, The Crescent "terrane", Olympic Peninsula and southern Vancouver Island. *In* Lasmanis, Raymond; Cheney, E. S., convenors, Regional geology of Washington State: Washington Division of Geology and Earth Resources Bulletin 80, p. 141-157. [http://www.dnr.wa.gov/publications/ger_b80_regional_geol_wa_2.pdf]

Ballantyne, C. K., 2002, Paraglacial geomorphology: Quaternary Science Reviews 21, p. 1935-2017.

Benn, D. I.; Evans, D. J. A., 1998, Glaciers and glaciation: Oxford University Press, 734 p.

Blakely, R. J.; Sherrod, B. L.; Hughes, J. F.; Anderson, M. L.; Wells, R. E.; Weaver, C. S., 2009, Saddle Mountain fault deformation zone, Olympic Peninsula, Washington—Western boundary of the Seattle uplift: Geosphere, v. 5, no. 2, p. 105-125.

Blunt, D. J.; Easterbrook, D. J.; Rutter, N. W., 1987, Chronology of Pleistocene sediments in the Puget Lowland, Washington. *In* Schuster, J. E., editor, Selected papers on the geology of Washington: Washington Division of Geology and Earth Resources Bulletin 77, p. 321-353.

Booth, D. B., 1994, Glaciofluvial infilling and scour of the Puget Lowland, Washington, during ice-sheet glaciation: Geology, v. 22, no. 8, p. 695-698.

Booth, D. B.; Troost, K. G.; Clague, J. J.; Waitt, R. B., 2004, The Cordilleran ice sheet. *In* Gillespie, A. R.; Porter, S. C.; Atwater, B. F., editors, The Quaternary period in the United States: Elsevier, p. 17-43.

Bowman, J. D.; Czajkowski, J. L.; Reidel, S. P.; Boschmann, D. E.; Fusso, L. A., 2014, Washington State rock geochemistry database—GIS data: Washington Division of Geology and Earth Resources Digital Data Series 5, version 1.0. [http://www.dnr.wa.gov/publications/ger_portal_geochemistry.zip]

Brandon, M. T.; Calderwood, A. R., 1990, High-pressure metamorphism and uplift of the Olympic subduction complex: Geology, v. 18, no. 12, p. 1252-1255.

Brandon, M. T.; Roden-Tice, M. K.; Garver, J. I., 1998, Late Cenozoic exhumation of the Cascadia accretionary wedge in the Olympic Mountains, northwest Washington State: Geological Society of America Bulletin, v. 110, no. 8, p. 985-1009, Data Repository item 9865. [http://minerva.union.edu/garverj/garver/pubs/Brandon_etal_1998.pdf]

Bretz, J H., 1910, Glacial lakes of Puget Sound—Preliminary paper: Journal of Geology, v. 18, no. 5, p. 448-458.

Bretz, J H., 1913, Glaciation of the Puget Sound region: Washington Geological Survey Bulletin 8, 244 p., 3 plates. [http://www.dnr.wa.gov/publications/ger_b8_glaciation_pugetsound.pdf]

Brocher, T. M.; Parsons, T. E.; Blakely, R. J.; Christensen, N. I.; Fisher, M. A.; Wells, R. E.; SHIPS Working Group, 2001, Upper crustal structure in Puget Lowland, Washington—Results from the 1998 seismic hazards investigations in Puget Sound: Journal of Geophysical Research, v. 106, no. B7, p. 13,541-13,564.

Cady, W. M.; Sorensen, M. L.; MacLeod, N. S., 1972a, Geologic map of the Brothers quadrangle, Jefferson, Mason and Kitsap Counties, Washington: U.S. Geological Survey Geologic Quadrangle Map GQ-969, 1 sheet, scale 1:62,500. [http://pubs.usgs.gov/gq/0969/report.pdf]

Cady, W. M.; Tabor, R. W.; MacLeod, N. S.; Sorensen, M. L., 1972b, Geologic map of the Tyler Peak quadrangle, Clallam and Jefferson Counties, Washington: U.S. Geological Survey Geologic Quadrangle Map GQ-970, 1 sheet, scale 1:62,500. [http://pubs.usgs.gov/gq/0970/report.pdf]

Cardozo, N.; Allmendinger, R. W., 2013, Spherical projections with OSXStereonet: Computers & Geosciences, v. 51, no. 0, p. 193-205. doi: 10.1016/j.cageo.2012.07.021

Carson, R. J., 1970, Quaternary geology of the south-central Olympic Peninsula, Washington: University of Washington Doctor of Philosophy thesis, 67 p., 4 plates.

Carson, R. J., 1979, Reinterpretation of the Skokomish Gravel, southwestern Puget Lowland, Washington [abstract]: Northwest Scientific Association, Annual Meeting, 52nd, Program and Abstracts, p. 31.

Carson, R. J., 1980, Quaternary, environmental, and economic geology of the eastern Olympic Peninsula, Washington: [Unpublished], 275 p.

Chan, C. F.; Tepper, J. H.; Nelson, B. K., 2012, Petrology of the Grays River volcanics, southwest Washington—Plume-influenced slab window magmatism in the Cascadia forearc: Geological Society of America Bulletin, v. 124, no. 7-8, p. 1324-1338.

Clague, J. J., 1978, Mid-Wisconsinan climates of the Pacific Northwest: Geological Survey of Canada Paper 78-1, Part B, p. 95–100.

Clark, K. P., 1989, The stratigraphy and geochemistry of the Crescent Formation basalts and the bedrock geology of associated igneous rocks near Bremerton, Washington: Western Washington University Master of Science thesis, 171 p., 1 plate.

Clement, C. R.; Pratt, T. L.; Holmes, M. L.; Sherrod, B. L., 2010, High-resolution seismic reflection imaging of growth folding and shallow faults beneath the southern Puget Lowland, Washington State: Bulletin of the Seismological Society of America, v. 100, no. 4, p. 1710-1723.

Clowes, R. M.; Brandon, M. T.; Green, A. G.; Yorath, C. J.; Sutherland Brown, A.; Kanasewich, E. R.; Spencer, C. J., 1987, LITHOPROBE—Southern Vancouver Island—Cenozoic subduction complex imaged by deep seismic reflections: Canadian Journal of Earth Sciences, v. 24, no. 1, p. 31-51.

Cong, S.; Ashworth, A. C. 1996, Palaeoenvironmental interpretation of Middle and Late Wisconsinan fossil coleopteran assemblages from western Olympic Peninsula, Washington, USA: Journal of Quaternary Science, v. 11, p. 345-356.

Compton, R. R., 1985, Geology in the Field: John Wiley and Sons, Inc., 398 p.

Contreras, T. A.; Legorreta Paulín, Gabriel; Czajkowski, J. L.; Polenz, Michael; Logan, R. L.; Carson, R. J.; Mahan, S. A.; Walsh, T. J.; Johnson, C. N.; Skov, R. H., 2010, Geologic map of the Lilliwaup 7.5-minute quadrangle, Mason County, Washington: Washington Division of Geology and Earth Resources Open File Report 2010-4, 13 p., 1 plate, scale 1:24,000. [http://www.dnr.wa.gov/Publications/ger_ofr2010-4_geol_map_lilliwaup_24k.zip]

Contreras, T. A.; Patton, A. I.; Legorreta Paulín, Gabriel; Hubert, I. J.; Cakir, Recep; Carson, R. J., 2014, Geologic map of the Quilcene 7.5-minute quadrangle, Jefferson County, Washington: Washington Division of Geology and Earth Resources Map Series 2014-03, 1 sheet, scale 1:24,000, with 27 p. text. [http://www.dnr.wa.gov/publications/ger_ms2014-03_geol_map_quilcene_24k.zip]

Contreras, T. A.; Spangler, Eleanor; Fusso, L. A.; Reioux, D. A.; Legorreta Paulín, Gabriel; Pringle, P. T.; Carson, R. J.; Lindstrum, E. F.; Clark, K. P.; Tepper, J. H.; Pileggi, Domenico; Mahan, S. A., 2012a, Geologic map of the Eldon 7.5-minute quadrangle, Jefferson, Kitsap, and Mason Counties, Washington: Washington Division of Geology and Earth Resources Map Series 2012-03, 1 sheet, scale 1:24,000, 60 p. text. [http://www.dnr.wa.gov/publications/ger_ms2012-03_geol_map_eldon_24k.zip]

Contreras, T. A.; Stone, K. A.; Legorreta Paulín, Gabriel , 2013, Geologic map of the Lofall 7.5-minute quadrangle, Jefferson and Kitsap Counties, Washington: Washington Division of Geology and Earth Resources Map Series 2013-03, 1 sheet, scale 1:24,000, with 19 p. text. [http://www.dnr.wa.gov/publications/ger_ms2013-03_geol_map_lofall_24k.zip]

Contreras, T. A.; Weeks, S. A.; Perry, B. B., 2012b, Analytical data from the Holly 7.5-minute quadrangle, Jefferson, Kitsap, and Mason Counties, Washington—Supplement to Open File Report 2011-5: Washington Division of Geology and Earth Resources Open File Report 2011-6, 16 p. [http://www.dnr.wa.gov/publications/ger_ofr2011-6_holly_supplement.pdf]

Contreras, T. A.; Weeks, S. A.; Stanton, K. M. D.; Stanton, B. W.; Perry, B. B.; Walsh, T. J.; Carson, R. J.; Clark, K. P.; Mahan, S. A., 2012c, Geologic map of the Holly 7.5-minute quadrangle, Jefferson, Kitsap, and Mason Counties, Washington: Washington Division of Geology and Earth Resources Open File Report 2011-5, 1 sheet, scale 1:24,000, with 13 p. text. [http://www.dnr.wa.gov/publications/ger_ofr2011-5_geol_map_holly_24k.zip]

Czajkowski, J. L., 2014, Washington State geochronology database—GIS data: Washington Division of Geology and Earth Resources Digital Data Series 6, version 1.0. [accessed at: http://www.dnr.wa.gov/publications/ger_portal_geochronology.zip]

Crandell, D. R.; Mullineaux, D. R.; Waldron, H. H., 1958, Pleistocene sequence in southeastern part of the Puget Sound lowland, Washington: Washington Division of Mines and Geology Reprint 2, 14 p. [http://www.dnr.wa.gov/publications/ger_reprint2_pleistocene_puget_lowlands.pdf]

Daneš, Z. F.; Bonno, M.; Brau, J. E.; Gilham, W. D.; Hoffman, T. F.; Johansen, D.; Jones, M. H.; Malfait, Bruce; Masten, J.; Teague, G. O., 1965, Geophysical investigation of the southern Puget Sound area, Washington: Journal of Geophysical Research, v. 70, no. 22, p. 5573-5580.

Deeter, J. D., 1979, Quaternary geology and stratigraphy of Kitsap County, Washington: Western Washington University Master of Science thesis, 175 p., 2 plates. [https://fortress.wa.gov/dnr/geologydata/library/thesis/Deeter_1979_thesis.pdf]

Dethier, D. P.; Pessl, Fred, Jr.; Keuler, R. F.; Balzarini, M. A.; Pevear, D. R., 1995, Late Wisconsinan glaciomarine deposition and isostatic rebound, northern Puget Lowland, Washington: Geological Society of America Bulletin, v. 107, no. 11, p. 1288-1303.

Dragovich, J. D.; Logan, R. L.; Schasse, H. W.; Walsh, T. J.; Lingley, W. S., Jr.; Norman, D. K.; Gerstel, W. J.; Lapen, T. J.; Schuster, J. E.; Meyers, K. D., 2002, Geologic map of Washington—Northwest quadrant: Washington Division of Geology and Earth Resources Geologic Map GM-50, 3 sheets, scale 1:250,000, with 72 p. text. [http://www.dnr.wa.gov/publications/ger_gm50_geol_map_nw_wa_250k.pdf]

Duncan, R. A., 1982, A captured island chain in the coast range of Oregon and Washington: Journal of Geophysical Research, v. 87, no. B13, p. 10,827-10,837.

Easterbrook, D. J., 1968, Pleistocene stratigraphy of Island County: Washington Department of Water Resources Water-Supply Bulletin 25, part 1, 34 p., 1 plate (in 4 parts). [http://www.ecy.wa.gov/programs/eap/wsb/wsb_All.html]

Easterbrook, D. J.; Briggs, N. D.; Westgate, J. A.; Gorton, M. P., 1981, Age of the Salmon Springs glaciation in Washington: Geology, v. 9, no. 2, p. 87-93.

Fairhall, A. W.; Schell, W. R.; Young, J. A., 1966, Radiocarbon dating at the University of Washington, III: Radiocarbon, v. 8, p. 498-506. [https://journals.uair.arizona.edu/index.php/radiocarbon/article/view/3340]

Florer, L. E., 1972, Quaternary paleoecology and stratigraphy of the sea cliffs, western Olympic Peninsula, Washington: Quaternary Research, v. 2, no. 2, p. 202-216.

Gale, A.; Dalton, C. A.; Langmuir, C. H.; Yongjun, S.; Schilling, J. G., 2013, The mean composition of ocean ridge basalts: Geochemistry, Geophysics, Geosystems, v. 14.3, p. 489-518. [http://onlinelibrary.wiley.com/doi/10.1029/2012GC004334/full]

Garling, M. E.; Molenaar, Dee, 1965, Water resources and geology of the Kitsap Peninsula and certain adjacent islands: Washington Division of Water Resources Water-Supply Bulletin 18, 309 p., 5 plates.

Garrison, Rick, 2007, Dam removal and stream restoration, Goldsborough Creek, WA [abstract]: AEG News, Program with Abstracts, 2007 Annual Meeting, v. 50, p. 84.

Glassley, W. E., 1974, Geochemistry and tectonics of the Crescent volcanic rocks, Olympic Peninsula, Washington: Geological Society of America Bulletin, v. 85, no. 5, p. 785-794.

Glassley, W. E., 1976, New analyses of Eocene basalt from the Olympic Peninsula, Washington; Discussion: Geological Society of America Bulletin, v. 87, no. 8, p. 1200-1201.

Globerman, B. R., 1981, Geology, petrology, and paleomagnetism of Eocene basalts from the Black Hills, Washington coast range: Western Washington University Master of Science thesis, 373 p., 1 plate.

Globerman, B. R.; Beck, M. E., Jr.; Duncan, R. A., 1982, Paleomagnetism and tectonic significance of Eocene basalts from the Black Hills, Washington coast range: Geological Society of America Bulletin, v. 93, no. 11, p. 1151-1159.

Gower, H. D.; Yount, J. C.; Crosson, R. S., 1985, Seismotectonic map of the Puget Sound region, Washington: U.S. Geological Survey Miscellaneous Investigations Series Map I-1613, 1 sheet, scale 1:250,000, with 15 p. text. [http://pubs.usgs.gov/imap/1613/plate-1.pdf]

Grigg L. D; Whitlock C., 2002, Patterns and causes of millennial-scale climate change in the Pacific Northwest during marine isotope stages 2 and 3: Quaternary Science Reviews, v. 21, p. 2067-2083

Hansen, B. S.; Easterbrook, D. J., 1974, Stratigraphy and palynology of late Quaternary sediments in the Puget Lowland, Washington: Geological Society of America Bulletin, v. 85, no. 4, p. 587-602.

Haugerud, R. A., 2009, Preliminary geomorphic map of the Kitsap Peninsula, Washington: U.S. Geological Survey, Open-File Report 2009-1033, 2 sheets, scale 1:36,000. [http://pubs.usgs.gov/of/2009/1033/]

Hebda, R. J.; Lian , O. B; Hicock, S. R., 2016, Olympia Interstadial: vegetation, landscape history, and paleoclimatic implications of a mid-Wisconsinan (MIS3) nonglacial sequence from southwest British Columbia, Canada: Canadian Journal of Earth Sciences, v. 53, No. 3, p. 304-320.

Heusser, C. J., 1972, Palynology and phytogeographical significance of a late-Pleistocene refugium near Kalaloch, Washington, Quaternary Research, 2, 189-201.

Heusser, C. J.; Heusser, L. E.; Peteet, D. M., 1999, Humptulips revisited—A revised interpretation of Quaternary vegetation and climate of western Washington, USA: Palaeogeography, Palaeoclimatology, Palaeoecology, v. 150, no. 3-4, p. 191-221.

Heusser, C. J.; Heusser, L. E.; Streeter, S. S., 1980, Quaternary temperatures and precipitation for the northwest coast of North America: Nature, v. 286, no. 5774, p. 702-704.

Hirsch, D. M.; Babcock, R. S., 2009, Spatially heterogeneous burial and high-P/T metamorphism in the Crescent Formation, Olympic Peninsula, Washington: American Mineralogist, v. 94, no. 8-9, p. 1103-1110.

Irvine, T. N.; Baragar, W. R. A., 1971, A guide to the chemical classification of the common volcanic rocks: Canadian Journal of Earth Sciences, v. 8, p. 523-548.

Irving, E., 1979, Paleopoles and paleolatitudes of North America and speculations about displaced terranes: Canadian Journal of Earth Sciences, v. 16, p. 669—694.

Johnson, S. Y.; Potter, C. J.; Armentrout, J. M.; Miller, J. J.; Finn, C. A.; Weaver, C. S., 1996, The southern Whidbey Island fault—An active structure in the Puget Lowland, Washington: Geological Society of America Bulletin, v. 108, no. 3, p. 334-354, 1 plate.

Johnson, S. Y.; Blakely, R. J.; Stephenson, W. J.; Dadisman, S. V.; Fisher, M. A., 2004, Active shortening of the Cascadia forearc and implications for seismic hazards of the Puget Lowland: Tectonics, v. 23, TC1011, 27 p.

Jones, M. A., 1999, Geologic framework for the Puget Sound aquifer system, Washington and British Columbia: U.S. Geological Survey Professional Paper 1424-C, 31 p., 18 plates. [http://pubs.er.usgs.gov/usgspubs/pp/pp1424C]

Kovanen, D. J.; Slaymaker, Olav, 2004, Relict shorelines and ice flow patterns of the northern Puget Lowland from LIDAR data and digital terrain modelling: Geografiska Annaler Series A: Physical Geography, v. 86, no. 4, p. 385-400.

Lamb, A. P.; Liberty, L. M.; Blakely, R. J.; Pratt, T. L.; Sherrod, B. L.; van Wijk, K., 2012, Western limits of the Seattle fault zone and its interaction with the Olympic Peninsula, Washington: Geosphere, v. 8, no. 4, p. 1-16.

Laprade, W. T., 2003, Subglacially reworked till in the Puget Lowland [abstract]: Geological Society of America Abstracts with Programs, v. 35, no. 6, p. 216.

Lea, P. D., 1984, Pleistocene glaciation at the southern margin of the Puget lobe, western Washington: University of Washington Master of Science thesis, 96 p., 3 plates.

Le Bas, M. J.; Le Maitre, R.W.; Streckeisen, A.; Zanettin, B., 1986, A chemical classification of volcanic rocks based on the total alkali silica diagram: Journal of Petrology, v. 27, p. 745-750.

Lewis, J. C.; Unruh, J. R.; Twiss, R. J., 2003, Seismogenic strain and motion of the Oregon coast block: Geology, v. 31, no. 2, p. 183-186.

Logan, R. L., compiler, 1987, Geologic map of the south half of the Shelton and south half of the Copalis Beach quadrangles, Washington: Washington Division of Geology and Earth Resources Open File Report 87-9, 15 p., 1 plate, scale 1:100,000. [http://www.dnr.wa.gov/publications/ger_ofr87-9_south_half_shelton_copalis_beach_100k.pdf]

Logan, R. L., 2003, Geologic map of the Shelton 1:100,000 quadrangle, Washington: Washington Division of Geology and Earth Resources Open File Report 2003-15, 1 sheet, scale 1:100,000. [http://www.dnr.wa.gov/publications/ger_ofr2003-15_geol_map_shelton_100k.pdf]

Logan, R. L.; Walsh, T. J., 2004, Geologic map of the Summit Lake 7.5-minute quadrangle, Thurston and Mason Counties, Washington: Washington Division of Geology and Earth Resources Open File Report 2004-10, 1 sheet, scale 1:24,000. [http://www.dnr.wa.gov/publications/ger_ofr2004-10_geol_map_summitlake_24k.pdf]

Logan, R. L.; Walsh, T. J.; Stanton, B. W.; Sarikhan, I. Y., 2009, Geologic map of the Maytown 7.5-minute quadrangle, Thurston County, Washington: Washington Division of Geology and Earth Resources Geologic Map GM-72. [http://www.dnr.wa.gov/publications/ger_gm72_geol_map_maytown_24k.pdf]

Mace, C. G.; Keranen, K. M., 2012, Oblique fault systems crossing the Seattle basin—Geophysical evidence for additional shallow fault systems in the central Puget Lowland: Journal of Geophysical Research, v. 117, B03105, 19 p.

Magsino, S. L.; Palmer, S. P.; Walsh, T. J., 2002, Geologic structure of southern Puget Sound revealed through detailed ground magnetic and gravity surveys [abstract]: Geological Society of America Abstracts with Programs, v. 34, no. 5, p. A-32.

Magsino, S.; Sanger, Elizabeth; Walsh, T. J.; Palmer, S. P.; Blakely, R. J., 2003, The Olympia structure—Ramp or discontinuity? New gravity data provide more information [abstract]: Geological Society of America Abstracts with Programs, v. 35, no. 6, p. 479.

Martens, Jo; Pringle, Patrick; Polenz, Michael, 2010, New radiocarbon ages on submerged forests in Eld and Henderson Inlets near Olympia, Washington [abstract]. *In* Northwest Scientific Association, From Mount St. Helens to Oak-Prairie Lowlands—Disturbances, biological legacies, and conservation: Northwest Scientific Association, p. 68. [http://www.centralia.edu/academics/earthscience/nwsa/NWSA_CPOP_2010_Program.pdf]

McCaffrey, Robert; Qamar, A. I.; King, R. W.; Wells, Ray; Khazaradze, Giorgi; Williams, C. A.; Stevens, C. W.; Vollick, J. J.; Zwick, P. C., 2007, Fault locking, block rotation and crustal deformation in the Pacific Northwest: Geophysical Journal International, v. 169, no. 3, p. 1315-1340.

McCaffrey, Robert; King, R. W.; Payne, S. J.; Lancaster, Matthew, 2013, Active tectonics of northwestern U.S. inferred from GPS-derived surface velocities: Journal of Geophysical Research Solid Earth, v. 118, 15 p. [http://onlinelibrary.wiley.com/doi/10.1029/2012JB009473/epdf]

Molenaar, Dee; Noble, J. B., 1970, Geology and related ground-water occurrence, southeastern Mason County, Washington: Washington Department of Water Resources Water-Supply Bulletin 29, 145 p., 2 plates. [http://www.ecy.wa.gov/programs/eap/wsb/wsb_All.html]

Morrison, R. B., 1991, Introduction. *In* Morrison, R. B., editor, Quaternary nonglacial geology—Conterminous U.S.: Geological Society of America DNAG Geology of North America, v. K-2, p. 1-12.

North Greenland Ice Core Project Members, 2004, High-resolution record of Northern hemisphere climate extending into the last interglacial period: Nature, v. 431, p. 147-151.

Pearce, J. A.; Harris, N. B. W.; Tindle, A. G., 1984, Trace element discrimination diagrams for the tectonic interpretation of granitic rocks: Journal of Petrology, v. 25, no. 4, p. 956-983.

Pease, M. H., Jr.; Hoover, Linn, Jr., 1957, Geology of the Doty-Minot Peak area, Washington: U.S. Geological Survey Oil and Gas Investigations Map OM-188, 1 sheet, scale 1:62,500. [http://pubs.er.usgs.gov/publication/om188]

Pettijohn, F. J., 1957, Sedimentary rocks: Harper and Brothers, 718 p.

Phillips, W. M.; Walsh, T. J.; Hagen, R. A., 1989, Eocene transition from oceanic to arc volcanism, southwest Washington. *In* Muffler, L. J. P.; Weaver, C. S.; Blackwell, D.D., editors, Proceedings of workshop XLIV—Geological, geophysical, and tectonic setting of the Cascade Range: U.S. Geological Survey Open-File Report 89-178, p. 199-256. [http://pubs.er.usgs.gov/publication/ofr89178

Polenz, Michael; Slaughter, S. L.; Thorsen, G. W., 2005, Geologic map of the Coupeville and part of the Port Townsend North 7.5-minute quadrangles, Island County, Washington: Washington Division of Geology and Earth Resources Geologic Map GM-58, 1 sheet, scale 1:24,000. [http://www.dnr.wa.gov/publications/ger_gm58_geol_map_coupeville_24k.pdf]

Polenz, Michael; Schasse, H. W.; Petersen, B. B., 2006, Geologic map of the Freeland and northern part of the Hansville 7.5-minute quadrangles, Island County, Washington: Washington Division of Geology and Earth Resources Geologic Map GM-64, 1 sheet, scale 1:24,000. [http://www.dnr.wa.gov/publications/ger_gm64_geol_map_freeland_hansville_24k.pdf]

Polenz, Michael; Alldritt, Katelin; Heheman, N. J.; Logan, R. L., 2009a, Geologic map of the Burley 7.5-minute quadrangle, Kitsap and Pierce Counties, Washington: Washington Division of Geology and Earth Resources Open File Report 2009-8, 1 sheet, scale 1:24,000. [http://www.dnr.wa.gov/publications/ger_ofr2009-8_geol_map_burley_24k.pdf]

Polenz, Michael; Alldritt, Katelin; Heheman, N. J.; Sarikhan, I. Y.; Logan, R. L., 2009b, Geologic map of the Belfair 7.5-minute quadrangle, Mason, Kitsap, and Pierce Counties, Washington: Washington Division of Geology and Earth Resources Open File Report 2009-7, 1 sheet, scale 1:24,000. [http://www.dnr.wa.gov/publications/ger_ofr2009-7_geol_map_belfair_24k.pdf]

Polenz, Michael; Contreras, T. A.; Czajkowski, J. L.; Legorreta Paulín, Gabriel; Miller, B. A.; Martin, M. E.; Walsh, T. J.; Logan, R. L.; Carson, R. J.; Johnson, C. N.; Skov, R. H.; Mahan, S. A.; Cohan, C. R., 2010, Supplement to geologic maps of the Lilliwaup, Skokomish Valley, and Union 7.5-minute quadrangles, Mason County, Washington—Geologic setting and development around the Great Bend of Hood Canal: Washington Division of Geology and Earth Resources Open File Report 2010-5, 27 p. [http://www.dnr.wa.gov/publications/ger_ofr2010-5_lilliwaup_skokomish_valley_union_suppl_24k.pdf]

Polenz, Michael; Czajkowski, J. L.; Legorreta Paulín, Gabriel; Contreras, T. A.; Miller, B. A.; Martin, M. E.; Walsh, T. J.; Logan, R. L.; Carson, R. J.; Johnson, C. N.; Skov, R. H.; Mahan, S. A.; Cohan, C. R., 2011, Geologic map of the Skokomish Valley and Union 7.5-minute quadrangles, Mason County, Washington: Washington Division of Geology and Earth Resources Open File Report 2010-3 revised, 21 p., 1 plate, scale 1:24,000. [http://www.dnr.wa.gov/publications/ger_ofr2010-3_geol_map_skokomish_valley_union_24k.zip]

Polenz, Michael; Favia, J. G.; Hubert, I. J.; Legorreta Paulín, Gabriel; Cakir, Recep, 2015, Geologic map of the Port Ludlow and southern half of the Hansville 7.5-minute quadrangles, Kitsap and Jefferson Counties, Washington: Washington Division of Geology and Earth Resources Map Series 2015-02, 1 sheet, scale 1:24,000, 40 p. text. [http://www.dnr.wa.gov/publications/ger_ms2015-02_geol_map_port_ludlow_hansville_24k.zip]

Polenz, Michael; Gordon, Harley O.; Hubert, Ian J.; Contreras, Trevor A.; Patton, Annette I.; Legorreta Paulín, Gabriel; Cakir, Recep, 2014, Geologic map of the Center 7.5-minute quadrangle, Jefferson County, Washington: Washington Division of Geology and Earth Resources Map Series 2014-02, 1 sheet, scale 1:24,000, with 35 p. text. [http://www.dnr.wa.gov/Publications/ger_ms2014-02_geol_map_center_24k.zip]

Polenz, Michael; Miller, B. A.; Davies, Nigel; Perry, B. B.; Clark, K. P.; Walsh, T. J.; Carson, R. J.; Hughes, J. F., 2012a, Geologic map of the Hoodsport 7.5-minute quadrangle, Mason County, Washington: Washington Division of Geology and Earth Resources Open File Report 2011-3, 1 sheet, scale 1:24,000, with 16 p. text. [http://www.dnr.wa.gov/publications/ger_ofr2011-3_geol_map_hoodsport_24k.zip]

Polenz, Michael; Miller, B. A.; Davies, Nigel; Perry, B. B.; Hughes, J. F.; Clark, K. P.; Walsh, T. J.; Tepper, J. H.; Carson, R. J., 2012b, Analytical data from the Hoodsport 7.5-minute quadrangle, Mason County, Washington—Supplement to Open File Report 2011-3: Washington Division of Geology and Earth Resources Open File Report 2011-4, 42 p. [http://www.dnr.wa.gov/publications/ger_ofr2011-4_hoodsport_supplement.pdf]

Polenz, Michael; Spangler, Eleanor; Fusso, L. A.; Reioux, D. A.; Cole, R. A.; Walsh, T. J.; Cakir, Recep; Clark, K. P.; Tepper, J. H.; Carson, R. J.; Pileggi, Domenico; Mahan, S. A., 2012c, Geologic map of the Brinnon 7.5-minute quadrangle, Jefferson and Kitsap Counties, Washington: Washington Division of Geology and Earth Resources Map Series 2012-02, 1 sheet, scale 1:24,000, with 47 p. text. [http://www.dnr.wa.gov/publications/ger_ms2012-02_geol_map_brinnon_24k.zip]

Polenz, Michael; Petro, G. T.; Contreras, T. A.; Stone, K. A.; Legorreta Paulín, Gabriel; Cakir, Recep, 2013, Geologic map of the Seabeck and Poulsbo 7.5-minute quadrangles, Kitsap and Jefferson Counties, Washington: Washington Division of Geology and Earth Resources Map Series 2013-02, 1 sheet, scale 1:24,000, with 39 p. text. [http://www.dnr.wa.gov/publications/ger_ms2013-02_geol_map_seabeck-poulsbo_24k.zip]

Porter, S. C.; Carson, R. J., 1971, Problems of interpreting radiocarbon dates from dead-ice terrain, with an example from the Puget Lowland of Washington: Quaternary Research, v. 1, no. 3, p. 410-414.

Porter, S. C.; Swanson, T. W., 1998, Radiocarbon age constraints on rates of advance and retreat of the Puget lobe of the Cordilleran ice sheet during the last glaciation: Quaternary Research, v. 50, no. 3, p. 205-213.

Pratt, T. L.; Johnson, S. Y.; Potter, C. J.; Stephenson, W. J.; Finn, C. A., 1997, Seismic reflection images beneath Puget Sound, western Washington State—The Puget Lowland thrust sheet hypothesis: Journal of Geophysical Research, v. 102, no. B12, p. 27,469-27,489.

Prescott, J. R.; Hutton, J. T., 1994, Cosmic ray contribution to dose rates for luminescence and ESR dating—Large depths and long-term time variations: Radiation Measurements, v. 23, no. 2-3, p. 497-500.

Rigg, G. B., 1958, Peat resources of Washington: Division of Mines and Geology Bulletin 44, p. 66-67. [http://www.dnr.wa.gov/publications/ger_b44_peat_reasources_wa_1.pdf]

Schasse, H. W.; Logan, R. L.; Polenz, Michael; Walsh, T. J., 2003, Geologic map of the Shelton 7.5-minute quadrangle, Mason and Thurston Counties, Washington: Washington Division of Geology and Earth Resources Open File Report 2003-24, 1 sheet, scale 1:24,000. [http://www.dnr.wa.gov/publications/ger_ofr2003-24_geol_map_shelton_24k.pdf]

Sceva, J. E., 1957a, Geology and ground-water resources of Kitsap County, Washington [abstract]: Geological Abstracts, v. 5, no. 4, p. 146-148.

Sceva, J. E., 1957b, Geology and ground-water resources of Kitsap County, Washington: U.S. Geological Survey Water-Supply Paper 1413, 178 p., 3 plates. [http://pubs.er.usgs.gov/usgspubs/wsp/wsp1413]

Sherrod, B. L., 2001, Evidence for earthquake-induced subsidence about 1100 yr ago in coastal marshes of southern Puget Sound, Washington: Geological Society of America Bulletin, v. 113, no. 10, p. 1299-1311.

Siddall, M.; Rohling, E. J.; Thompson, W. G.; Waelbroeck, C., 2008, Marine isotope stage 3 sea level fluctuations: Data synthesis and new outlook, Reviews of Geophysics, v. 46, RG4003. [doi:10.1029/2007RG000226.]

Singhroy, V. H.; Kenny, F. M.; Barnett, P. J., 1992a, Imagery for Quaternary geological mapping in glaciated terrains: Canadian Journal of Remote Sensing, v. 18, n. 2, p. 112-117.

Singhroy, V. H.; Kenny, F. M.; Barnett, P. J., 1992b, Quaternary Mapping in Glaciated and Vegetated Areas Using SAR and Multispectral Images: Proceeding I, XVII International Society of Photogrammetry and Remote Sensing congress, Washington, D.C., v. XXIX, part B7. [http://www.isprs.org/proceedings/XXIX/congress/part7/874_XXIX-part7.pdf]

Smith, G. R.; Montgomery, D. R.; Peterson, N. P.; Crowley, Bruce, 2007, Spawning sockeye salmon fossils in Pleistocene lake beds of Skokomish valley, Washington: Quaternary Research, v. 68, no. 2, p. 227-238.

Snavely, P. D., Jr.; Brown, R. D., Jr.; Roberts, A. E.; Rau, W. W., 1958, Geology and coal resources of the Centralia-Chehalis district, Washington, with a section on Microscopical character of Centralia-Chehalis coal, by J. M. Schopf: U.S. Geological Survey Bulletin 1053, 159 p., 6 plates.[http://pubs.er.usgs.gov/usgspubs/b/b1053]

Squires, R. L.; Goedert, J. L., 1994, New species of early Eocene small to minute mollusks from the Crescent Formation, Black Hills, southwestern Washington: Veliger, v. 37, no. 3, p. 253-266.

Staley, A. E., 2015, Glacial geomorphology and chronology of the Quinault Valley, Washington, and broader evidence of Marine Isotope Stages 4 and 3 glaciation across northwestern United States: Idaho State University Master of Science thesis, 177 p. [http://geology.isu.edu/thesis/Staley.AmieElizabeth.2015.pdf]

Sun, S. S.; McDonough, W. F., 1989, Chemical and isotopic systematics of oceanic basalts: implications for mantle composition and process: Geological Society of London Special Publications 1989, v. 42, p. 313-345.

Tabor, R. W.; Cady, W. M., 1978a, Geologic map of the Olympic Peninsula, Washington: U.S. Geological Survey Miscellaneous Investigations Series Map I-994, 2 sheets, scale 1:125,000. [http://pubs.er.usgs.gov/publication/i994]

Tabor, R. W.; Cady, W. M., 1978b, The structure of the Olympic Mountains, Washington—Analysis of a subduction zone: U.S. Geological Survey Professional Paper 1033, 38 p. [http://pubs.er.usgs.gov/publication/pp1033]

Tepper, J. H., 2016, Eocene breakoff and rollback of the Farallon slab—an explanation for the "Challis" event? [abstract]: Geological Society of America Abstracts with Programs, v. 48, no. 4.

Thackray, G. D., 1996, Glaciation and neotectonic deformation on the western Olympic Peninsula, Washington: University of Washington Doctor of Philosophy thesis, 139 p., 2 plates.

Thackray, G. D., 2001, Extensive early and middle Wisconsin glaciation on the western Olympic Peninsula, Washington, and the variability of Pacific moisture delivery to the northwestern United States: Quaternary Research, v. 55, no. 3, p. 257-270.

Thackray, G. D.; Gavin, Dan; Ritchie, Andy; Wegmann, K. W.; Ashworth, Allan; Ely, Lisa, 2015, Late Pleistocene to Modern Geomorphic and Biotic History of the Olympic Peninsula, Washington: Friends of the Pleistocene, Pacific Northwest Cell Field Trip, 2015, 121 p.

Thorson, R. M., 1981, Isostatic effects of the last glaciation in the Puget Lowland, Washington: U.S. Geological Survey Open-File Report 81-370, 100 p., 1 plate. [http://pubs.er.usgs.gov/publication/ofr81370]

Thorson, R. M., 1989, Glacio-isostatic response of the Puget Sound area, Washington: Geological Society of America Bulletin, v. 101, no. 9, p. 1163-1174.

Troost, K. G., 1999, The Olympia nonglacial interval in the south-central Puget Lowland, Washington: University of Washington Master of Science thesis, 123 p.

Troost, K. G.; Booth, D. B., 2008, Geology of Seattle and the Seattle area, Washington. *In* Baum, R. L.; Godt, J. W.; Highland, L. M., editors, Landslides and engineering geology of the Seattle, Washington, area: Geological Society of America Reviews in Engineering Geology XX, p. 1-35. [http://www.wou.edu/las/physci/taylor/g473/seismic_hazards/troost_booth_2008_geo_seattle.pdf]

U.S. Department of Agriculture, Natural Resource Conservation Service, Soil Survey Staff, 2013, Web Soil Survey, Mason County, Washington: U.S. Department of Agriculture. [accessed on 12/2013 and 7/2014 at http://websoilsurvey.nrcs.usda.gov/]

U.S. Geological Survey Geologic Names Committee, 2010, Divisions of geologic time—Major chronostratigraphic and geochronologic units: U.S. Geological Survey Fact Sheet 2010-3059, 2 p. [http://pubs.usgs.gov/fs/2010/3059/]

Van Wagoner, T. M.; Crosson, R. S.; Creager, K. C.; Medema, G. F.; Preston, L. A.; Symons, N. P.; Brocher, T. M., 2002, Crustal structure and relocated earthquakes in the Puget Lowland, Washington, from high-resolution seismic tomography: Journal of Geophysical Research, v. 107, no. B12, 2381, p. ESE 22-1–22-23. [doi:10.1029/20012JB000710]

Walsh, T. J.; Logan, R. L., 2005, Geologic map of the East Olympia 7.5-minute quadrangle, Thurston County, Washington: Washington Division of Geology and Earth Resources Geologic Map GM-56, 1 sheet, scale 1:24,000. [http://www.dnr.wa.gov/publications/ger_gm56_geol_map_eastolympia_24k.pdf]

Walsh, T. J.; Korosec, M. A.; Phillips, W. M.; Logan, R. L.; Schasse, H. W., 1987, Geologic map of Washington—Southwest quadrant: Washington Division of Geology and Earth Resources Geologic Map 34, 2 sheets, with 28 p. text. Geologic map: Sheet 1, scale 1:250,000. [http://geopubs.wr.usgs.gov/open-file/of99-382/]

Wang, Kelin, 1996, Simplified analysis of horizontal stresses in a buttressed fore arc sliver at an oblique subduction zone: Geophysical Research Letters, v.23, n. 16, p. 2021-2024.

Washington Division of Geology and Earth Resources, 2010a, Surface geology, 1:250,000—GIS data, June 2010: Washington Division of Geology and Earth Resources. [http://www.dnr.wa.gov/publications/ger_portal_surface_geology_250k.zip]

Washington Division of Geology and Earth Resources, 2010b, Surface geology, 1:100,000—GIS data, June 2010: Washington Division of Geology and Earth Resources. [http://www.dnr.wa.gov/publications/ger_portal_surface_geology_100k.zip]

Wells, R. E., 1982, Paleomagnetism and geology of Eocene volcanic rocks in southwest Washington—Constraints on mechanisms of rotation and their regional tectonic significance: University of California at Santa Cruz Doctor of Philosophy thesis, 229 p., 1 plate, scale 1:62,500.

Wells, R. E.; Bukry, David; Friedman, Richard; Pyle, Doug; Duncan, Robert; Haeussler, Peter; Wooden, Joe, 2014, Geologic history of Siletzia, a large igneous province in the Oregon and Washington Coast Range—Correlation to the geomagnetic polarity time scale and implications for a long-lived Yellowstone hotspot: Geosphere, v. 10, no. 4, p. 692-719.

Wells, R. E.; Engebretson, D. C.; Snavely, P. D., Jr.; Coe, R. S., 1984, Cenozoic plate motions and the volcano-tectonic evolution of western Oregon and Washington: Tectonics, v. 3, no. 2, p. 275-294.

Wells, R. E.; Heller, P. L., 1988, The relative contribution of accretion, shear, and extension to Cenozoic tectonic rotation in the Pacific Northwest: Geological Society of America Bulletin, v. 100, no. 3, p. 325-338.

Wells, R. E.; Weaver, C. S.; Blakely, R. J., 1998, Forearc migration in Cascadia and its neotectonic significance: Geology, v. 26, no. 8, p. 759-762.

Wlodarski, Wojciech, 2014, Geometry and kinematics of glaciotectonic deformation superimposed on the Cenozoic fault-tectonic framework in the central Polish Lowlands: Quaternary Science Reviews, v. 94, p. 44-61.

Appendix A. New Radiocarbon, Luminescence, and $^{40}Ar/^{39}Ar$ Age Estimates

Table A1. Radiocarbon ages from the map area. ^{14}C yr BP age estimates (including AMS) are in radiocarbon years before 1950 and uncertainty estimates are reported at 1σ (68% confidence). Ages in ka are calendar years before 1950 divided by 1,000 and have 2σ uncertainty range. An age range is preferred because uncertainties are unequally distributed as a result of the calibration curves used to convert between radiocarbon and calendar years. Age and method in quotation marks are those reported by the cited publication. Uncertainty statements reflect random and lab errors; errors from unrecognized sample characteristics or flawed methodological assumptions (for example, ^{14}C sample contamination from younger carbon flux) are not known. Radiocarbon 'greater than' age statements (for example, >43,500 BP) include a 2σ variance against background radiation. Ages (including AMS) are adjusted for measured $^{13}C/^{12}C$ ratio (a 'conventional' age) if a $^{13}C/^{12}C$ ratio is shown.

Geologic units are the interpretation of this study. Elevations were estimated using Puget Sound Lidar Consortium lidar data projected to State Plane South, NAD 83 HARN, US Survey feet, supplemented by visual elevation estimates on bluffs. Lidar level 0 is theoretically 3.41 to 3.47 ft below base map level 0 [http://www.ngs.noaa.gov/cgi-bin/VERTCON/vert_con.prl]. Lidar elevation statements were not adjusted to account for systematic projection differences relative to the base map. Latitude and longitude coordinates are in WGS84. – – – indicates no data.

^{14}C site ID (geologic unit)		Reference	Material	Method	$^{13}C/^{12}C$ (o/oo)	Age estimate
GD1 (Qc$_O$)		this study	plant material	^{14}C	-27.9	14,430 ±50 ^{14}C yr BP (17.690–17.475 ka)
Lab ID[a]	Beta-423292	Homogenized plant material from 2 in.-thick peaty gyttja overlain by 2–3 in. of compact, pale gray clayey silt beneath an unconformable contact with loose colluvium on the right (southwestern) bank of a southeast-flowing unnamed creek at the northwest end of Shelton Valley. The gyttja is the uppermost of three similar gyttja layers separated by interbeds of similar silt. The lowest gyttja is the thickest (1.5–2 ft) and overlies at least 3 ft of pale gray silt that extends to the base of the exposure at the valley floor. The entire exposure is broken by fractures and clastic dikes with uncompacted sediment fill; the silt and gyttja may therefore be part of a Holocene slide block from up to 90 ft higher elevation. Geologic unit for sample differs from map unit because map is simplified to limit complexity.				
TRS	sec. 27, T20N R4W					
Lat/long. (degrees)	47.19236 -123.16769					
Elev. (ft)	179					
GD2 (Qc$_O$)		this study	plant material	^{14}C (AMS)	-28.7	23,030 ±90 ^{14}C yr BP (27.480–27.235 ka)
Lab ID[a]	Beta 423290	Plant material from flattened concentrations of organic material in the upper part of a roughly 6 in.-thick, lilac-brown gyttja that we described as a probable paleosol. The sample is from about 4 ft above channel level at the base of a more than 50 ft-high cliff on the right (southern) bank of Goldsborough Creek (Fig. 8). The gyttja is the upper of two similar gyttja layers that appear to be the same single deposit repeated by a gently northeast-dipping thrust. The gyttja overlies Olympic Mountains-sourced diamicton interpreted as a debris flow deposit into a lacustrine setting. The gyttja layer is overlain by lacustrine silt. The lacustrine mud is truncated by an erosional unconformity overlain by 17–20 ft of basalt-rich pebble gravel (Olympic Mountains source). The contact with the lacustrine deposits—and bedding within the gravel—rise gently southwest and appear to record post-depositional tilting. At the top of the exposure, the Olympic Mountains-sourced gravel is overlain by 7 ft of silt (?) that in turn is overlain by 3 ft of pebble gravel.				
TRS	sec. 14, T20N R4W					
Lat/long. (degrees)	47.21690 -123.15154					
Elev. (ft)	135					
GD3 (Qp$_O$)		this study	wood	^{14}C	-24.7	> 43,500 ^{14}C yr BP
Lab ID[a]	Beta 418908	Detrital 1 in. wood stick about 12 in. long, embedded in silty glaciolacustrine matrix with dropstones and layers and lenses of debris flow slurries rich in locally derived subangular basaltic clasts. Deposit records the arrival or melting of ice against northeast-facing slopes at 370 ft elevation.				
TRS	sec. 29, T20N R4W					
Lat/long. (degrees)	47.1955 -123.22032					
Elev. (ft)	370					

^{14}C site ID (geologic unit)		Reference	Material	Method	$^{13}C/^{12}C$ (o/oo)	Age estimate
GD4 (Qc_o)		this study	wood	^{14}C (AMS)	-27.9	> 43,500 ^{14}C yr BP
Lab ID[a]	Beta 422697	Wood fragment (0.3 g) from 8 in.-thick, dark gray to brown, interbedded silt and organic-rich mud (Fig. I). Sampled layer is underlain by 2 ft of interbedded and laminated silt and sandy pebble gravel. The gyttja, silt, and pebble gravel comprise a nonglacial deposit that is overlain by about 8 ft of surficial drift that is probably partly waterlain in a subglacial setting and includes undulating interbedded sand, silt, pebble gravel and till. The provenance of the drift is at least partly northern-sourced, but a clast count from the basal two feet of the drift contains much basalt and may be sourced from the Olympic Mountains. A subvertical southeast-striking shear plane offsets the entire exposed section with about 2 ft of apparent southwest-up displacement.				
TRS	sec. 15, T20N R4W					
Lat/long. (degrees)	47.21903 -123.16879					
Elev. (ft)	183					
GD5 (Qpu_{op})		this study	plant material	^{14}C (AMS)	-29.0	> 49,510 ^{14}C yr BP
Lab ID[a]	Beta 423291	Small plant fragments from the lower of two dark-brownish-black seams of gyttja (organic-rich silt and very fine sand with abundant flattened debris of plant or algal matter). Each gyttja is about 0.5 in. thick and is interbedded in a 2 ft-thick layer of planar-laminated to massive very compact silt to very fine sand with scattered delicate plant or algal bits throughout. The silt is planar-bedded where sampled and thickens to 5 ft about 30 ft west of the sample site. The silt overlies basalt-rich lodgment till that in turn overlies sandy, basalt-rich pea gravel. Both the till and the pea gravel contain mostly rotten clasts. The exposure is located in the north-facing slope at the edge of a bouldery Vashon recessional outwash gravel terrace south of Goldsborough Creek, about 250 ft west of the former Goldsborough Creek dam site. On the USGS topographic base map, the former dam site is located at (and can be identified by) the east edge of a lake. (Historic aerial orthophotos suggest a dam location about 100 ft farther east, about 350 ft from our sample site.)				
TRS	sec. 24, T20N R4W					
Lat/long. (degrees)	47.20978 -123.13983					
Elev. (ft)	106					
GD6 (Qpu_{op}—now likely unit ml)		Fairhall and others (1966)	wood	"^{14}C"	– – –	"> 40,000" ^{14}C yr BP
Lab ID[a]	UW-50	Wood from a bluff of mostly nonglacial gravel sourced from the Olympic Mountains overlain by Vashon Drift. Fairhall and others (1966) reported sample site as "ca. 12 ft above creek level" and "ca. 1" mi west of Shelton, "100 ft downstream from toe" of former Rayonier-Simpson dam; it was not stated which side of the stream the sample was collected from. If accurately identified, sample location is now modified land due to extensive earth movement associated with dam removal. Fairhall and others (1966) added that the sample was submitted by John B. Noble, and that he commented "sequence probably the same as the one that contained UW-48"—in apparent reference to the "Skokomish Gravel" type section near UW-48.				
TRS	sec 24, T20N R4W					
Lat/long. (degrees)	47.210 -123.138					
Elev. (ft)	~88					

[a] Letters identify radiocarbon labs: Beta, Beta Analytic; UW, University of Washington Department of Chemistry.

Table A2. New infrared stimulated luminescence (IRSL) results from the map area. Analyses were performed on fine-grained feldspar by Shannon Mahan and Harrison Gray, USGS. Uncertainty estimates are 1σ (68% confidence) and are the values reported by the lab. Uncertainty statements reflect random and lab errors; errors from unrecognized sample characteristics or flawed methodological assumptions (for example, incomplete pre-depositional resetting of luminescence samples) are not known.

Luminescence site ID (geologic unit)		Water content (%)[a]	K (%)[b]	U (ppm)[b]	Th (ppm)[b]	Cosmic dose additions (Gy/ka)[c]	Equivalent dose (Gy)	Total dose rate (Gy/ka)	N[d]	Scatter (%)[e]	Method	Age (ka)[f]
GD7 (Qc$_O$)		13 (50)	1.16 ±0.05	1.15 ±0.14	4.20 ±0.45	0.05 ±0.01	96 ±7.7	2.02 ±0.13	8 (12)	49	IRSL	47.31 ±4.9 ka
Lab ID	C461B	Sand sampled 6 ft above stream level from a 7 ft-thick section of orange to gray, medium- to fine-grained sand that is mostly medium to very thinly planar bedded with minor cross beds and ripples. The upper 3 ft of the exposure coarsen upwards to pebble gravelly sand. The sand overlies 4 ft of cross-bedded sandy pebble gravel that appears to be part of the same unit; a clast count from this unit 600 ft downstream to the southeast showed mild weathering and northern provenance (clast count site C31).										
TRS	sec. 15, T20N R4W											
Lat/long. (degrees)	47.21702 -123.16770											
Elev. (ft)	170	Downsection of the dated unit is an apparently alpine glacial unit sourced from the Olympic Mountains that ranges from diamicton to pebble gravel and sand and may be glaciolacustrine drift or till (possible Qat? in Columnar Section 2). The alpine drift at the base of the section can be traced up valley at stream level, where it also underlies radiocarbon infinite age site GD4 (Fig. I), but the stratigraphic relationship between age site GD4 and the luminescence age site GD7 (Columnar Section 2) remains unresolved because the sections above the basal drift differ from each other at the two age sites.										
Material	sand	Upsection of sample GD7 is an 8 ft-thick section of Vashon-age recessional outwash pebble gravel; a cliff exposure 600 ft farther southwest reveals more than 100 ft of section stratigraphically between GD7 and the 8 ft-thick section of Vashon recessional outwash. The exposure 600 ft southwest of GD7 includes apparent Vashon (?) advance outwash pebble gravel (clast count site C34) above planar-laminated advance outwash silt (paleomagnetic sample M3) that in turn overlies about 100 ft of lightly weathered pebble gravel of likely Olympic provenance (clast count site C30; Columnar Section 2).										
GD8 (Qc$_O$)		9 (22)	0.67 ±0.04	1.00 ±0.11	2.50 ±0.24	0.05 ±0.01	66 ±4.2	1.51 ±0.08	16 (18)	53	IRSL	43.69 ±3.7 ka
Lab ID	C259C	Sand sampled from the south side of a channel about 4.5 ft above the base of a steeply incised v-shaped drainage. The sampled exposure consists of a 20 ft-thick yellowish-dark brown interbedded sand and pebble gravel; fluvial channel margins appear to be defined by bedded (3.5 in.-thick) sets of tangential cross beds; bedding dips as steep as 25° were observed and interpreted as channel structure, not evidence of post-depositional tilting. A clast count (site C22) of pebbles stratigraphically equivalent to the sand of GD8 suggests northern provenance, as does 3 ft of northern-sourced gravel observed upslope above a 53.5 ft gap in exposure (clast count site C21).										
TRS	sec. 16, T19N R4W											
Lat/long. (degrees)	47.13733 -123.19439											
Elev. (ft)	320	Upsection of the dated unit and clast count site C21 is 1.5 ft-thick pale tan and reddish brown sandy diamicton—possibly a till—with moderately abundant medium pebbles and a sharp, undulating contact with the underlying outwash gravel. The diamicton is overlain by 8.5 ft of probable Vashon advance outwash. Within this outwash, the lower 1.5 ft is compact, pale tan, horizontally laminated to massive silt; the upper 7 ft is mildly weathered, moderately sorted, interbedded and faintly cross bedded sand and pebble gravel (clast count site C20). The degree of compaction of these layers—and the presence of surficial till elsewhere on the nearby upland surface—suggest that Vashon-age till lies somewhere above these units, likely within the uppermost 35 ft of the valley wall.										
Material	sand											

[a] Field moisture, with number in parentheses indicating the complete sample saturation percent. Ages calculated using approximately 50 percent of saturation values.

[b] Analyses obtained using high-resolution gamma spectrometry (HPGe detector).

[c] Cosmic doses (in Grays per 1,000 yr) and attenuation with depth were calculated using the methods of Prescott and Hutton (1994). See text for details.

[d] Number of replicated equivalent dose (De) estimates used to calculate the equivalent dose. Numbers in parentheses indicate total number of measurements included in calculating the represented equivalent dose and age using the weighted mean

[e] Defined as 'over-dispersion' of the De values. Obtained by taking the average over the standard deviation. Values >35 percent are considered to be poorly bleached sediments.

[f] Dose rate and IRSL age for feldspar from 250–90 micron k-feldspar, post IR230C. Errors to one sigma, exponential + linear fit used on equivalent dose. No fade indicated.

Table A3. $^{40}Ar/^{39}Ar$ ages for sites GD9 and GD10. Analysis by Daniel Miggins and staff, Argon Geochronology Lab, College of Oceanic and Atmospheric Sciences, Oregon State University, Corvallis, Oregon. Uncertainty values span 2σ (95% confidence). Uncertainty statements reflect random and lab errors; errors from unrecognized sample characteristics or flawed methodological assumptions (for example, unrecognized post-depositional re-setting of $^{40}Ar/^{39}Ar$ ratios) are not known. – – – indicates no data

$^{40}Ar/^{39}Ar$ site (sample ID) (geologic unit)							
GD9 (C227) (Evc)			Gray, fine-grained, slightly altered basalt; sampled from 13 ft-high exposure, parts of which resemble siltstone but appear to be fine-grained basalt throughout; the basalt appears relatively fresh. Sample is the northwestern-most date in basalt from the Black Hills and is the same location as geochemistry site G15.				
TRS	sec. 32, T20N R4W						
Lat/long (degrees)	47.18448 -123.22300						
Elev. (ft)	610						
Result Type	**$^{40}Ar^{(r)}/^{39}Ar^{(k)}$**	**±2σ**	**$^{39}Ar^{(k)}$ (%.n)**	**K/Ca ±2σ**	**Age (Ma) ±2σ**		**MSWD**
Age Plateau	15.81427	±0.0507	56.95	0.0475 ±0.0039	50.51	±0.21	1.99
		±0.32%	15			±0.41%	1%
					Full external error	±1.15	
					Analytical error	±0.16	
Total Fusion	15.62029	±0.03315	40	0.0484 ±0.0001	49.90	±0.17	
		±0.21%	– – –			±0.34%	

GD10 (C350) (Evc)			Basalt from 23 ft-high by 80 ft-wide exposure of well-developed colonnade with 1–1.5 ft-diameter columns. Gently west-southwest-dipping flow orientation inferred from platy column top joints and surfaces. Sample site is the same as geochemistry site G14.				
TRS	sec. 24, T20N R5W						
Lat/long (degrees)	47.20076 -123.24422						
Elev. (ft)	255						
Result Type	**$^{40}Ar^{(r)}/^{39}Ar^{(k)}$**	**±2σ**	**$^{39}Ar^{(k)}$ (%.n)**	**K/Ca ±2σ**	**Age (Ma) ±2σ**		**MSWD**
Age Plateau	15.66077	±0.03347	38.77	0.060 ±0.009	50.14	±0.17	1.58
		±0.21%	14			±0.34%	8%
					Full external error	±1.14	
					Analytical error	±0.11	
Total Fusion	14.83155	±0.01925	38	0.099 ±0.0001	47.52	±0.14	
		±0.13%	– – –			±0.30%	
					Full external error	±1.07	
					Analytical error	±0.06	

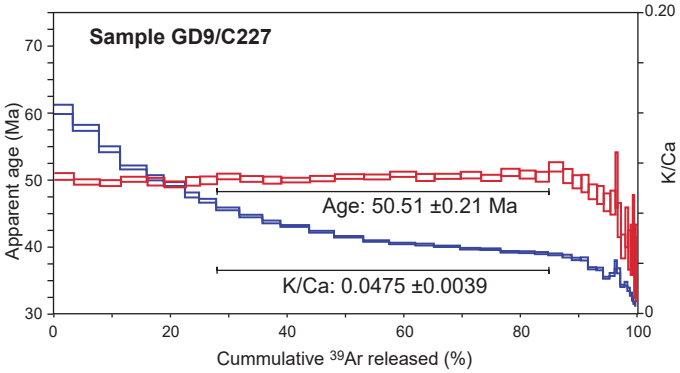

Figure A1. $^{40}Ar/^{39}Ar$ step-heating age and K/Ca spectra for site GD9.

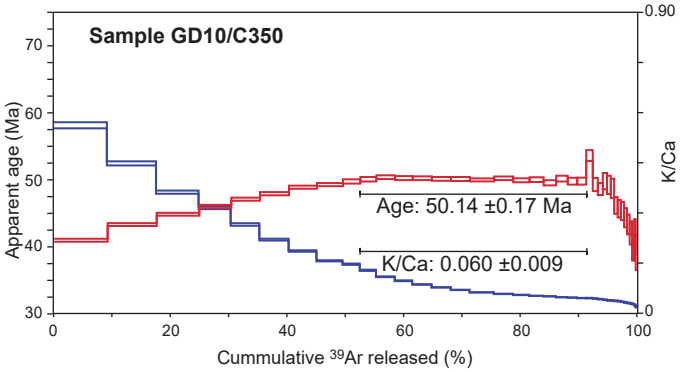

Figure A2. $^{40}Ar/^{39}Ar$ step-heating age and K/Ca spectra for site GD10.